Schweizerische Eidgenossenschaft
Confédération suisse
Confederazione Svizzera
Confederaziun svizra

Federal Department of the Environment, Transport, Energy and Communications DETEC

Swiss Federal Office of Energy SFOE
Energy Research and Cleantech

Final report dated 10 May 2021

HybridStock

Hybrid Seasonal Storage of Renewable Heat and Electricity with an Aluminium Redox Cycle

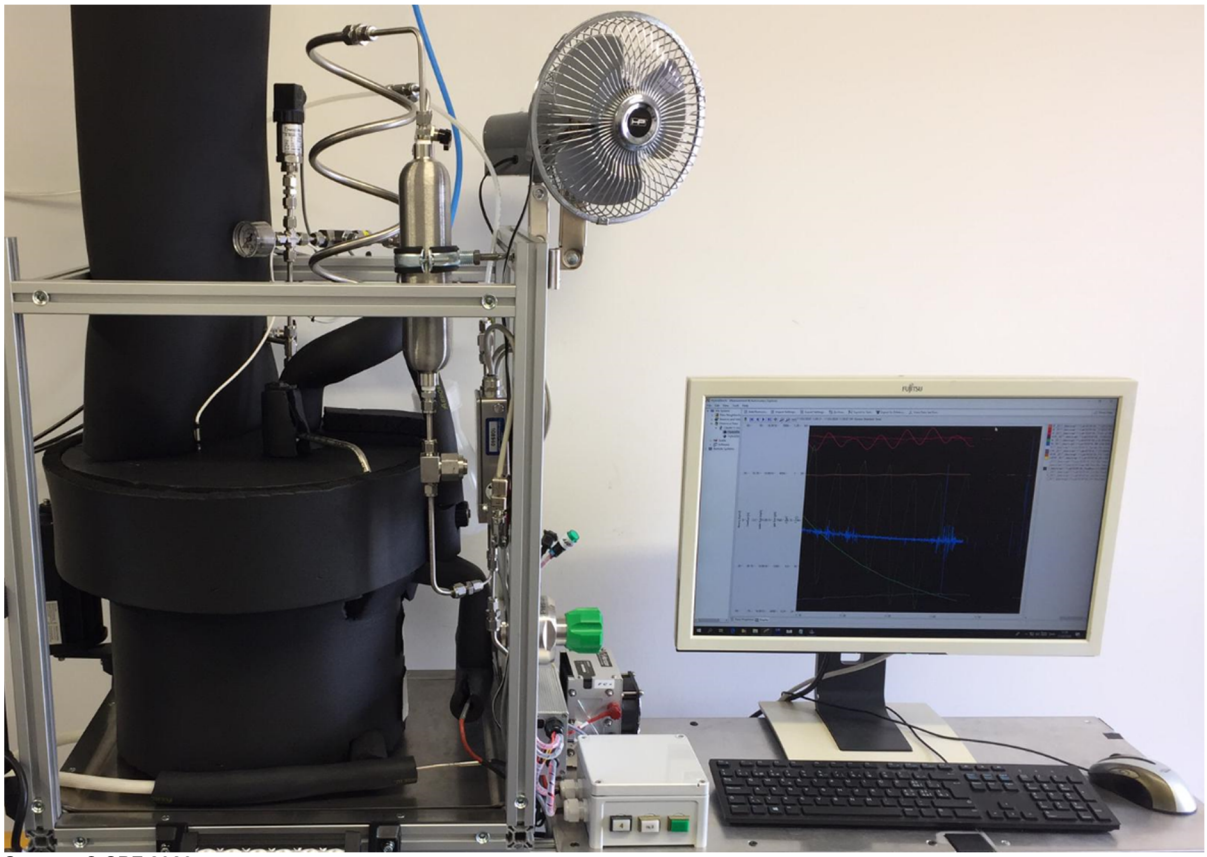

Source: © SPF 2020

Date: 10 May 2021

Location: Rapperswil

Subsidiser:
Swiss Federal Office of Energy SFOE
Energy Research and Cleantech Section
CH-3003 Bern
www.bfe.admin.ch

Subsidy recipients:
SPF Institute for Solar Technology, HSR University of Applied Sciences
Oberseestr. 10, CH-8640 Rapperswil
www.spf.ch

Authors:
Michel Haller, michel.haller@spf.ch
Dominik Amstad, dominik.amstad@spf.ch
Mihaela Dudita, mihaela.dudita@spf.ch
Daniel Carbonell, dani.carbonell@spf.ch
Daniel Zenhäusern, daniel.zenhaeusern@spf.ch
With contributions from Meryem Farchado, Alexander Englert, Dario Niggli, Ivo Caduff, Fabio Lichtensteiger

SFOE project coordinators:
Andreas Eckmanns, andreas.eckmanns@bfe.admin.ch
Elimar Frank, elimar.frank@frank-energy.com

SFOE contract number: SI/501693-01

Zusammenfassung

Aluminium kann als Energievektor eingesetzt werden der beliebig lange gespeichert werden kann und aus dem sehr hohe Energiemengen freigesetzt werden können. Die Produktion von Wärme und Wasserstoff auf der Basis von Aluminium wurde untersucht, und es wurde ein 400 W Prototyp-Reaktor gebaut, der mittels Aluminium-Wasser Reaktion 4.3 kWh Wärme und 0.11 kg Wasserstoff pro kg Al erzeugte. Die Reinheit des erzeugten Wasserstoffs war sehr hoch, so dass dieser direkt in einer PEM-Brennstoffzelle zur Stromerzeugung verwendet werden konnte. Simulationen ergaben, dass für Gebäude die nach heutigen Standards gebaut werden, 300 - 500 kg Al pro Wohnung benötigt würden, um Solarenergie vom Sommer in den Winter zu speichern und in Kombination mit einem PV-Wärmepumpensystem den Strom- und Wärmebedarf über das ganze Jahr vollständig zu decken. Eine Lebenszyklusanalyse zeigte, dass dieses neue 100% solare Energieversorgungskonzept für Gebäude insgesamt wesentlich geringere Treibhausgasemissionen aufweist als ein konventionelles System. Die verbleibenden Emissionen können erheblich reduziert werden, wenn für die Aluminium-Produktion statt des herkömmlichen Hall-Héroult-Verfahrens ein Inert-Elektroden-Prozess verwendet wird, und wenn die Elektrizität durch Wasser- oder Windkraft statt durch Photovoltaik bereitgestellt wird.

Résumé

L'aluminium peut être utilisé comme un vecteur d'énergie qui peut être stocké pendant une durée indéterminée et à partir duquel de très grandes quantités d'énergie peuvent être libérées. La production de chaleur et d'hydrogène à base de l'aluminium a été étudiée et un prototype de réacteur de 400 W a été construit, capable de produire 4.3 kWh de chaleur et 0.11 kg d'hydrogène par kg d'Al grâce à la réaction aluminium-eau. La pureté de l'hydrogène produit était très élevée, de sorte qu'il pouvait être utilisé directement dans une pile à combustible PEM pour la production d'électricité. Les simulations ont montré que pour les bâtiments construits selon les normes actuelles, il faudrait 300 à 500 kg d'Al par appartement pour stocker l'énergie solaire d'été à hiver et de couvrir complètement la demande d'électricité et de chaleur tout au long de l'année en combinaison avec un système de pompe à chaleur et PV. Une analyse du cycle de vie montre que ce nouveau concept d'alimentation des bâtiments à 100% d'énergie solaire a globalement des émissions de gaz à effet de serre nettement inférieures à celles d'un système conventionnel. Les émissions restantes peuvent être considérablement réduites si un procédé à électrode inerte est utilisé pour la production d'aluminium au lieu du procédé Hall-Héroult classique, et si l'électricité est fournie par l'énergie hydraulique ou éolienne au lieu du photovoltaïque.

Summary

Aluminium can be used as an energy vector that can be stored as long as desired and from which very high amounts of energy can be released. The production of heat and hydrogen was investigated and a 400 W prototype reactor was built that produced roughly 4.3 kWh of heat and 0.11 kg hydrogen per kg Al from an Al-water reaction. The purity of the produced hydrogen was very high, such that it can be used directly in a PEM fuel cell for the production of electricity. Simulations showed that 300 – 500 kg Al per dwelling would be needed for buildings that are built according to current standards in order to store solar energy from summer to winter and to fully cover the electricity and heat demand over the whole year in combination with a PV and heat pump system. A life cycle analysis showed that the overall global warming potential of this new 100% solar building energy supply concept is substantially lower than for a conventional system. Remaining emissions can be reduced substantially when an inert electrode process is used for Al smelting instead of the conventional Hall-Héroult process, and when electricity is provided by hydro or wind power instead of photovoltaics.

Main findings

- Aluminium (Al) can be used to store solar energy with an energy storage density of 8.7 kWh/kg (23.5 MWh/m^3), and 0.112 kg of H_2 can be produced from 1 kg of Al.
- The production of hydrogen with high efficiency from Al and water under alkaline conditions has been demonstrated in the HSR laboratory and the produced hydrogen was used successfully for the production of electricity using a small fuel cell
- Simulations showed that 300 – 500 kg Al would be needed for a modern low energy house to store solar energy from summer to winter and to fully cover the electricity and heat demand of the whole year based on this storage in combination with a PV and heat pump system.
- The Al seasonal energy storage combined with a PV and heat pump system is an environmental friendly solution for providing the building's heat and electricity demand, as shown by the environmental life cycle assessment, and the system could become cost-effective by 2030.

Contents

Abbreviations

CAPEX	Capital Expenditures
CED	Cumulated Primary Energy Demand
DC	Direct Current
DHW	Domestic Hot Water
DSC	Differential Scanning Calorimetry
EDX	Energy Dispersive X-ray Spectroscopy
El.	Electricity
EMPA	Swiss Federal Laboratories for Material Science and Technology
ENTSO-E	European Network of Transmission System Operators for Electricity
ETH	Swiss Federal Institute of Technology
EU	European Union
fH	French degree of hardness
GWP	Global Warming Potential
HH	Household
HHV	Higher Heating Value
HSR	University of Applied Sciences Rapperswil HSR
ICP-OES	Inductively Coupled Plasma Optical Emission Spectrometry
IWK	Materials Technology and Plastics Processing Institute from HSR
KPI	Key Performance Indicator
LCA	Life Cycle Assessment
M	Molarity
MEC	Minimum Explosive Concentration
MIE	Minimum Ignition Energy
OPEX	Operational Expenditures
PCM	Phase Change Material
PEM	Polymer Electrolyte Membrane (fuel cell)
PV	Photovoltaics
SEM	Scanning Electron Microscopy
SFOE	Swiss Federal Office of Energy
SH	Space Heat
SIA	Swiss Society of Engineers and Architects
SPF	Seasonal Performance Factor, or SPF Institute for Solar Technology of HSR
SPF	SPF Institute for Solar Technology
SUVA	Schweizerische Unfallversicherung
TES	Thermal Energy Storage
TGA	Thermogravimetric Analysis

XRD	X-Ray Diffraction

Symbols

c_p	specific heat, kJ/kgK
f	purity, -
K_{sp}	solubility product constant
K_{st}	maximal explosioin overpressure, bar m s^{-1}
m	mass, kg
$\dot{m}$	mass flow rate, kg/s
M	molar mass, g/mol
n	stoichiometric amount of substance participating in a reaction, -
p	pressure, Pa
$\dot{Q}$	heat flow rate, thermal power, W
R	ratio, -; or gas constant (8.314472 L kPa K^{-1} mol^{-1})
t	time, s
T	thermodynamic temperature, K
u	uncertainty, variable units
V	volume, mL
V_M	molar volume for H_2 at normal conditions: 22.42 L/mol (273.15 K, 101.325 kPa)
V_n	gas volume at normal conditions, mLn
W	work, W
η	efficiency of hydrogen production, -
ΔH_r	enthalpy of reaction, kJ/kg

Subscripts

100a	100 years (for GWP)
Al	aluminium
C	carbon
el	electric
H_2	hydrogen
max	theoretical maximum
n	normal conditions (T_n = 273.15 K, p_n = 101.325 kPa)
nr	non-renewable
tot	total

1 Introduction

1.1 Motivation

The energy consumption of buildings is responsible for 40% of the final energy use of Switzerland. Substantial savings are expected in this field according to the Swiss energy strategy 2050[1]. These shall be achieved by better insulation of the building shell and a substantial increase of decentralized renewable energy production for heat and electricity, as well as more efficient electric appliances.

Photovoltaic and heat pump systems in combination with short-term electric and thermal storage and intelligent control are able to provide 50% of the electricity consumption (and thus of the final energy consumption) of a new building. At the same time, these systems generate additional electricity in summer that is not used on site and could cover the missing 50% of electric end energy use in winter, if an economic seasonal energy storage would be available.

Seasonal thermal energy storage in combination with solar thermal collectors have demonstrated to be able to cover 100% of the heating demand of single- and multi-family buildings all year around [1,2]. However, in these systems, electricity demand in winter is not covered, and the volume of the thermal storage usually exceeds 10 m^3 per apartment. The potential for multiplication of this concept into denser populated areas or zones with high real estate prices is thus limited.

With the multifamily-building in Brütten [3–5], it was demonstrated that it is also possible to cover 100% of the yearly electricity and heat demand with a combination of thermal energy storage, batteries and hydrogen tanks. However, in this system the storage volumes are also quite large (> 10 m^3 per apartment) and the overall concept of storing hydrogen is associated with very high cost as well as safety issues.

The HybridStock project aims to develop a seasonal energy storage concept with considerably higher energy density compared to water, hydrogen or any Power-to-Gas system, and can be used to provide 100% of electricity and heat demand of a building in winter from solar energy that has been used for charging the storage in summer. The concept is based on an aluminium redox-cycle that has been evaluated in the feasibility study “HePoStAl – Heat and Power Storage in Aluminum” (SFOE project nr. SI/500315-03).

1.2 Purpose of the project

Aluminium was used in the past as an energy carrier for rocket propulsion systems and it has been discussed for powering cars, boats and submarines. Aluminium powder can be burnt directly [6] or it can be converted to hydrogen and heat [7,8]. A literature review that focuses on this latter conversion path has been given in the feasibility study previously published by SPF [9]. General literature about aluminium as an energy storage or as a starting point for the formation of hydrogen has been reviewed by different authors [10–12].

[11] https://www.bfe.admin.ch/bfe/en/home/policy/energy-strategy-2050.html

In the HybridStock project, we propose to develop a seasonal energy storage process based on the aluminium redox cycle (chemical reduction and oxidation of aluminium). Electricity from solar or other renewable sources is used to convert aluminium oxide or aluminium hydroxide to elementary aluminium by a chemical reduction process ($Al^{3+} \rightarrow Al$) and thus "charge the storage". The discharging takes place in decentralized small units in winter, when aluminium is chemically oxidized ($Al \rightarrow Al^{3+}$). This process releases hydrogen, heat, and aluminium hydroxide or oxide. Hydrogen is used in a fuel cell to produce electricity, and heat produced in the fuel cell and in the aluminium oxidation process is used for domestic hot water production (DHW) and space heating. The overall concept is shown in Figure 1. It differs from previous work involving aluminium as an energy carrier in the following ways:

- We propose a concept of decentralized production of heat and electricity based on aluminium, which reduces thermal losses, since almost all heat is used directly on site and is not discarded (or wasted).
- We propose the use of the (chemically) stored energy in aluminium primarily for heating (75%), with the positive side effect that we can produce as well electricity (25%).
- In addition to the obvious temporal separation of the aluminium reduction (storage charging) and oxidation processes (storage discharging), we also propose a spatial separation of the two processes. The discharging of the energy that is stored in aluminium can take place in many small units that are distributed in different buildings and homes (decentralized). The regeneration of the aluminium by a smelter process is done in a central facility, since this is a metallurgic high temperature process that requires an industrial environment.
- Last, but not least, we propose a closed cycle as Al is not released in the environment after it is oxidized, but recycled and converted to elementary Al again in a central facility.

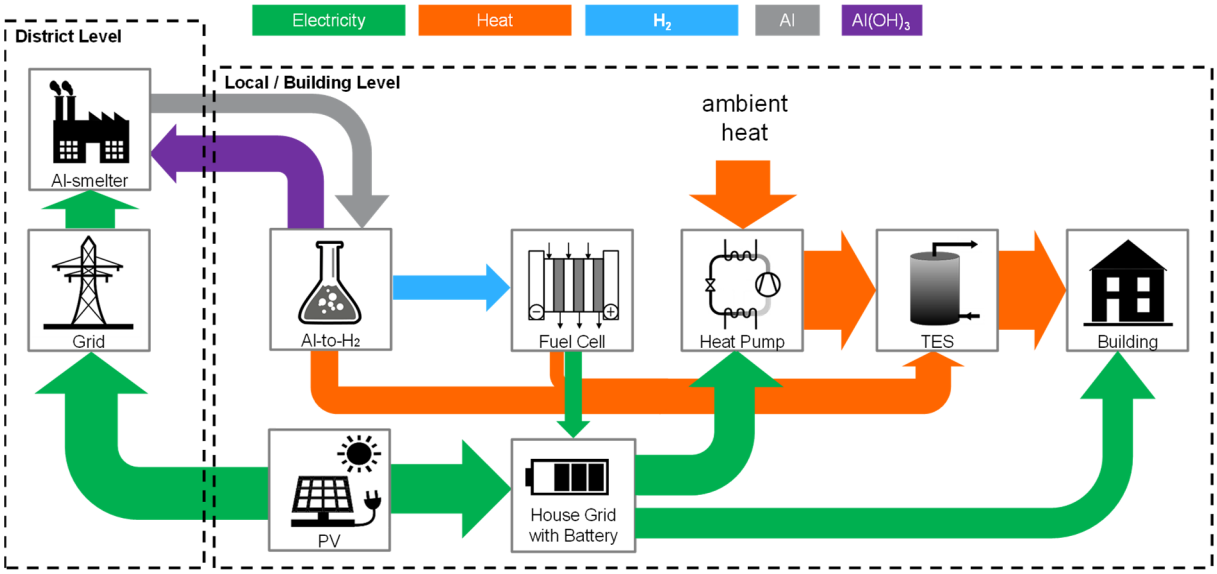

Figure 1: Electricity and heat supply for 100% solar coverage with aluminium seasonal energy storage.

The HybridStock discharging process and system is shown in Figure 2. The reaction of aluminium (Al) with water produces heat and hydrogen and, depending on the reaction temperature, either aluminium hydroxide or aluminium oxide. Each kg of Al generates 0.11 kg of hydrogen. Using this hydrogen in a fuel cell with an electric efficiency of 50% ideally produces 2.2 kWh_{el} and 2.2 kWh_{th} per kg Al. In the system shown in Figure 2, an additional 4.3 kWh_{th} of heat is produced from the aluminium oxidation reaction. Thus, the total energy density of Al as an energy storage medium is 8.7 kWh/kg, or 23.5 MWh/m^3, respectively. This value is calculated considering the heat and the hydrogen (based on the higher heating value or HHV) produced in the aluminium oxidation process. The energy density of aluminium is much higher than the volumetric storage density of all conventional energy carriers we know of – with the exception of nuclear fuels (Figure 3).

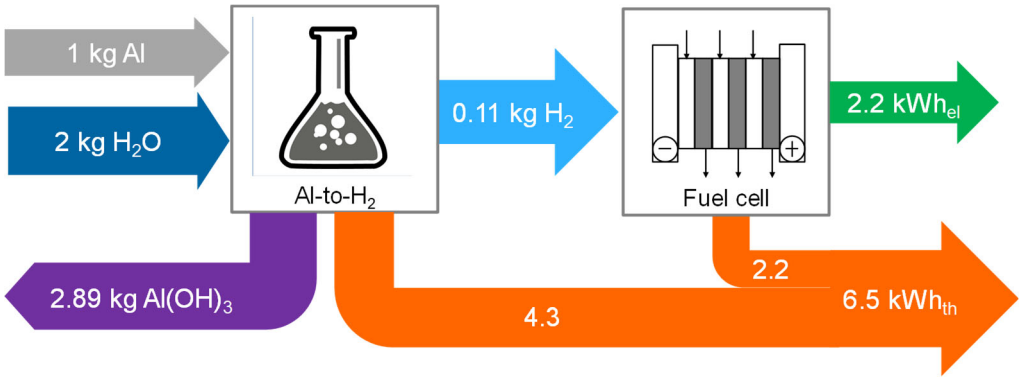

Figure 2: Conversion of aluminium to heat and electricity with aqueous oxidation that releases heat and hydrogen and subsequent production of electricity with a fuel cell, idealized.

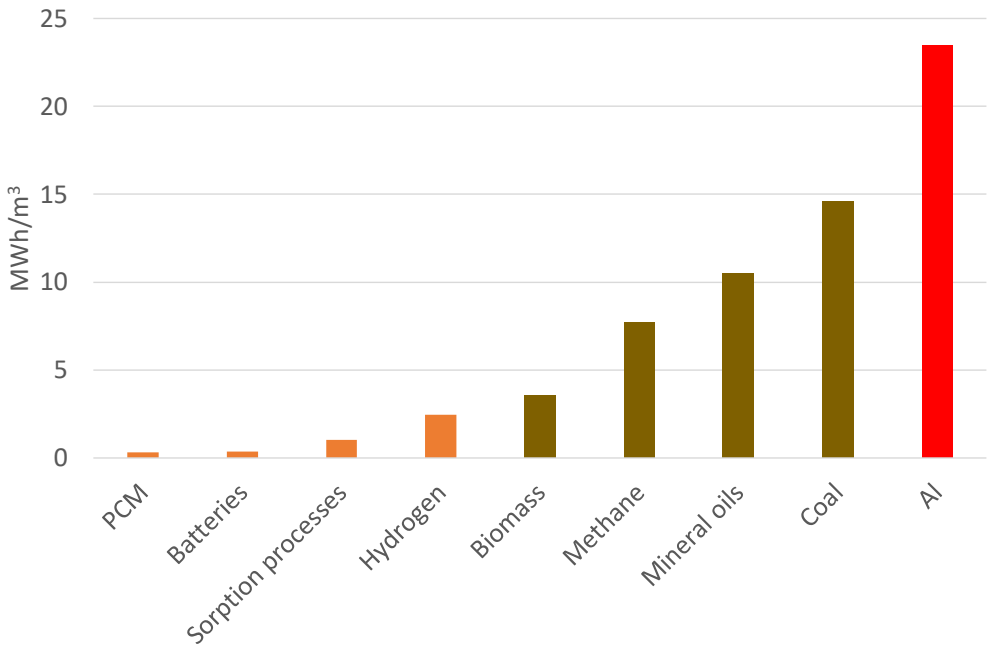

Figure 3: Volumetric storage density of different technologies, PCM = phase change materials, brown bars = needs a carbon source, e.g. CO_2, for synthesizing these materials.

1.3 Objectives

The overarching goal of this project is to demonstrate the feasibility of the hybrid seasonal storage of heat and electricity with an aluminium redox-cycle. The charging is an inert smelter process that is driven by electric energy, which is provided by renewable electricity at times of high availability of wind, solar or other renewable resources. The discharging is based on the oxidation of aluminium that releases hydrogen and heat on demand, and the subsequent use of the hydrogen in a fuel cell.

Within the overall storage cycle, two steps may be considered as being critical:

1. The controlled production of hydrogen from aluminium oxidation with a high energetic efficiency.
2. The conversion of aluminium hydroxide to alumina (calcination) and the reduction of alumina to elementary aluminium without the use of carbon electrodes (inert electrode smelters).

The following goals were to be reached within the project:

1. The controlled production of hydrogen by aqueous oxidation of Al shall be demonstrated at the lab scale. This includes the determination of ideal boundary conditions for the reaction (temperature, solvent, catalysts, and shape of aluminium) as well as the possibilities to control the reaction.
2. The state of development of low-carbon aluminium production from alumina (inert electrode smelters) shall be evaluated on site at the respective developers and the potential and feasibility for the intended application shall be evaluated.

Based on the results of these first two steps, the following goals shall be reached after a go/no-go decision:

3. Optimization of the oxidation process and control of the process as well as direct coupling with a fuel cell at lab-scale.
4. Energy balance, cost estimation, and environmental balance that includes the results of the above mentioned tasks, with the help of energy system simulations.

1.4 Outline of the report

Chapter 2 of this report deals with questions concerning aluminium as a renewable fuel, in particular the shape or size of aluminium material for safe storage, transport and efficient use. In chapter 3, small-scale laboratory experiments for the production of hydrogen and heat are presented. Solubility and precipitation of the solid reaction product $Al(OH)_3$ is analysed in chapter 4. In chapter 5 and 6, a 400 W prototype converter is designed and tested, and the reaction products of this converter are analysed. The Power-to-Al charging process is evaluated on a theoretical base in chapter 7, and system simulations for building heat and electricity supply based on photovoltaics in combination with seasonal energy storage in aluminium are presented in chapter 8. The main findings of this project have also been published in journal articles on the system concept and simulations [13], and on the experiments with the 400 W prototype reactor [14].

2 Aluminium Renewable Fuel

2.1 Procedures and methodology

The ideal "renewable fuel" should have a number of properties, such as:

- high energy density
- non-toxic to humans and the environment
- inert in natural environment, even under humid conditions
- non-flammable, low vapour pressure
- easy transportable and storable

Elementary aluminium seems to be an ideal candidate for a renewable fuel with respect to a number of these requirements:

- it has an extremely high energy density
- it does not bear risks of intoxication, neither to humans nor to the environment, in its elementary form
- the oxygen layer that forms rapidly on its surface when in contact with air makes it inert in natural environments.
- its vapour pressure is negligible for our application

Closer attention has to be paid to the requirements of non-flammability, transportability and storage properties. For this reason, a literature survey and personal communication with experts were used in order to obtain a clear overview of risks of explosion or flammability from small aluminium particles. Based on this analysis, the different options for Al fuel shape were evaluated.

2.2 Results

2.2.1 Flammability and explosion risk

Literature as well as own experiments reported in chapter 3 show that large specific surfaces of the aluminium particles lead to high hydrogen production rates. Consequently, the finer the aluminium "solar fuel", the faster the reaction will be. However, the finer a metal powder, the higher are the risks of dust explosions. A detailed literature study on this subject has been conducted and is reported in Annex C. The main results are summarized in this section.

According to SUVA, dust explosions can be avoided by using particle sizes above 500 µm. Different sources showed that aluminium shapes as powder or chips made by drilling or milling with particle sizes smaller than 63 µm have a high explosion risk and can ignite even at small concentrations. The risk decreases when the particle size is larger than 100 µm and is almost zero when the particle size is greater than 125 µm, as long as the particles do not fall apart as suggested by experiments made with aluminium pellets that are made from finer particles.

Therefore, it is recommended to use particles, which have a median size of 500 µm or larger in order to be on the safe side. Thus, no special regulations regarding explosion safety have to be considered also during transportation. However, it is recommended to test the explosion

potential of the aluminium grains once the final shape of the Al renewable fuel is determined. Furthermore, depending on the friction between the particles when being transported, it cannot entirely excluded that fine abrasion products may form and accumulate in some parts or corners of a transport or storage vessel or in a transport pipe. Therefore, care has to be taken to avoid frictions in the first place, and to detect the formation of fine powders from transport frictions if this shows to be an issue. There are extended studies and guidelines for handling Al fines, e.g. from the Aluminium Association[2].

2.2.2 Evaluation of different shapes of fuel

Based on the available information, a preliminary evaluation of different shapes for the Al renewable fuel has been carried out according to the following criteria:

- reaction time: higher scores for faster reaction with water and sodium lye
- Safety: higher scores for lower risk of explosion or abrasion
- Cost: higher scores for presumably lower cost of production
- Feeding: higher scores for easy and available solutions for feeding to the reaction vessel
- Transport: higher scores if transport is thought to be easy, including also transport from a lorry to a storage in the technical room of a building

According to Table 1 the highest score is obtained for small grains with a size > 0.5 mm.

Table 1: Evaluation table for the selection among different shapes of aluminium renewable fuel

Shape	Reaction time	Safety	Cost	Feeding	Transport	Total
Powder	10	No Go	5	4	4	No Go
Pellets (pressed particles)	6	No Go	5	6	8	No Go
Small grains (> 0.5 mm)	**8**	**5**	**6**	**6**	**8**	**33**
Foil	10	10	2	4	4	30

2.3 Discussion

Although aluminium may be considered largely inert under environmental conditions and of low or even no concern from a toxicological point of view, the size of Al particles that are used as a bulk material for energy storage purposes is relevant from a safety point of view. Fine metal powders typically may react violently with air, and Al is no exception to this rule. Therefore, it is recommended that the particle size is not finder than 500 µm, or that Al is used in another form that is safe to handle such as a thin foil.

[2] Guidelines for Handling Aluminum Fines Generated During Various Aluminum Fabricating Operations.

3 Hydrogen Production from Al-water Reactions

The discharge reaction is based on a controlled production of hydrogen and heat from aluminium (Al). Different types of Al (alloys, shape) were tested and the produced hydrogen was measured. For this purpose, two types of small-scale batch laboratory installations were used (3.1.1), and reaction speed and amount of hydrogen produced were quantified (3.2.1 and 3.2.2). Based on these results, a small-scale batch reaction system was designed (3.1.2) for a continues feed of hydrogen to a small fuel cell, and the purity of the produced hydrogen gas was analysed (3.2.3).

3.1 Procedures and Methodology

3.1.1 Measurement of H_2 production by gas displacement and by pressure increase

Different samples of Al were used in order to evaluate the influence of Al shape on the reaction rate. To avoid the influence of impurities when optimizing the technological parameters, high purity materials were used from Sigma Aldrich and Merck. Additionally, a commercially available Al foil and recycled aluminium grit were included in the analysis (Table 2).

Table 2: Samples of aluminium tested in the lab.

Type / Shape	Size	Purity	Source	Identifier / lot
Al-foil	0.013 mm	n.d.	Toppits	9993260960133
Al-foil pure	0.25 mm	99.999%	Sigma-Aldrich	326852
Granular	n.d.	>99%	Merck-Schuchardt	231-072-3
Al pellets	3 – 12 mm	99.99%	Sigma-Aldrich	MKBX5212V
Wire	1.0 mm	>99%	ThermoFisher (Kandel)	F24I24
Al recycled	variable	98 – 98.75%	HSR	EN-AW6060 / AlMgSi0.5

As composition of the commercial foil was not known, Scanning Electron Microscopy coupled with Energy Dispersive X-ray Spectroscopy (SEM/EDX) was performed. Results indicate that the aluminium foil contains small amounts of iron and manganese. These impurities were found also in the other aluminium samples (see Annex D - SEM/EDX of different aluminium samples).

After a literature review, sodium hydroxide was chosen as a reaction promoter. Solutions with different concentrations were prepared with different types of water:

- ordinary tap water at HSR, Oberseestr. 10, Rapperswil, Sep – Nov 2018, 34 °fH – 38 °fH (546.2 µS/cm at 21.6°C)
- soft de-ionized tap water, 8 ° fH (537.8 µS/cm at 21.1°C)
- deionized water (5.77 µS/cm at 21.2°C)

Sodium hydroxide solutions were prepared using $Na(OH)_{(l)}$ 50% in H_2O (1.515 g/mL at 25°C) from Sigma-Aldrich Chemie GmbH, PCode: 101707073, Lot: STBG0124V.

Two types of lab-setup have been tested and used:

- Measurement of hydrogen by ***volume displacement*** and volume flow rates. Initial experiments were performed with a lab setup that collects the produced hydrogen by volume displacement, using an upside-down water-filled cylinder that is immersed in a water bucket (Figure 4, left). The handling of this setup was time-consuming, and care had to be taken to avoid leakages in the many tube connections that were present. The reaction can be considered isobaric in this case, since the pressure does not change notably during the experiment. In some cases the flow rate was also measured using an H_2 flow meter (red-y smart series by Vögtlin Instruments) calibrated specifically for hydrogen measurements. The material used for this lab setup is listed in Annex B.2.

1. Measurement of hydrogen by ***pressure increase***: An alternative for the measurement of total gas production by volume displacement has been found with the ANKOM^{RF} Gas Production System. In this case, a bottle contains the aqueous solution in which the Al sample is introduced. Al was inserted in a capsule that dissolves with time in the aqueous solution. After placement of the capsule, the bottle is closed and remains closed (Figure 4, right). The amount of hydrogen is obtained from the pressure increase in combination with the initial gas volume of the bottle. The reaction in this case cannot be considered isobaric. The material used for this lab setup is listed in Annex B.3.

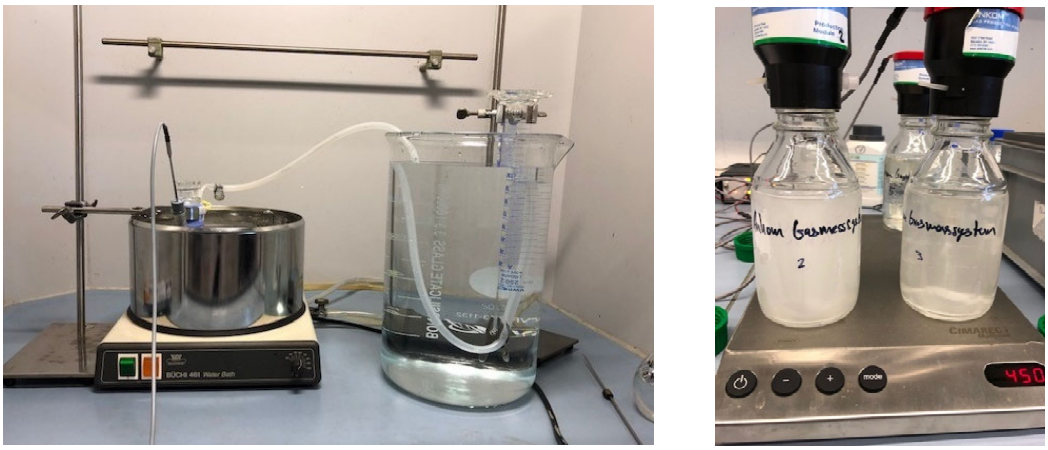

Figure 4: Lab setup for the measurement of produced hydrogen by displacement (left) and by pressure increase with the ANKOM system (right).

The formation of a black precipitate was noted after the reaction stops. Further investigations were performed to check the chemical composition of this precipitate by ICP-OES (see Annex E).

The procedure for the gas production samples was as follows:

- NaOH solutions (1 – 8 M) were prepared at room temperature,
- 75 mL NaOH solution were used for the volume displacement experiments, 450 mL for the ANKOM pressure increase experiments,
- Erlenmeyer-flasks or ANKOM bottles containing the NaOH solutions were placed in a water bath and conditioned to the temperature at which the reaction shall take place,
- for the Erlenmeyer assays (volume displacement), the temperature in the solution was measured with a temperature probe (Annex B.2),

- Al samples were weighed using a Mettler Toledo AT 261 Delta Range (weighing capacity 62 g, accuracy ±0.1 mg) balance, roughly 0.1 g was used for the volume displacement experiments, 0.05 g for the ANKOM pressure increase measurements,
- the Al foil was introduced directly (Erlenmeyer) or within a dissolvable capsule (ANKOM) into the assay and the system closed (Erlenmeyer with a tap, ANKOM bottles with a screw cap),
- reaction was monitored until gas volume or pressure seized to increase.

3.1.2 Small scale prototype for batch reactions

A lab-scale prototype of an aluminium batch converter that is able to deliver hydrogen for roughly 15 minutes to 1 h to a 12 W fuel cell was built (Figure 5) in order to demonstrate the experimental proof of the concept for the production of heat and electricity based on Al. This prototype is composed of the following components:

- Stainless steel converter vessel of 250 mL;
- Heat ribbon to preheat the converter vessel
- Manual double valve system for feeding the aluminium to the converter vessel;
- Pressure relief valve and safety trough in order to collect possible NaOH leakage;
- Drying column filled with molecular sieve (3 Å) from (Sigma-Aldrich Chemie GmbH, PCode: 208574-1kg, Lot: MKCG2396) in order to dry the produced hydrogen;
- Filter of 5 µm in order to prevent a carry-over of molecular sieve dust into the flow meter;
- Pressure regulator fixed at 0.5 bar (recommended pressure for the operating fuel cell is between 0.45 - 0.55 bar);
- H_2-Flow meter (red-y smart series by Vögtlin Instruments) calibrated specifically for hydrogen measurements;
- Fuel cell (Horizon 12 W PEM fuel cell H-12);
- Electrical load (LED lamp).

All the components, connections and valves are made of stainless steel because of the high corrosive environment of the NaOH solution and also in order to prevent hydrogen leakage.

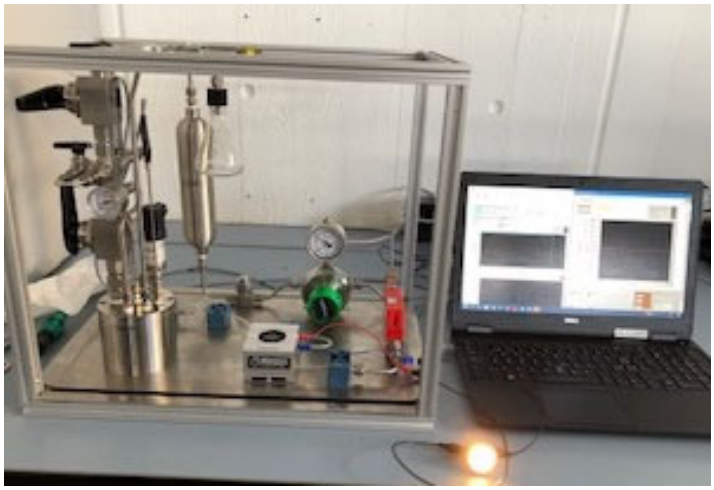

Figure 5: Prototype batch Al-to-Energy converter with an LED light powered by the fuel cell.

The converter was pre-heated to 60°C with a heat ribbon. A piece of commercial aluminium foil was rolled up and added to the converter through the valve system, where it reacted with the 6 M NaOH lye in the converter and produced hydrogen and heat. Hydrogen flows through the dryer, filter, pressure regulator and flow meter into the fuel cell. The gas outlet of the fuel cell was closed in order to prevent excessive flow through the cell. Measurements included the temperature of the lye and the gas inside of the converter, pressure, gas flow rate of hydrogen and electric power of the fuel cell.

3.2 Results

3.2.1 Gas displacement measurements

The influence of temperature, NaOH concentration and type of water was tested with pieces (0.1 g) of commercially available aluminium foil.

The dependent variables that were analysed were the time of reaction (in seconds, until the volume of H_2 stops to increase), and the efficiency of the reaction. The reaction efficiency was calculated as the ratio between the hydrogen produced and the theoretical amount of hydrogen expected considering the stoichiometric reaction of 0.1 g Al. This theoretical hydrogen amount is 124.6 mL (at normal conditions of 0 °C and 1 atm). The calculation of the efficiency as well as the uncertainty estimation are detailed in Annex A. Results are shown in Figure 6 and Figure 7. Both temperature and alkalinity – or NaOH concentration - have an influence on the reaction kinetics, whereas the influence on reaction efficiency is within the range of the measurement uncertainty. Other parameters such as the type of water had no significant influence for the samples tested.

Results of more than 100% efficiency (Figure 6 and Figure 7) are not of concern as long as the uncertainty range includes the 100% value. However, in some of the measurements this is not the case. This indicates an underestimation of the uncertainty, and possibly a systematic bias by another reaction that is occurring and that is producing yet another gas. In order to

reduce the uncertainty, another method for the measurements has been searched for and found with the ANKOM system for which results are presented in section 3.2.2.

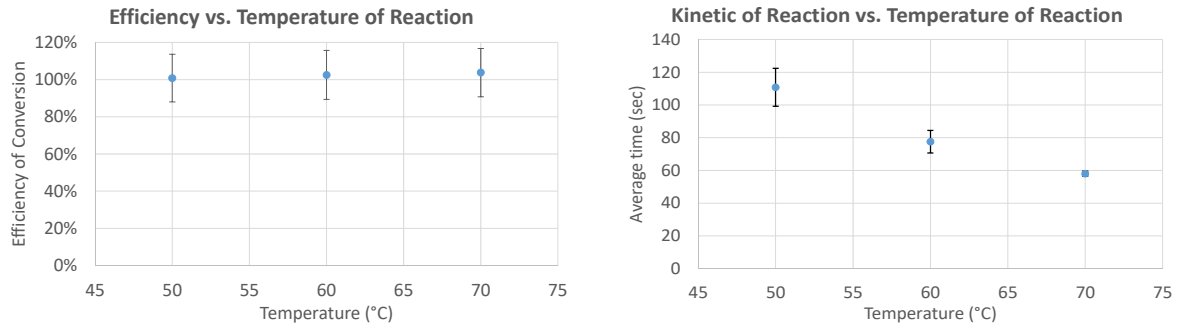

Figure 6: Effect of temperature on efficiency of the reaction and on time for the reaction to complete, with 0.1 g Al and 2 M NaOH.

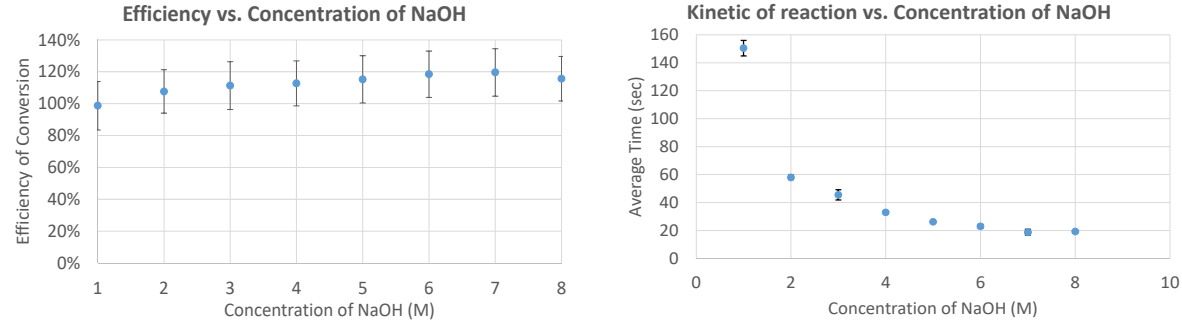

Figure 7: Effect of lye concentration (NaOH) on efficiency of the reaction and on time for the reaction to complete, with 0.1 g Al at 70 °C.

For controlling the reaction, it might be advantageous to be able to stop the reaction completely by cooling the reaction volume to room temperature or by reducing the concentration of the reaction promoter. Therefore, it was tested under which conditions the reaction can be slowed down so far that no measurable amounts of hydrogen are produced (Figure 8). It can be seen that with 1 M NaOH, the reaction does not start or is not producing significant amounts of hydrogen at room temperature.

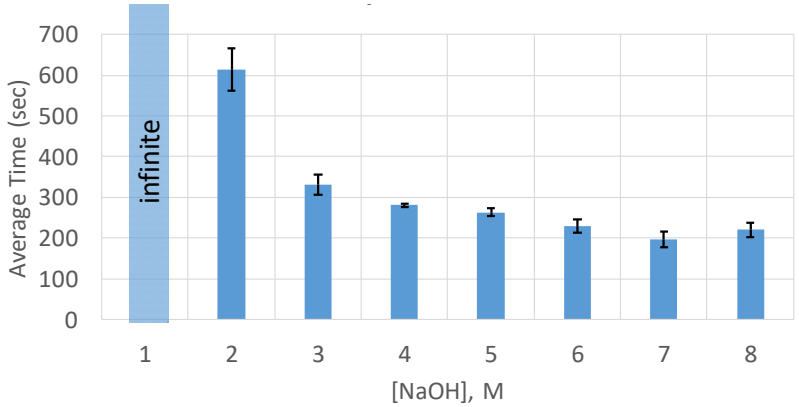

Figure 8: Effect of lye concentration (NaOH) on the reaction kinetics when starting at room temperature (25±2 °C).

3.2.2 Measurements with pressure increase

Different shapes of aluminium (0.05 g samples) were studied using the ANKOM method with a concentration of NaOH 6 M at room temperature. The purpose of these experiments was to determine the influence of the aluminium fuel shape on the hydrogen production rates.

The results from Table 3 and Figure 9 indicate that the Al shape has not a significant influence on the reaction efficiency, which is close to 100%. A slightly higher efficiency was measured for Al-foil in comparison to the other Al shapes. As could be expected from the different surface to mass ratios, the reaction rates show a high dependency on the Al shape. There was a great variation in the specific hydrogen production rate from 0.1 up to 2.3 mL/min. The minimum rate was obtained with the Al pellet. The maximum hydrogen production rate was reached with the commercial Al foil.

The smaller the particle size of the aluminium, the higher is the surface area for the reaction, thus the faster is the kinetic of the reaction.

Table 3: Volume of H_2 produced and efficiency of the reaction depending on the Al shape.

Parameter	Al granular	Al foil	Al wire	Al pellet
mV_{H2} (mL)	59.4 ± 0.4	61.2 ± 0.2	59.3 ± 0.3	60.2 ± 0.2
Efficiency (%)	96.1 ± 3.6	98.9 ± 3.7	95.8 ± 3.6	97.3 ± 3.6

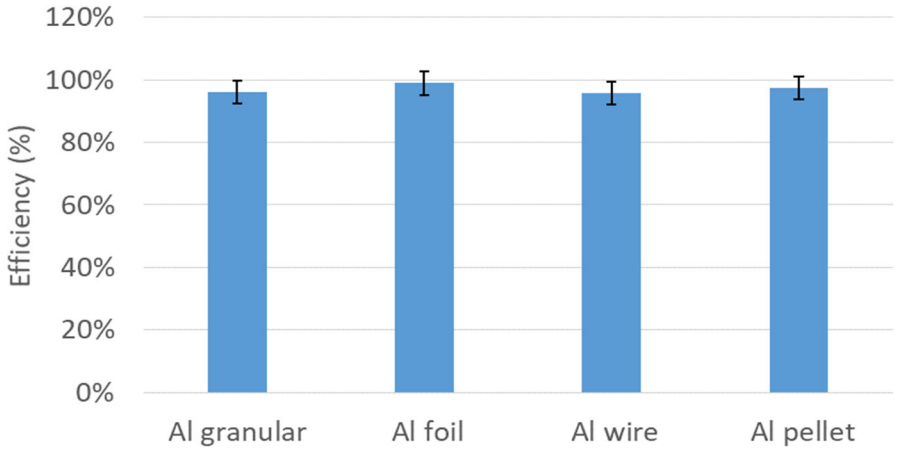

Figure 9: Effect of the aluminium shape on the volume of H_2 produced and the efficiency of the reaction, with 0.05 g Al and 6 M NaOH at room temperature.

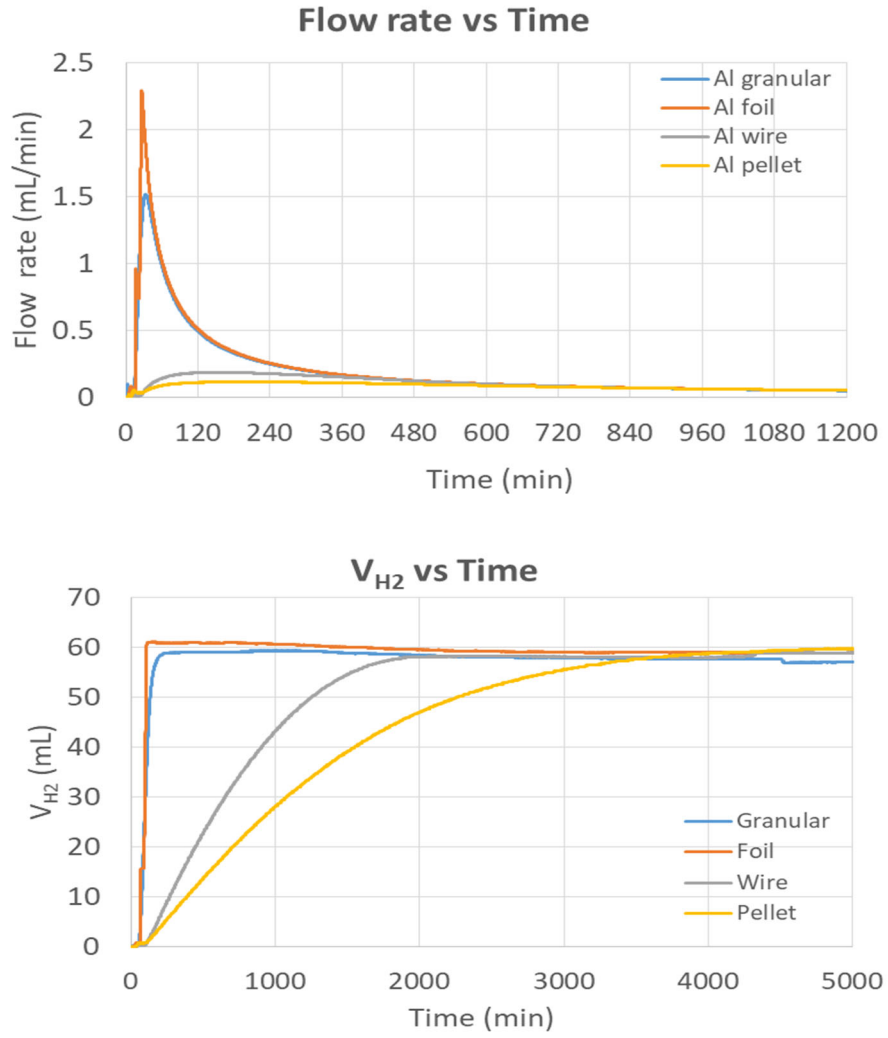

Figure 10: Effect of the aluminium shape on the flow rate (top) and volume (bottom) of H_2 produced, with 0.05 g Al and 6 M NaOH at room temperature.

3.2.3 Small prototype batch reactor

Experiments were performed with the batch reaction system that was described in section 3.1.2, using 6 M NaOH solution and Al foil. Temperature and pressure in the reactor rose after the Al was added at 13:20, for about 2 minutes (Figure 11). Shortly after, when the pressure was high enough for the pressure regulator to open, a gas flow rate was detected.

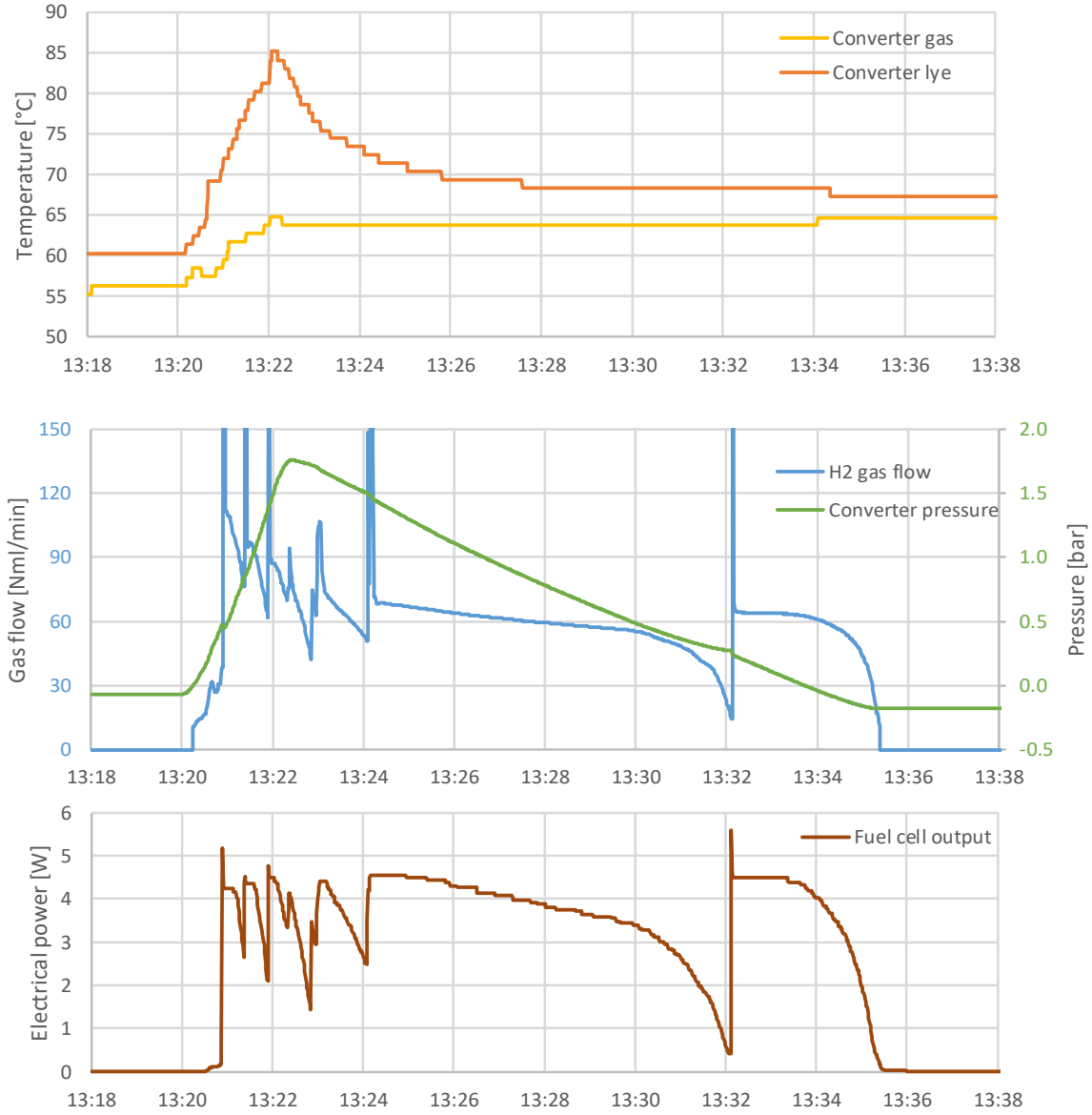

Figure 11: Measured parameters during a test of the small-scale lab demonstrator.

The power output of the fuel cell is dependent on the gas flow rate, but has its upper limits, as visible in the graphs between 13:21 and 13:24. The short peaks of the gas flow occurred

because the valve after the fuel cell was quickly opened in order to keep the gas flow running. If it was closed for too long, the gas flow would eventually stop, as it almost happened at 13:32. These peaks of high gas flow rates result in small pressure drops. The over-pressure in the converter serves as a buffer, so the gas flow and power output can be maintained long after the Al foil has presumably been consumed at around 13:22. The flow only ceases when the over-pressure is depleted at around 13:35. Thus, the duration of the whole experiment was about 15 minutes.

In order to measure the purity of the produced hydrogen, another experiment was carried out using the same principle and the gas from the reaction was fed into a mass spectrometer (GAM 200 by IPI) instead of a fuel cell. The analysis included H_2, O_2, N_2, CO_2, H_2O, CH_4, Ar, NH_2 and H_2S. Figure 12 shows the results of the mass spectrometry. During normal operation (17:02 – 17:10), a hydrogen purity of ≥ 99.999% vol was measured. Just when the aluminium was added to the converter, the purity of H_2 decreased temporarily below the purity limit for the H-12 fuel cell of 99.995%, due to air entering the system through the aluminium inlet, i.e. oxygen and nitrogen could temporarily be measured in the gas. Before the H_2-curve drops around 16:45, there was some argon left in the system from the flushing of the mass spectrometer with argon gas, thus the purity was not at its highest value yet.

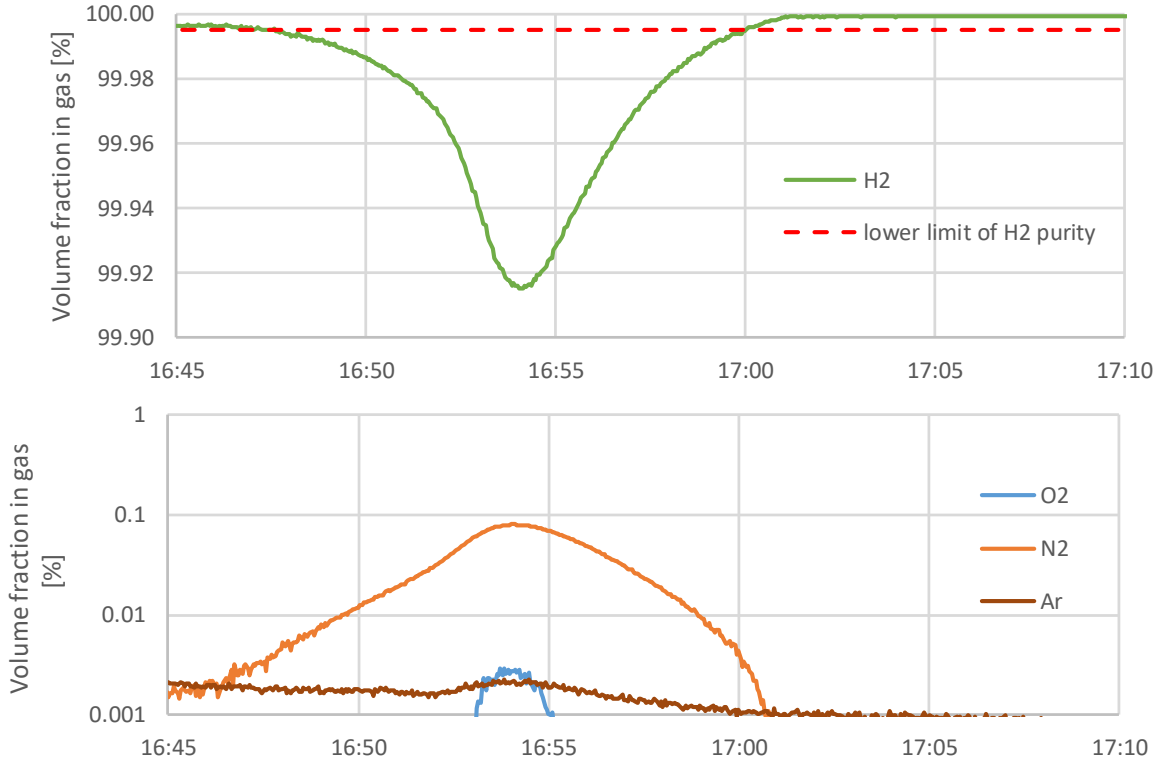

Figure 12: Hydrogen purity and traces of other gases measured by mass spectrometry.

3.3 Discussion

It has been shown that for 1 – 6 M NaOH solutions and temperatures at around 60 °C, different shapes of Al samples may react completely (100% within the uncertainty of the measurements) and produce the amount of hydrogen that can be expected from the stoichiometry of the reaction. Temperature and alkalinity have a strong influence on the kinetics, i.e. the reaction speed, and also the shape of the particles, in particular the ratio of surface to bulk material, has a strong influence on the time needed for the reaction to complete.

The design of a small lab scale prototype batch reactor for the continues feeding of hydrogen from Al-water reactions to a 12 W fuel cell has been successful, and electricity from the fuel cell was used to power DC electric loads such as an LED lamp or a rotator.

The purity of the produced hydrogen was very high with 99.999% vol. in steady operation. A carry-over of air into the system while feeding Al samples leads to a temporary reduction of gas purity to about 99.92%, trace gases being nitrogen and oxygen from the air.

4 Solubility and Precipitation of $Al(OH)_3$

4.1 Procedures and methodology

A literature study was carried out in order to understand under which conditions precipitation of aluminium hydroxide occurs, and its results are presented in section 4.2.

In order to determine the solubility and precipitation of $Al(OH)_3$ for the specific conditions that are expected for a hydrogen production unit that is in the focus of this project, laboratory experiments were carried out that are specified in more detail in section 4.1.1 and 4.1.2.

4.1.1 Chemicals used

The following material and chemicals were used in the experiments:

- Al grit (minimum 99% Al): CAS 7429-90-5, molar mass 26.98 g/mol, lot S7594917838, Merck code 8.14917.0100, impurities: iron;
- reaction promoter: sodium hydroxide, NaOH 50 wt.% (±2%) in H_2O, density: 1.515 g/mL at 25 °C, molar mass: 40.0 g/mol, CAS number: 1310-73-2, Sigma-Aldrich code 415413, Lot #STBH6577;
- precipitation seeds: aluminium hydroxide powder, $Al(OH)_3$ x H_2O (hydrargillite), density: 2.42 g/mL at 20 °C, molar mass: 78.00 g/mol, CAS 21645-51-2, Merck code: 1.01091.1000.

4.1.2 Experimental installation and procedures

Three main approaches were followed to investigate the solubility and precipitation of aluminium hydroxide in highly alkaline solutions with high concentrations of Al^{3+} species. These are represented schematic in Figure 13. Details and specifications of the equipment and sensors used are given in Table 4.

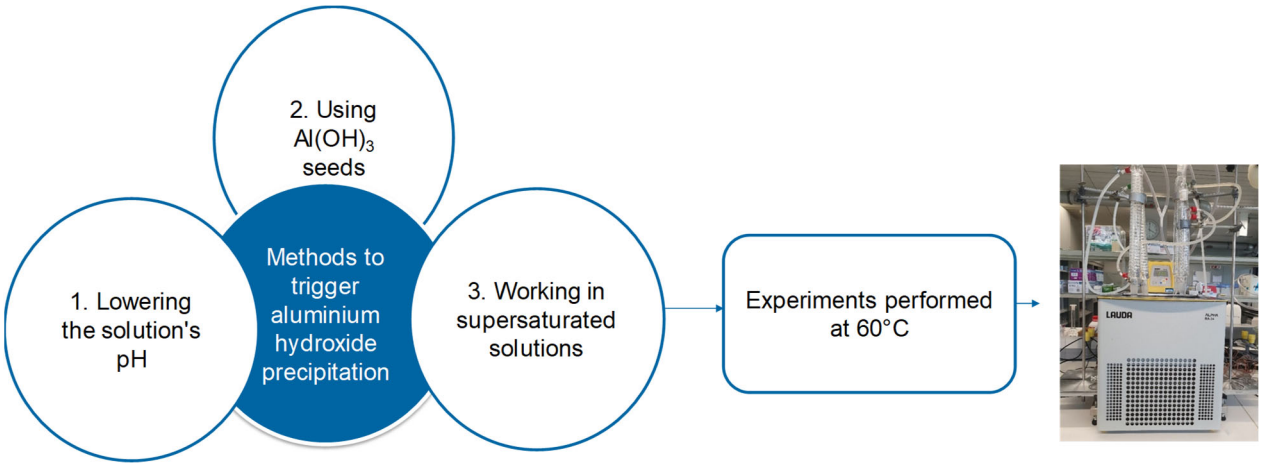

Figure 13: Schematic representation of the experiments performed for the solubility and precipitation of aluminium hydroxide using boundary conditions that are specific for HybridStock: pH close to 14, supersaturated solutions with Al^{3+}.

Four round bottom flask assays were used in parallel. A thermostatic bath was used to control the temperature to 60 °C. This temperature was chosen because the heat extraction in the HybridStock converter is planned to be in the range of 60 °C for DHW preparation and space heating. It is important to note that in the case of 6 M NaOH the reaction, and therefore also the release of heat, occurs very fast. Thus, the temperature in the reactor increased temporarily to values that were 10 – 15 K higher than 60 °C for short time periods. The temperature of the solution inside the round bottom flask assays was measured using fast responding thermocouples (Figure 17). A data logger (Figure 15) was used for recording the temperature during the Al-water reaction in all four flask assays.

A condensation unit was connected to each assay to condense the water vapours and thus limit the water loss during reaction.

A special stirring system (Figure 14) was necessary as, for higher amounts of added aluminium, a voluminous and precipitate was forming. This stirring system can be submerged in water at high temperatures (up to 200 °C) and it includes adjustable magnet field power and strong, temperature insensible, magnetic stirring bars. The system is strong enough to stir also when high amounts of precipitate are formed. Without stirring, it was observed that the reaction rate slowed down considerably during the experiment and eventually would even drop below a measurable value.

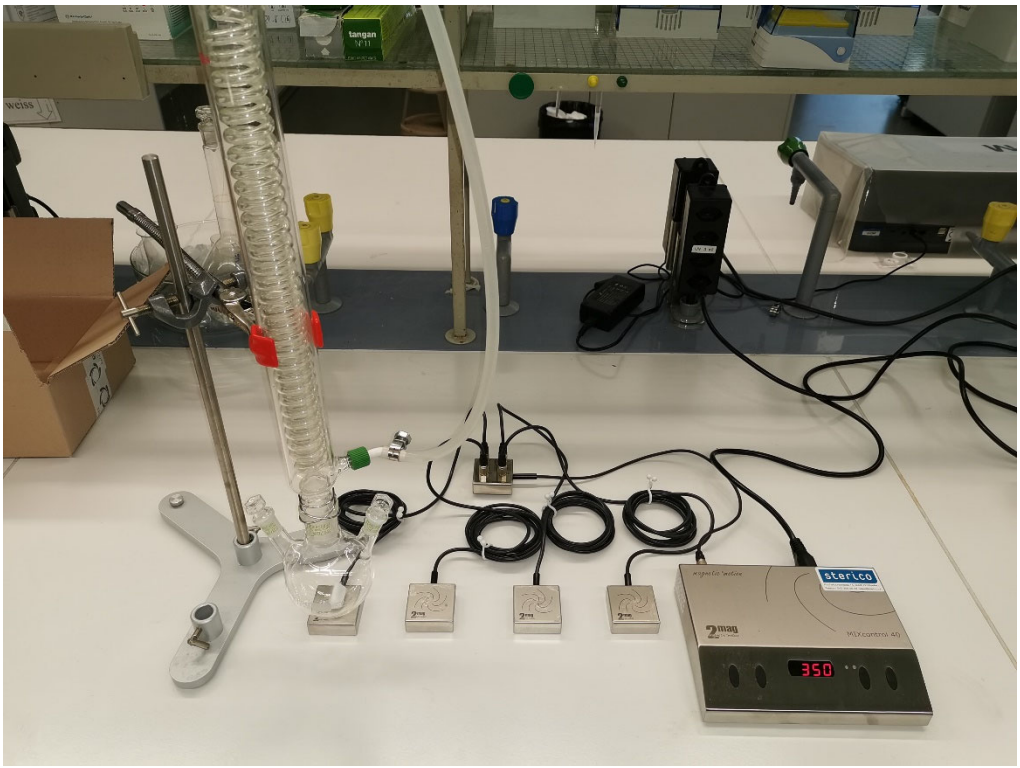

Figure 14: Stirring system for submersion in the thermostatic bath for performing four chemical experiments in parallel; a round bottom flask together with the condensation unit is shown in the left side, while on the right the controlling unit for the stirring system is visible.

A gas flow meter (Figure 16) was used to monitor the combined hydrogen flow of all four assays and assess when the aluminium oxidation reaction was complete, i.e. when no more hydrogen was produced.

Table 4: Details and technical specifications of the sensors and components used for the chemical experiments.

Item	***Technical specifications***
Thermostatic bath	Lauda Alpha RA24, temperature stability ±0.05 K, heater power 1.5 kW, cooling power 0.3 – 0.425 kW, bath volume: min 14 L
Stirring system	The system from 2 mag composes of four MIXdrive 1 XS HT stirrers with MIXcontrol 20 control unit and DistriBOX 4, four stirring bars; the stirrers can be used for high temperature (HT-version) up to +95 °C when submerged in water baths and up to +200 °C when they are used in ovens.
Gas flowmeter	Vögtlin red-y smart series, type: GSM-A9ST-BN00, measuring range: 12-600 mln/min, accuracy: ±1% full scale, reference pressure: 1013 mbar, reference temperature: 0 °C
Temperature sensors	RS PRO type T, accuracy ± 0.5 °C, temperature range: -75°C to +250°C, 316 stainless steel sheath, 1.6 mm diameter x 100 mm long, tolerance in accordance with IEC 584-2 specifications
Data logger	GRAPHTEC GL 220
Centrifuge	Hermle Labortechnik Universal Centrifuge Z 306
Condenser	Witeg coil type 300 mm, borosilicate glass 3.3, Graham pattern

The main experimental parameters are presented in Table 6. As solubility is influenced by temperature, samples were removed from the thermostatic bath after the temperature settled to 60°C. For the 6 M NaOH case, the time to settle back to 60 °C was longer than for 0.25 M NaOH, since the temperature increase was higher during the fast reaction at this NaOH concentration.

In order to separate the precipitate from Al species in solution and to quantify Al species in solution, the following procedure was applied:

- a sample of 70 mL was taken from the round bottom flask assay;
- liquid and solid phases were separated using the centrifuge at 4000 rpm for 10 minutes;
- the liquid samples were additionally filtered using a 0.45 µm syringe filter;
- samples of 1 mL from the filtered solution were preserved before ICP-OES (Inductively Coupled Plasma Optical Emission Spectrometry) measurements by adding 1 mL of HNO_3;
- a microwave digestion was performed using 1 mL of sample, 4 mL HNO_3 65%, 2 mL HCl 35% and deionized water (to obtain a sample of 50 mL), at 210 °C for 15 min;
- for ICP-OES measurements, the digested samples were diluted from 1:100 to 1:1000, depending on the amount of Al that was expected in solution.

Figure 15: Logger used to monitor and record the reaction temperature during the experiments.

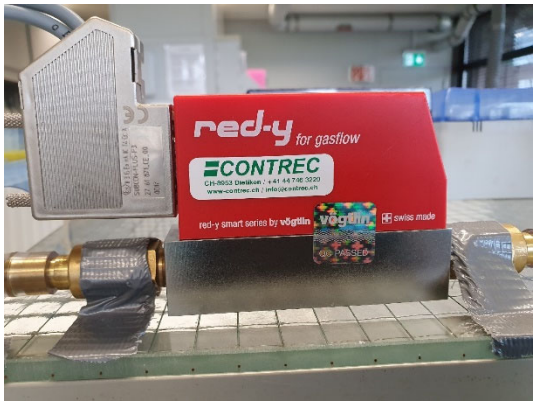

Figure 16: Gas flow meter used for indicating when the reaction has stopped, i.e. when no more hydrogen is produced.

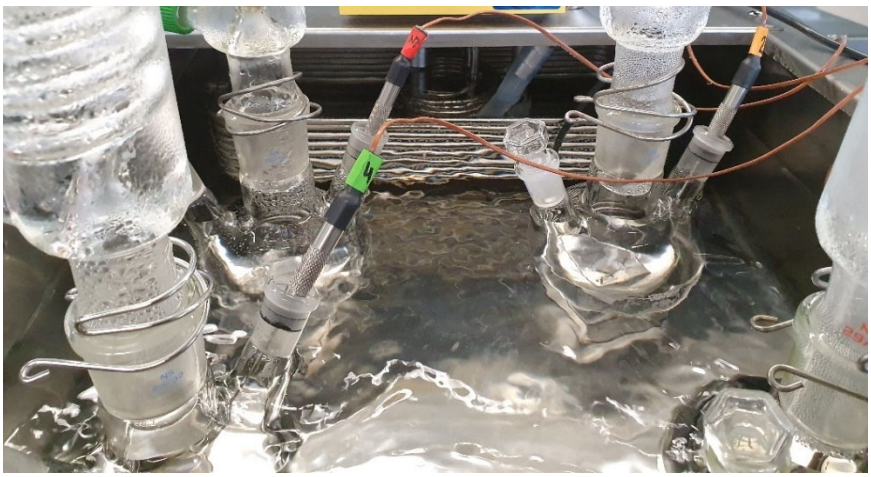

Figure 17: Positioning of the temperature sensor and details with condensation unit attached to the reactor.

Table 5: Experimental conditions for the chemical experiments performed at 60°C in 150 mL assays for three different concentrations of NaOH and four different amounts of Al added.

	Total amount (g) of Al added in each assay (A)			
NaOH concentration	A1	A2	A3	A4
0.25 M NaOH	0.1	0.25	0.5	1.0
1 M NaOH	1.5	3.0	4.5	6.0
6 M NaOH	5.0	15	25	35

4.2 Results

4.2.1 Literature study

A general method for the calculation of the solubility of metal hydroxides in water is presented by Scholz and Kahlert [15]. Data on the solubility of aluminium hydroxide in acidic and basic media has been reported by various authors [16–18]. Further literature includes theoretical studies [19] and a mass spectrometric study of the hydrolysis of aluminium salts [20]. The precipitation of $Al(OH)_3$ is also a step of the industrial Bayer process, which may be more representative for the conditions of the HybridStock project. In the Bayer process, bauxite ore is heated to a temperature of 150 to 200 °C in a pressure vessel and concentrated sodium hydroxide solution (with pH close to 14) is added. In these conditions, aluminium compounds dissolve primarily as aluminate ions $[Al(OH)_4]^-$. After precipitation of non-aluminium species and formation of "red mud" that contains e.g. iron compounds, the remaining liquid is cooled and diluted. Fine-grained, crystalline aluminium hydroxide particles are added in order to facilitate the precipitation of $Al(OH)_3$. This process may take several hours to several days. Thus, precipitation of $Al(OH)_3$ under these conditions seems to be feasible, but is possibly a very slow process.

The investigated literature indicates that above pH 8, the major Al specie in aqueous solution is the aluminate ion $[Al(OH)_4]^-$ (Figure 18). According to [20], $Al(OH)_3$ forms and precipitates easily at a neutral pH range (solubility constant $pK_{s,\ 25°C}$= 31.5).

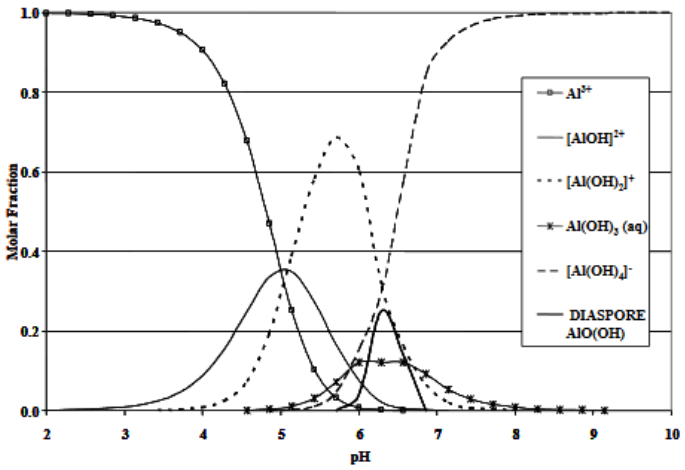

Figure 18: An example of the aluminium-ions distribution in aqueous solutions depending on the pH (in 10^{-9} M $AlCl_3$ solution) [20].

The main conclusion of this literature study is that $Al(OH)_3$ may precipitate from aqueous solutions up to a certain pH, but it may be a very slow process. Precipitation can be promoted by a decrease of pH, lowering the temperature and addition of crystalline aluminium hydroxide seeds. The crystallization seeds size has an influence on the duration of the precipitation process. Most of the studies or models found in literature focus on chemical conditions that differ from those that are relevant for the HybridStock project, e.g. much more diluted solutions, lower pH values or presence of other ions (e.g. ClO_4^-, Cl^-).

In the HybridStock project, solutions with a high concentration of Al^{3+} and pH close to 14 are obtained from the Al-water reaction (see for example section 5.4). Thus, several chemical experiments were carried out in order to assess the possibilities for precipitation of $Al(OH)_3$ in these specific conditions.

4.2.2 Lowering the solution's pH

The first method identified for triggering aluminium hydroxide precipitation is decreasing the pH of the aqueous solution to a neutral range. In order to investigate this possibility for the specific conditions of HybridStock, a sample containing soluble Al^{3+} was prepared using the solution obtained after the aluminium oxidation reaction at room temperature (5 g of Al-foil were added in 150 mL NaOH 1M). The sample was collected after no more hydrogen formation was observed. The solid part (shown in Figure 19) was separated via centrifugation and then a sample from the liquid phase was titrated with HCl until precipitation was occurring (Figure 20). A white precipitate started to form already at pH around 12.

Figure 19: Solid by-products obtained from the aluminium reaction with 1 M NaOH without further treatment.

Figure 20: Precipitation of Al^{3+}occurs when the pH of a saturated solution decreases from 14+ to 12.

4.2.3 Triggering by $Al(OH)_3$ seeds

Another method for triggering precipitation of aluminium hydroxide is the use of fine-grained aluminium hydroxide crystal seeds. The influence of two types of $Al(OH)_3$ seeds was tested: a commercially available $Al(OH)_3$ x H_2O (S1, hydrargillite) and a sample obtained from the white gelatinous precipitate (S2) from Figure 20 after drying (Figure 21) and grinding into a fine powder with mortar and pestle.

Three samples were prepared: two using a very small amount (in the range of 1-2 mg) of aluminium hydroxide seeds (S1 and S2) and one reference sample in which case no seeds were added. The samples were homogenized using a Biosan programmable rotator (Multi Bio RS-24, Figure 22) that performs several motion types: vertical rotation, reciprocal rotation, as well as vibration. The samples were visually investigated after 1 day.

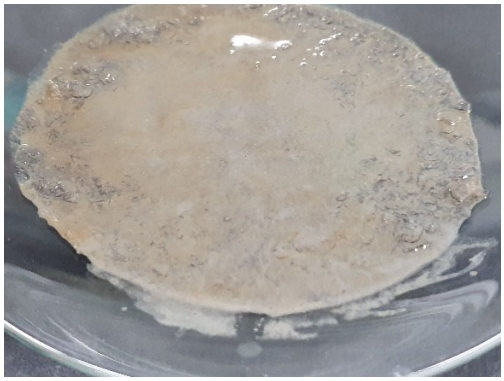

Figure 21: White precipitate after drying and before grinding for obtaining the S2 seeds.

Figure 22: The system used to homogenise the three samples.

From the three samples, precipitation was observed only in the samples in which the seeds were added. More precipitate was observed in case of S1. This may be explained by the smaller particle size (<150 µm) of the commercially available S1 seeds.

Figure 23: The three samples prepared for studying the influence of using $Al(OH)_3$ seeds: S1 - commercially available (particle size <150 µm), S2 - obtained in the chemistry lab (unknown particle size) and a reference sample (no seeds).

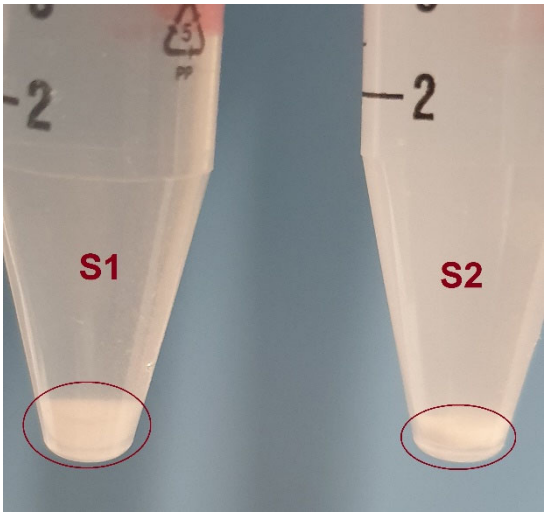

Figure 24: Adding $Al(OH)_3$ seeds triggers precipitation: left: after adding S1, right: after adding S2. The finer the seeds are, the more precipitate is formed

4.2.4 Spontaneous precipitation from supersaturated solutions

It was observed that after adding a certain amount of aluminium to the NaOH solutions while stirring, the initially black precipitate that is composed of non-aluminium compounds described in Annex E is changing to grey colour. This is due to the precipitation of white aluminium hydroxide, which is assumed to occur after a supersaturated solution with Al^{3+} is reached.

Preliminary experiments performed in summer 2019 showed a significant decrease in reaction rate or even (probably temporary) reaction stop after adding about 20 g of Al (foil) in 150 mL of 6 M NaOH solution (equivalent to an Al concentration of 133 g/L). Therefore, experiments

were made in order to determine the maximum amount of Al that would react before a reaction or solubility limit is reached at 0.25 M, 1 M and 6 M NaOH concentration at 60 °C. The experimental parameters are presented in Table 6. Higher amounts of aluminium were added in steps, and a stronger stirring system was used compared to the experiments performed in summer 2019 (Figure 14).

As can be seen from Figure 25 - Figure 26, precipitation started at about 5 g/L, 21 g/L (Figure 26) and above 100 g/L (Figure 25) for samples with NaOH concentrations of 0.25, 1 and 6 M, respectively.

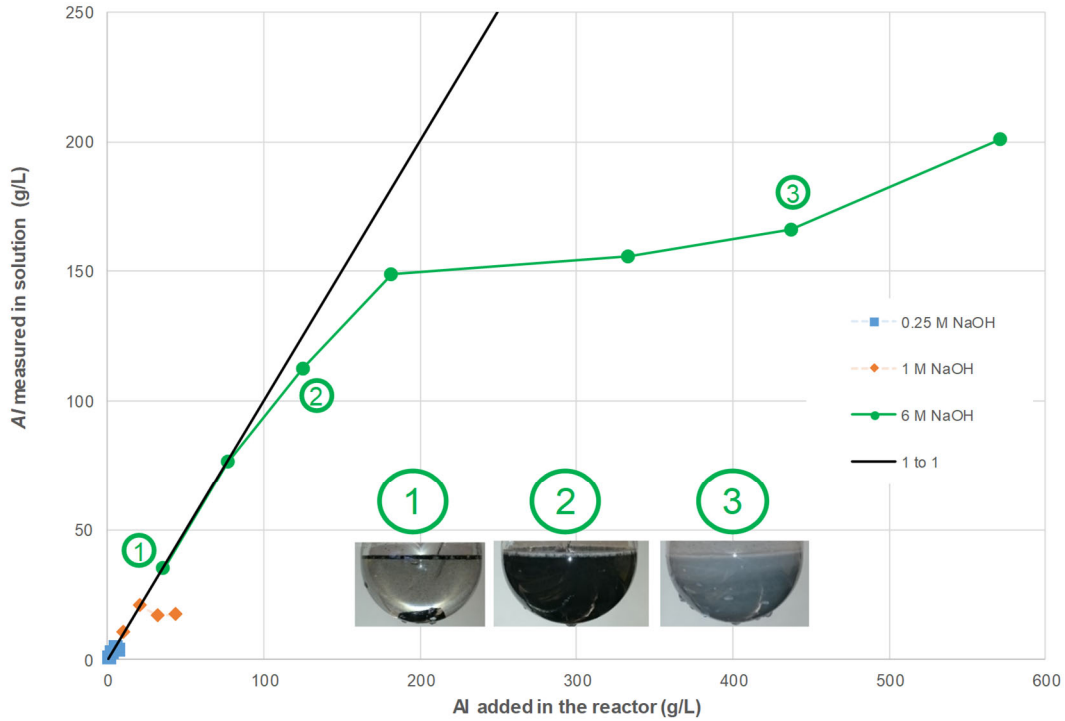

Figure 25: Amount of dissolved aluminium in solution vs. the amount of added aluminium in solution for experiments at 60°C [14].

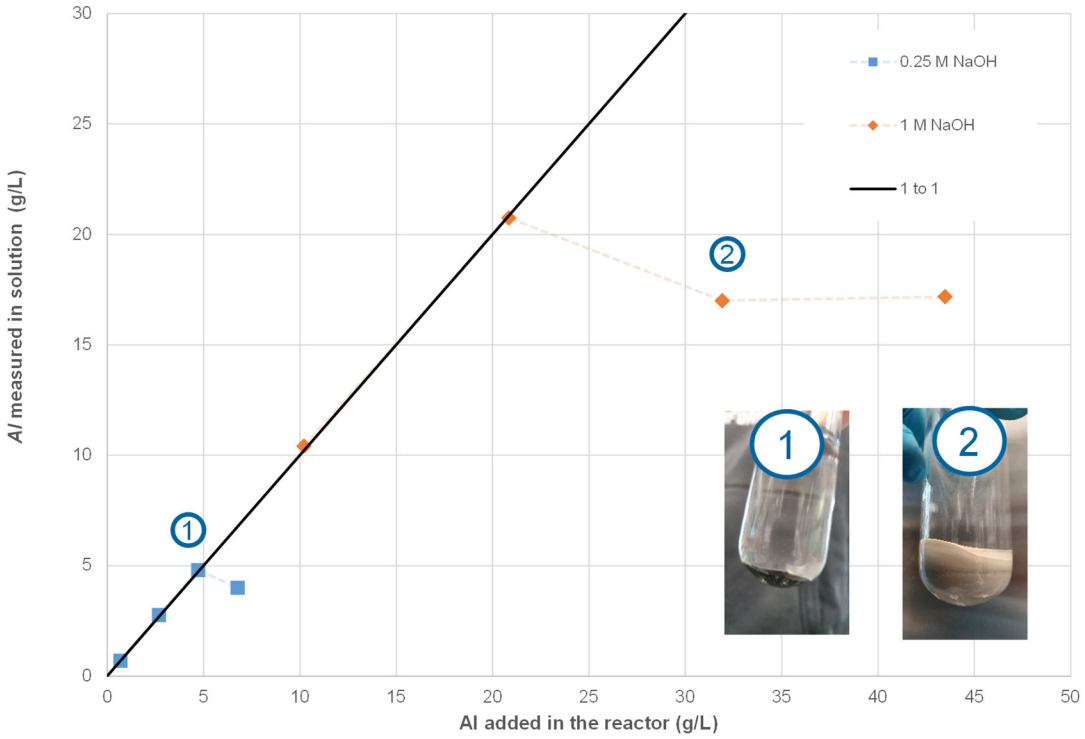

Figure 26: Amount of dissolved aluminium in solution vs. the amount of added aluminium in solution for the 0.25M and 1 M NaOH experiment at 60°C.

For the assay of 6 M NaOH, the formation of aluminium hydroxide precipitate can be visually observed in the insets 1 to 3 of Figure 25. When an amount smaller than 50 g/L is added to the round bottom flask assay, only a limited amount of black precipitate is formed (likely due to iron compounds, see Annex E. For higher values, a white precipitate starts to form (see the upper part from inset 2 of Figure 25). Even after adding more than 400 g/L, which is much more than in the preliminary experiments (133 g/L) from summer 2019, the Al concentration in solution was found to be only 166 g/L, although the Al that was added reacted completely. A similar effect is observed for the 1 M NaOH solution and 2 M NaOH (see insets from Figure 26).

A visual aspect of the four assays at the end of the experiments that were performed at 60°C with 1 M NaOH solution is given Figure 27. It can be observed that, after saturation is reached, the more aluminium is added, the more precipitate is formed.

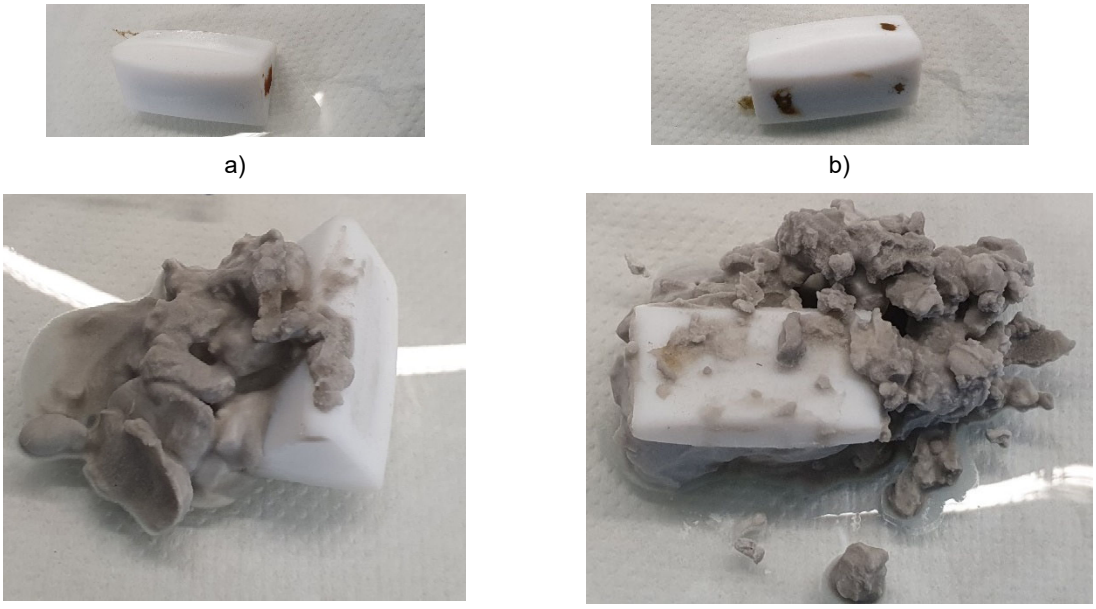

Figure 27: The influence of the amount of aluminium added to the assay of 150 g 1 M NaOH at 60°C, and the amount of precipitate: a) 1.5 g Al added, b) 3 g Al added, c) 4.5 g Al added, d) 6 g Al added.

4.3 Discussion

Based on the experimental investigations, the following concluding remarks can be made:

- The solubility of Al^{3+} ions is high in the alkaline and in the acidic regions, and lowest around pH 5-6. Precipitation is most likely to occur at a more or less neutral pH.
- Even in high alkaline solutions, precipitation happens when the solution is oversaturated with Al^{3+} ions; for a solution of 6 M NaOH, the point when precipitation starts after about 112 g/L of solid Al was added to the alkaline solution;
- A higher amount of Al can be oxidized until aluminium hydroxide starts to precipitate at 6 M NaOH solution compared to lower NaOH concentrations (e.g. 112 g/L for 6 M NaOH compared to 21 g/L for the 1 M NaOH);
- Triggering precipitation by decrease of pH (e.g. by adding water to the assay) showed to be effective;
- Adding crystalline $Al(OH)_3$ helped the precipitation, but only adding seeds without changing the pH of the solution is not as effective as a change in pH;
- Stirring helps to maintain a high reaction rate, even when a voluminous precipitate is formed.

The main conclusion of these chemical experiments is that even at high pH (close to 14), the precipitation of Al ions can occur. Once that a certain amount of precipitate is formed, it can be mechanically removed from the reactor.

5 Prototype 400 W Converter with Fuel Cell

5.1 Objective

Based on the experiments presented in chapters 3 and 4, a larger converter was built with the following goals:

- realizing an automated, gas-tight, Al feeding system;
- quantify the produced hydrogen and heat of the aluminium oxidation;
- compare the produced hydrogen and heat with the theoretical maximum that is to be expected for a complete conversion of the Al in the converter.

Two automatic feed systems were tested, and one of them was chosen for the final converter test-runs. The prototype system was designed to power a fuel cell with an electrical and thermal power of 100 W each (50% electric efficiency[3]), although current market available fuel cells of this power range have somewhat lower efficiency. This demands a hydrogen flow of 5.1 g/h and an aluminium flow 45.3 g/h according to the energy content of hydrogen and the stoichiometry of the aluminium-water reaction. The reaction of 45.3 g/h of aluminium will lead to a heat production of about 200 W (according to Eq. 28). All target values of power and flow are summarized in Table 6 and Table 7.

Table 6: Target power value of the system.

Fuel cell electric power [W_{el}]	Fuel cell thermal power [W_{th}]	Reaction heat in converter [W_{th}]	System total power [W]
100	100	200	400

Table 7: Flow rate of educts and products.

H_2 mass flow rate [g/h]	Al mass flow rate [g/h]	H_2O consumption [g/h]	$Al(OH)_3$ production [g/h]
5.1	45.3	90.7	130.9

5.2 Procedures and methodology

Aluminium oxidation is carried out in an 8.3 litre stainless steel (1.4404) pressure vessel, the "converter" (see Figure 28). Experiments were performed with 5 litres of NaOH aqueous solution with a concentration of 6 M, 1 M and 2 M, respectively. Recycled aluminium grit (0.8 – 1.2 mm) with a purity of 97-98% was used (specification in Annex F.4). The hydrogen that was produced during the experiment was measured with a gas flow sensor. Used sensors, their uncertainties, and propagation of measurement uncertainties are given in Annex F.

[3] all efficiencies and enthalpies in this report are based on gross heating values.

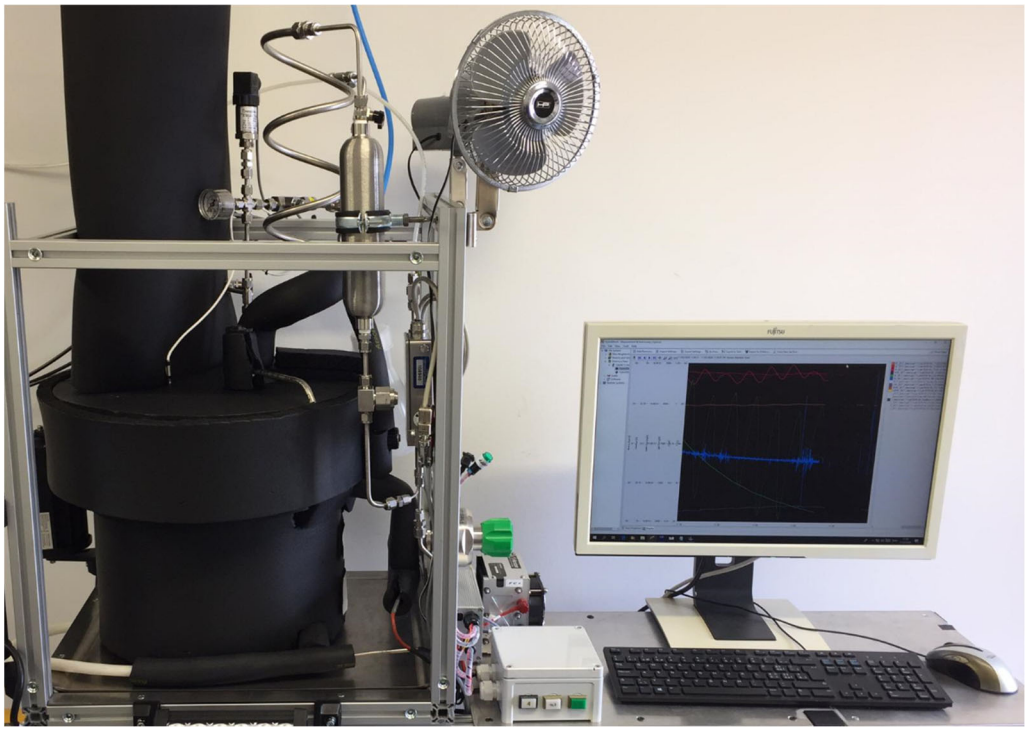

Figure 28: 400 W Al-to-Energy converter with automatic Al feeding system.

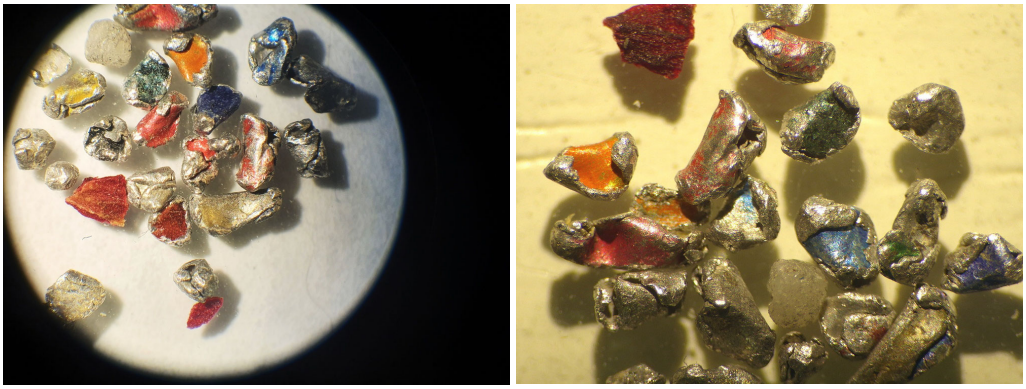

Figure 29: Sample of recycled aluminium grit used for the experiments [14].

During the operation of the system, heat is removed from the converter by heat exchanger tubes that are attached to the outside walls of the converter. The extracted heat is quantified considering the temperature difference of the inlet and outlet of the heat exchanger, and the mass flow rate of the cooling water. The converter and heat exchanger are thermally insulated and the water vapours from the gas outlet are cooled and condensed in order to reduce heat losses.

Before each experiment, the tightness of the system was evaluated by filling the converter with nitrogen up to 3 bar gauge and then, if no leakage was detected with a leakage detection spray, with hydrogen up to 3 bar gauge, heated to 60 °C, and left overnight. With this procedure, a hydrogen leakage of 0.047 g over the course of 6 h was calculated based on

pressure drop, which corresponds to 0.15% of the targeted hydrogen production rate of 5.1 g/h. The measured heat loss was 28 ±2.2 W.

Experiments for the measurement of heat and hydrogen production of the converter were based on the following procedure, exemplary for the 6 M NaOH solution as reaction promoter:

- fill the converter with 5 litres of NaOH solution, close the converter;
- flush the converter and system piping with nitrogen;
- preheat the converter using a thermostatic bath and maintain a constant temperature of 60°C at the outlet of the heat exchanger ;
- feed aluminium through the valve feeding system with a target mass flow rate of 45.3 g/h, control of the feeding rate via a LabVIEW program;
- monitor the heat flow, hydrogen flow and temperature;
- run the experiment for several hours;
- stop Al-feeding and (time-delayed) the cooling system at the end of the experiment;
- monitor the hydrogen flow until it fades out and it can be assumed that all Al that will oxidize under these conditions has reacted.

For the experiment with the 1 M and 2 M NaOH solution, the same procedure was followed except for the following points:

- converter was also flushed with hydrogen from the bottle after it was flushed with nitrogen;
- dosing rate was kept constant during the experiment;
- cooling system was kept in operation after stopping the Al-feeder in order to measure the heat production until all aluminium has reacted.

Additionally, for the 2 M experiment, the produced hydrogen was fed into a 100 W_{el} fuel cell, which produced electricity to power three LED spotlights with a total power of 85 W and two ventilators with 15 W each. These loads could be switched on and off separately, and the electric power delivered by the fuel cell was quantified based on measurements of DC voltage and current (see Annex F.4).

In order to determine the heat and mass balances based on several phases of continuous operation, four consecutive phases of about 30 minutes were evaluated. In each of these phases, the Al consumption as well as hydrogen and heat production was analysed. The results of these consecutive phases were compared in order to detect possible trends that would indicate that a quasi-steady state operation has not been reached. The final results are reported as the mean of the four periods and the standard deviation of the mean of the four phases has been combined with the uncertainty of the measurement devices in order to determine the combined random and systematic uncertainty of the results.

5.3 Results with 6 M NaOH solution

5.3.1 General observations

Results of the measurement of the hydrogen and heat production during the experiment, including the selection of the four phases for the determination of heat and mass balances, are

depicted in Figure 30. In this experiment, a total of 324 g, together with additional experiments with this setup that are not reported here, a total of 510 g Al was used, from which an Al^{3+} concentration of 3.78 mol/L or 102 g/L can be expected. According to the experiments of chapter 4, precipitation is expected to start when a threshold of 150 g/L is surpassed, which has not been reached in these experiments. The measurements of hydrogen and heat show a similar course, as they are the result of the same chemical reaction. The heat production is slightly delayed, due to the system's thermal inertia. After the first dosing of aluminium at 12:11, hydrogen and heat production start to increase rapidly. Between 12:30 and 13:00, the Al-feeding was stopped to implement a software change in the feeding system. After that, the Al-feeding was kept on roughly the same rate with only small changes in attempt to reach a constant production rate. Control was rather difficult due to the system's high inertia. The gas flow meter stopped working two times for short periods (at 15:50 and 18:10) due to software problems. Al feeding was stopped at 19:17, together with the cooling system, therefore the measurement of the heat production stops there abruptly.

Figure 31 shows a detailed view of phase 2 as an example. A phase is defined as four feed cycles, with four dosings each (16 dosing in total) carried out by the feeder. A phase starts with the first dosing after a refill of the Al buffer of the feeding system (see Figure 31). For this experiment, the phases have not the same length because the time between the dosings were adjusted to control the aluminium flow. The hydrogen flow rate increases after every dosing, indicating that aluminium is reacting fast after it is dropped into the solution. The fact that the amount of aluminium varies slightly even for equal opening times of the dosing valve results in some fluctuations of the hydrogen production. The fluctuations of the heat production are mainly caused by the control of the thermostatic bath of the cooling system, i.e. by the compression chiller of the cooling system that turns on and off.

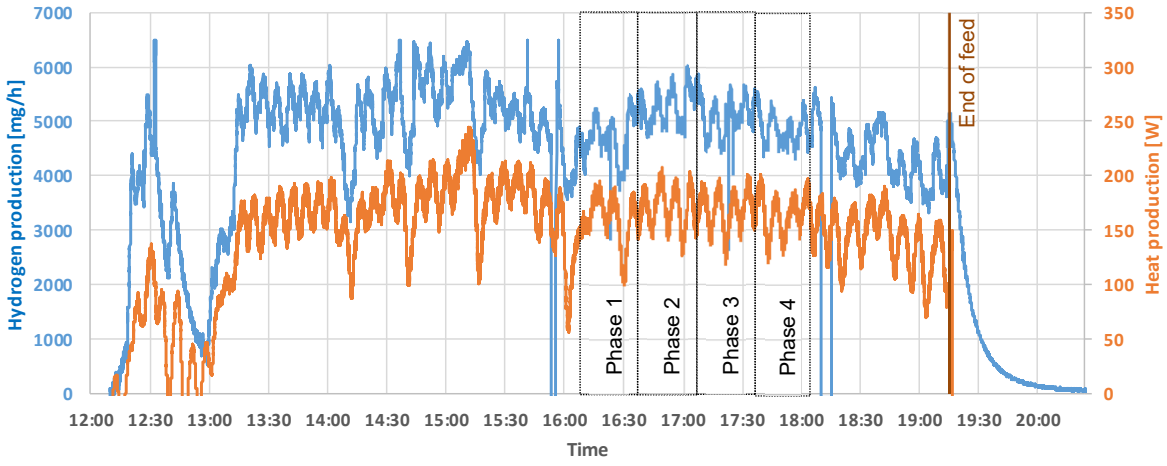

Figure 30: Hydrogen and heat production during the 6 M NaOH experiment with the 400 W converter.

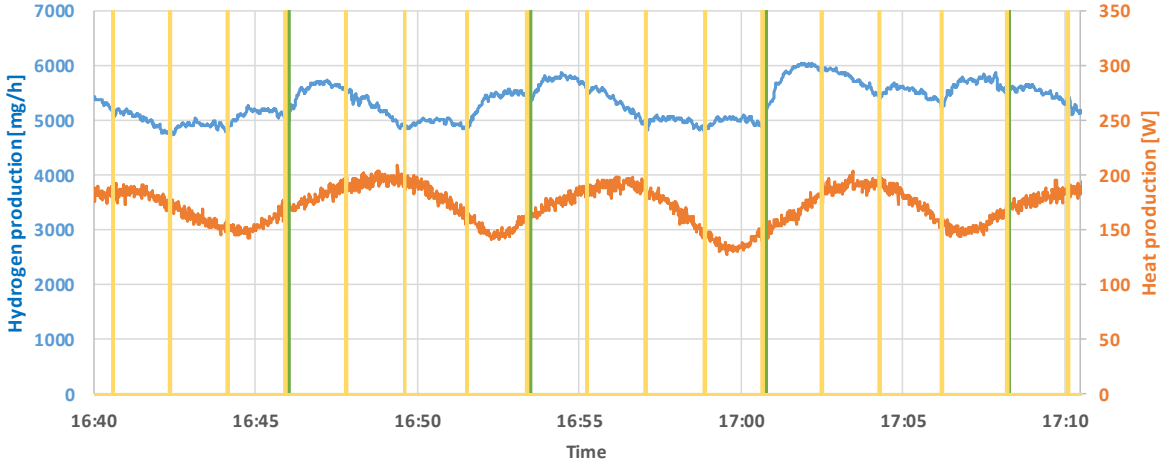

Figure 31: Phase 2 with 16 dosings (yellow) by the valve of the feeding system and the periodic reloads of the Al-grit buffer above the dosing valve (4 cycles, green).

5.3.2 Quantification of hydrogen and heat production from the 6 M NaOH experiment

The hydrogen and heat production is analysed for each of the four selected phases and results have been compared in order to ensure that a quasi steady state has been reached, as shown in Figure 30.

The measured hydrogen and heat production are compared with the theoretical values, which are calculated according to the stoichiometry of the reaction, based on the added amount of aluminium. The detailed calculation procedure, including the determination of uncertainties, are reported in Annex F. The results are summarized in Table 8 and show a good agreement between the experimental and theoretical values.

Figure 32 shows the comparison between the calculated and the measured hydrogen production for each phase and for the average of the phases. The hydrogen produced (5.02 g/h) would be enough to operate a fuel cell with an electric power of 99 W and 50% efficiency. The calculated values are not constant because the aluminium flow was not constant during the experiment as a result of the feeding rate control.

The differences between measured heat and hydrogen production rates and the calculated production rates that would result from 100% stoichiometric reaction of the Al with water are within the uncertainties of the measurements or calculations. The average conversion efficiency, defined as the ratio of measured value to the calculated one is 99.6%. Thus, it can be assumed that added aluminium has fully reacted. This was confirmed by a visual inspection after opening of the converter that showed no solid Al particles.

The comparison between the calculated and measured heat production is given in Figure 33. To compare the two values, the previously measured heat losses of 28 W were added to the usable heat that was measured during the experiment. The values and differences between calculated and measured heat vary for the same reasons as described above for hydrogen, but are within the uncertainties. In average, the conversion efficiency of heat is 99.6%, i.e. very much the same as the one for hydrogen production, which is a further confirmation that all aluminium has been converted completely.

The usable heat that can be extracted from the system is 166 W. With a total heat production of 194 W, this leads to an efficiency of the heat utilization of 85.6%.

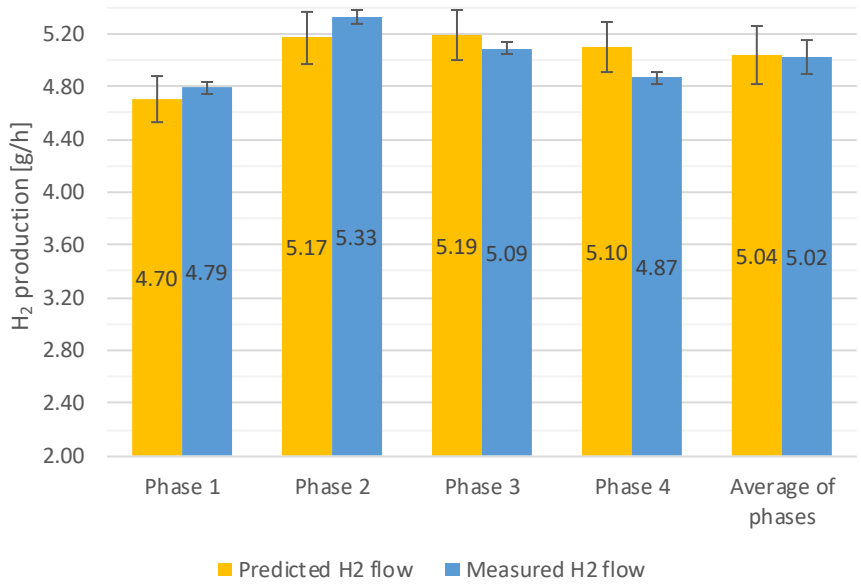

Figure 32:Comparison of calculated (based on Al feed) and measured H_2 production of each phase and of the average of all phases for the 6 M experiment. Uncertainties are given as 2σ (±95%).

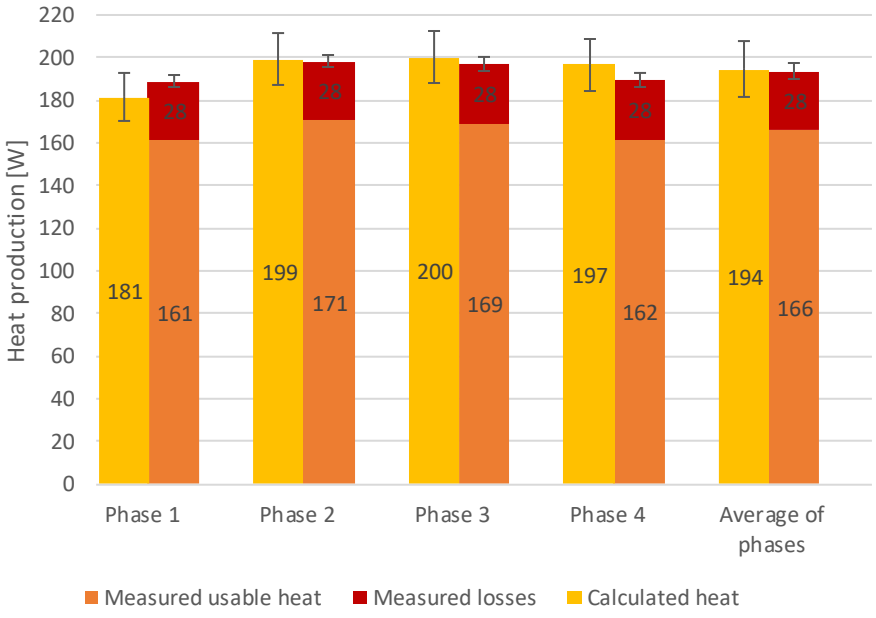

Figure 33: Comparison of calculated (based on Al feed) and measured heat production for each selected phase and the average values of all four phases for the 6 M NaOH experiment, uncertainties are given as 2σ (±95%).

Table 8: 6 M experiment: Measured and calculated values of hydrogen and heat production for each phase and for the average.

	Phase 1	Phase 2	Phase 3	Phase 4	Average of 1 to 4
Start of phase	16:08:12	16:40:37	17:10:07	17:39:29	
End of phase	16:40:36	17:10:06	17:39:28	18:09:21	
Duration of phase [min]	32.4	29.5	29.4	29.9	30.9
Cycles per phase [ ]	4	4	4	4	4
Avg. Al flow [g/h]	42.0 ±1.57	46.1 ±1.73	46.3 ±1.74	45.5 ±1.71	45.0 ±1.97
Temperature of solution [°C]	66.3 ±0.28	66.7 ±0.28	67.0 ±0.28	66.8 ±0.28	66.7 ±0.32
Meas. avg. H_2 flow [g/h]	4.79 ±0.04	5.33 ±0.05	5.09 ±0.05	4.87 ±0.04	5.02 ±0.13
Calculated theoretical maximum of H_2 flow [g/h]	4.70 ±0.18	5.17 ±0.19	5.19 ±0.19	5.10 ±0.19	5.04 ±0.22
H_2 production compared to theoretical maximum [%]	***101.9 ±3.9***	***103.1 ±4.0***	***98.0 ±3.8***	***95.4 ±3.7***	***99.6 ±4.2***
Meas. avg. heat flow [W]	161 ±2.2	171 ±2.2	169 ±2.2	162 ±2.1	166 ±3.3
Meas. heat + losses [W]	189 ±3.1	198 ±3.1	197 ±3.1	190 ±3.1	194 ±4.0
Efficiency heat utilization [%]	*85.2* ±1.0	*85.9* ±1.0	*85.9* ±1.0	*85.3* ±1.0	*85.6* ±1.0
Calculated theoretical maximum of heat flow [W]	181 ±11.3	199 ±12.5	200 ±12.5	197 ±12.3	194 ±12.9
Heat production compared to theoretical maximum [%]	***104.2 ±6.7***	***99.6 ±6.4***	***98.5 ±6.3***	***96.4 ±6.2***	***99.6 ±6.6***

5.3.3 Solid reaction products

After a total operation time of about 11 h with 6 M NaOH solution and 510 g of added aluminium in two experimental runs, the converter was opened. Figure 34 shows the impurities (brown / black) that are on the converter's wall and suspended in the solution. The type of impurities in the aluminium grit are given in Annex F.4. There was no visible precipitation of $Al(OH)_3$, as with 510 g of aluminium in 5 litres of solution (102 g Al /L), the point after which Al^{3+} starts to precipitate is not yet reached (see section 4.2.4). The converter was cleaned with water only, and solid products came off easily without scrubbing.

Figure 34: Solid and liquid products from the reaction of 0.5 kg Al grit with the 6 M NaOH solution (left) and vessel after cleaning (right) [14].

5.4 Results with 1 M NaOH solution

5.4.1 General observations

The measurement of the hydrogen and heat production with the 1 M NaOH solution is shown in Figure 35. The Al-feed started at 11:00 and was kept constant during the whole experiment. The hydrogen flow almost reached the target flow of 5.1 g/h. At 12:45 (marked with red line), after 15 feed cycles, the amount of aluminium (17 g/L) that is needed to reach saturation with Al^{3+} is reached (compare section 4.2.4). However, it cannot be assumed that all aluminium that was added has reacted at this point. The hydrogen production rate as well as the heat production are decreasing around the same time as the limit of solubility is theoretically reached. Thus, it must be assumed that increasing concentrations of Al^{3+} species in aqueous alkaline solutions slow down the reaction. At around 14:45, the H_2 mass flow rate and heat production start to increase again. At this point, the formation of $Al(OH)_3$ presumably sets in and the reaction rates recover to their "normal" values. Precipitation of $Al(OH)_3$ may have been triggered by the taking of a 60 mL sample of the solution through the sampling pipe. However, in the 2 M NaOH experiment reported later, precipitation happened also without any intervention (see section 5.5.1). The crystallization seed effect of $Al(OH)_3$ particles correspond to the literature (e.g. on the Bayer process and in [21]) as well as own observations (4.2.3). After this point, the hydrogen and heat production remains constant. From this last phase, four periods were selected and analysed. Toward the end of the experiment, the hydrogen mass flow rate and temperature increased for unknown reasons. The production rates start to decrease after the Al-feed was stopped at 18:26. The hydrogen flow only stopped (dropped below 50 mg/h) at around 15:00 the next day, 20.5 h after the feed was stopped. This shows that the reaction is much slower with the 1 M NaOH solution than with the 6 M NaOH solution, where the hydrogen mass flow rate decreased below 50 mg/h about 2 h after the Al feeding stopped.

Figure 36 shows a detailed view of phase 1 as an example of the nearly steady state conditions. Contrary to the experiment at 6 M NaOH, there is no noticeable change in the

hydrogen production immediately after a dosing occurs. This indicates again that the reaction is much slower. The fluctuations of the heat remain, since they are caused mainly by the cooling behaviour of the thermostatic bath.

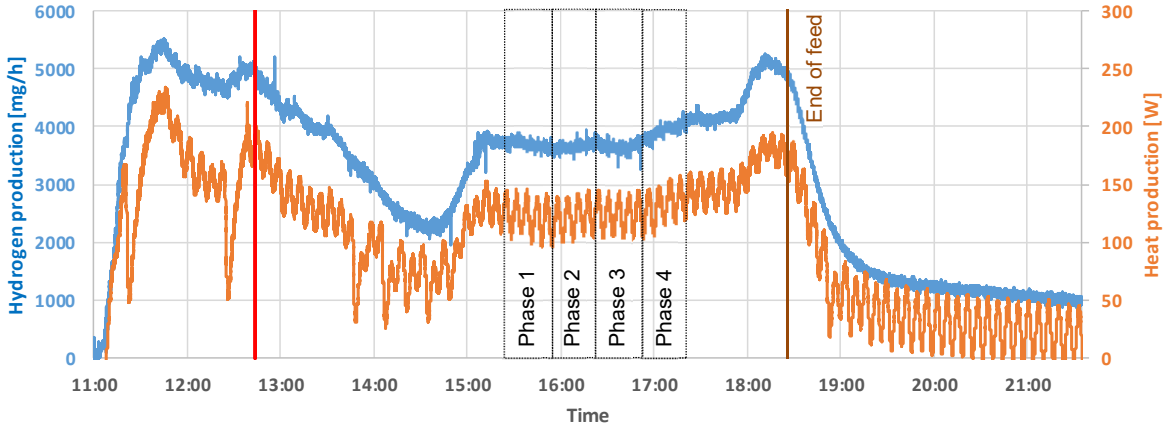

Figure 35: Hydrogen and heat production during the 1 M NaOH experiment

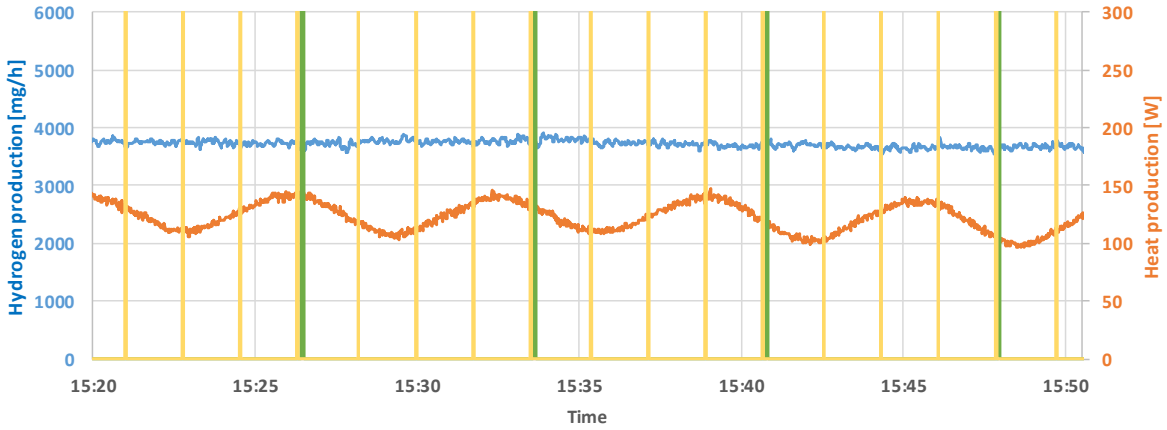

Figure 36: Phase 1 with the 16 dosings (yellow) by the valve of the feeder and the reloads of the Al-grit buffer above the valve (4 cycles, green).

5.4.2 Quantification of hydrogen and heat production from the 1 M NaOH experiment

Hydrogen and heat production were analysed for all four phases and are reported for the average of the four phases. The results are summarized in Table 10. The detailed calculations and uncertainties are given in Annex F.

Figure *37* shows the comparison between the theoretical maximum (calculated based on the Al feeding rate) and the measured hydrogen production for each phase of roughly 30 min duration and for the average of all four phases. The calculated values are the same for all phases, since the aluminium feeding rate was kept constant. The measured values vary only slightly from phase to phase. The conversion efficiency for hydrogen is 70.1% for the average of all phases. This suggests that the aluminium does not fully react under these conditions

within the evaluated time-span. The conversion efficiency of the heat production (presented in Figure *38*) is similar with 70.8% (total of utilized heat and estimated heat losses according to the heat loss measurements, compared to calculated theoretical maximum), which indicates the same incompleteness of reaction as the measured H_2 production.

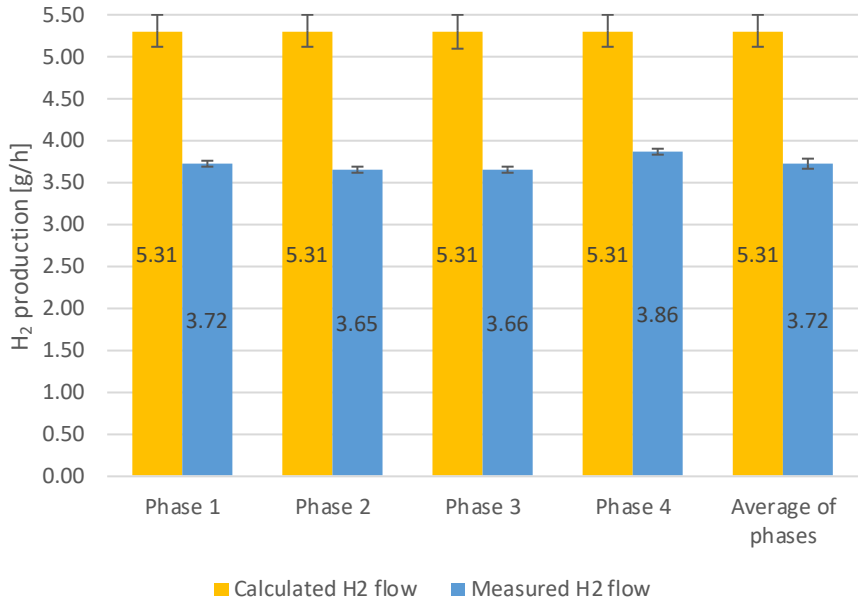

Figure 37: Comparison of the calculated theoretical maximum and of the measured H_2 production of each phase and of average of all phases for the 1 M NaOH experiment.

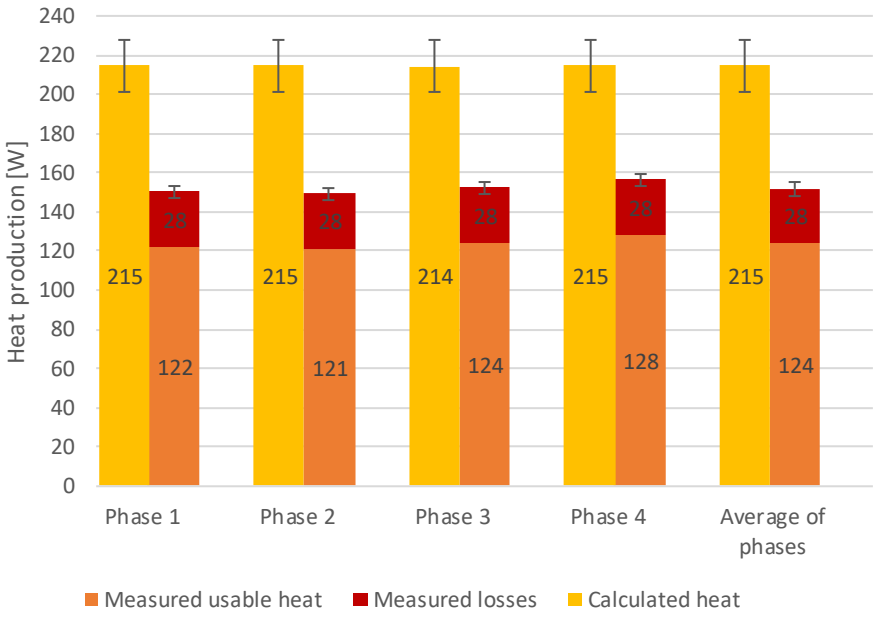

Figure 38: Comparison of the calculated theoretical maximum with the measured heat production of each phase and of average of all phases for the 1 M NaOH experiment.

Because the aluminium oxidation reaction is very slow, it takes up to 20.5 h to reach the full reaction turnover. The conversion efficiency of hydrogen and heat for the whole experiment with heat and hydrogen measurements including the 20.5 h after the end of Al feeding is presented in Table 9. The duration of the whole experiment, including this post-feeding time, is 28 h (from the beginning of aluminium feeding at 11:00 until the end of the reaction, the next day at 15:00, when no hydrogen mass flow was recorded anymore). The results of this evaluation are shown in the second line of Table 9, with much higher values of 92% for hydrogen production and 99% for heat production. For this reason, the efficiency calculation shown in Table 10 are probably based on a section of the experiment where it is unlikely that a quasi steady state has already been reached, and with time almost all or even all aluminium is reacting. The difference between the efficiencies of hydrogen and heat production until the considered end of reaction are within the uncertainty of the (heat) measurements. After feeding stops, the heat production decreases slowly, thus the heat losses have a very high influence on the results and increase its uncertainty substantially.

Table 9: 1 M NaOH experiment: Conversion efficiency during selected period of the experiment and until the end of the reaction.

	Hydrogen production	**Heat production**
Total conversion efficiency until end of Al-feeding	68.0 ±2.6%	67.9 ±4.5%
Total conversion efficiency until end of reaction	92.0 ±3.6%	99.3 ±6.6%

Table 10: 1 M NaOH experiment: Measured and theoretical maximum values of hydrogen and heat production for each phase and for the average of all four phases.

	Phase 1	**Phase 2**	**Phase 3**	**Phase 4**	**Average of 1 to 4**
Start of phase	15:21:01	15:49:44	16:18:27	16:47:11	
End of phase	15:49:43	16:18:26	16:47:10	17:15:53	
Duration of phase [min]	28.7	28.7	28.7	28.7	28.7
Cycles per phase [ ]	4	4	4	4	4
Avg. Al flow [g/h]	47.4 ±1.78	47.4 ±1.78	47.4 ±1.78	47.4 ±1.78	47.4 ±1.78
Temperature of solution [°C]	63.1 ±0.28	63.3 ±0.28	63.4 ±0.28	63.6 ±0.28	63.3 ±0.29
Meas. avg. H_2 flow [g/h]	3.72 ±0.04	3.65 ±0.04	3.66 ±0.04	3.86 ±0.04	3.72 ±0.06
Calculated theoretical maximum of H_2 flow [g/h]	5.31 ±0.20	5.31 ±0.20	5.31 ±0.20	5.31 ±0.20	5.31 ±0.20
H_2 production compared to theoretical maximum [%]	**70.0 ±2.7**	**68.8 ±2.7**	**69.0 ±2.7**	**72.7 ±2.8**	**70.1 ±2.9**
Meas. avg. heat flow [W]	122 ±2.3	121 ±2.3	124 ±2.3	128 ±2.3	124 ±2.8
Meas. heat + losses [W]	150 ±3.2	149 ±3.2	152 ±3.2	156 ±3.2	152 ±3.6
Efficiency heat utilization [%]	81.3 ±1.2	81.3 ±1.2	81.6 ±1.2	82.1 ±1.2	81.6 ±1.2
Calculated theoretical maximum of heat flow [W]	215 ±13.4	215 ±13.4	215 ±13.4	215 ±13.4	215 ±13.4
Heat production compared to theoretical maximum [%]	**70.0 ±4.6**	**69.6 ±4.6**	**71.0 ±4.7**	**72.9 ±4.8**	**70.8 ±4.7**

5.4.3 Solid reaction products

After a total operation time of about 20 h and 930 g of added aluminium (in several experiments), the converter was opened and visually inspected (Figure 39) three weeks after the last experiment has ended. The level of the aqueous solution was slightly lower compared to the level before the experiments. A strongly adherent layer, likely composed of iron and aluminium compounds, covered the middle part of the walls of the converter. The layer was removed with difficulty.

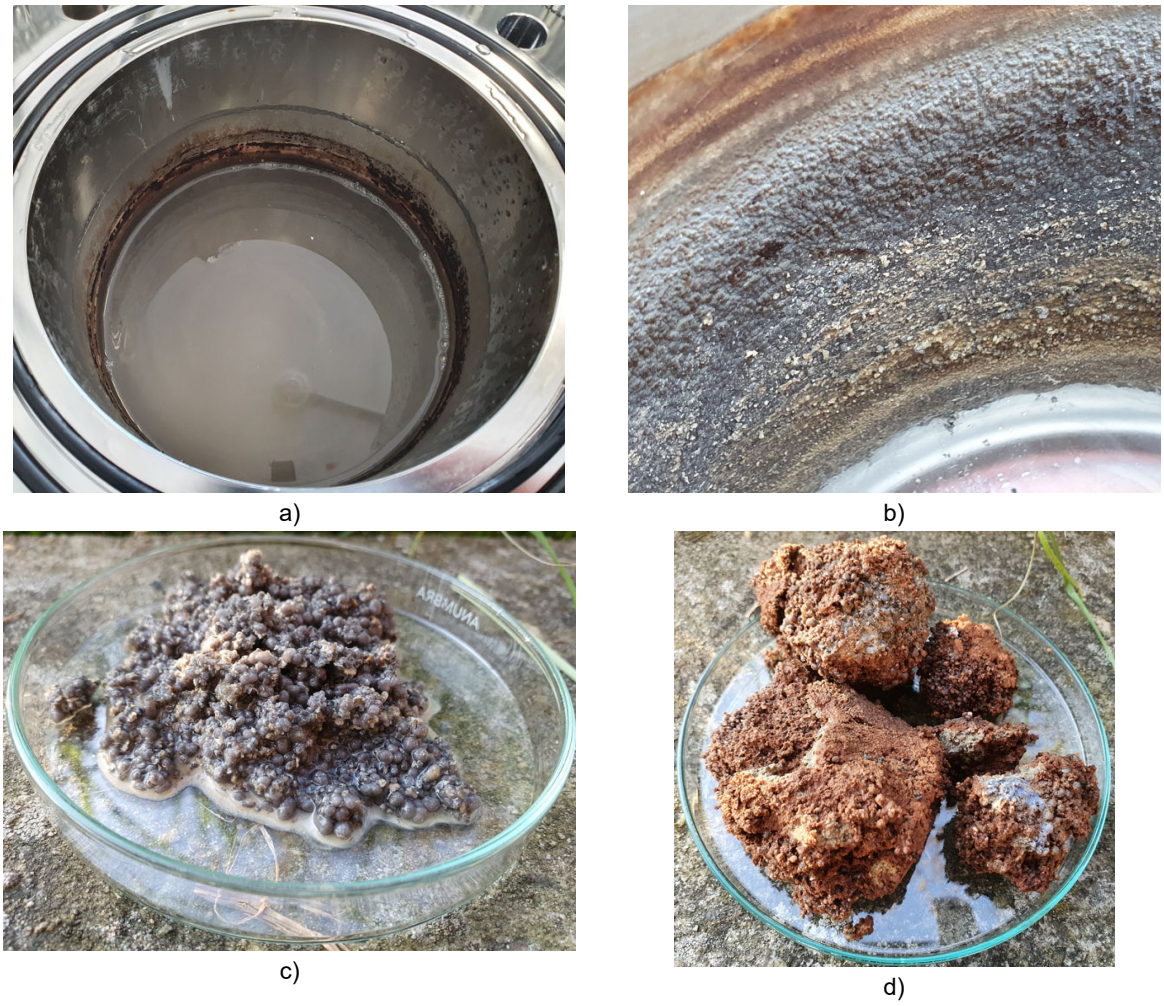

Figure 39: Visual inspection of the converter vessel after the 1 M NaOH experiments: a) converter vessel after opening, b) fouling on the converter wall, c) loose precipitate with spherical shaped elements d) rocky precipitate from the middle part in the bottom of the converter, below the loose precipitate [14].

While removing the content of the reactor, several phases were observed: a liquid one on top (Figure 39a), a solid one in the middle and a very viscous one in the bottom part. The liquid one was mainly sodium hydroxide solution with dissolved aluminium compounds. The one in the middle was made of two zones: on top there were particles of the size of the Al grit (Figure 39c), which probably stemmed from a slow oxidation of the grit that might have led to this spherical form of products. Adding a 6 M NaOH solution showed no gas evolvement, therefore

it may be assumed that they contained no or only minor amounts of unreacted aluminium. The second part (Figure 39d) was a hard, rocky precipitate, which presumably has been formed slowly since the spherical form of the Al particles was still visible, although the Al had reacted completely. The brown-red aspect on the outside may be due to Fe^{3+} compounds, while inside, there is a white-grey colour. This is likely due to solid white $Al(OH)_3$ and Fe^{2+} or Fe_3O_4 black compounds, the spherical shape of the Al particles was not maintained in this material.

5.5 Results from 2 M NaOH experiments with fuel cell

5.5.1 General observations

The hydrogen and heat production during the experiment with the 2 M NaOH solution is shown in Figure 40. From the beginning of the experiment until 15:15, hydrogen was directed into the fuel cell and converted to electrical power. After that, because the H_2 production dropped and could not maintain the needed pressure, the fuel cell was turned off and the hydrogen was vented to the outside. Thus, the graph shows the real time H_2 production. The hydrogen flow fluctuates more during the operation of the fuel cell because the fuel cell purges every 10 seconds, which increases the flow shortly. Also, the load of the fuel cell was turned off some times, which causes the flow to stop.

The red line marks the point where the total addition of 170 g Al was reached. This is roughly the amount of 34 g/L that is needed to reach saturation with Al^{3+} according to extrapolation of the results of section 4.2.4. After that the hydrogen and heat production start to decrease slowly to a point (16:00), where presumably precipitation starts. Then they increase again, thus, showing the same behaviour as with the 1 M NaOH solution in the previous experiment. After 18:00, a constant production rate seems to be reached. The four phases for the analysis of the quantification of hydrogen and heat production were selected there. The aluminium feed was stopped at 20:00. The hydrogen production stopped (dropped below 50 mg/h) 8 hours later at 04:00 the next day.

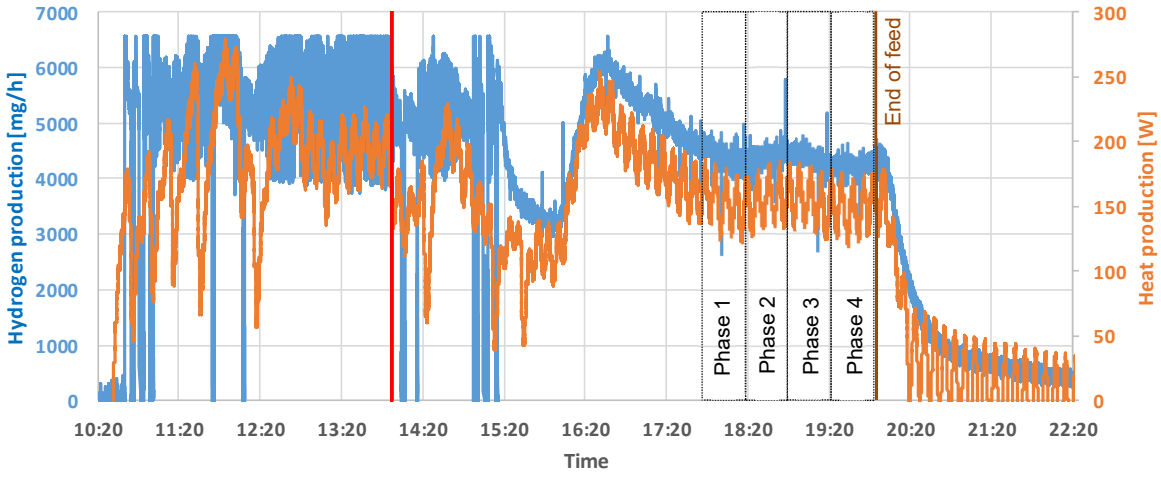

Figure 40: Hydrogen and heat flow rates during the experiment with the 2 M NaOH solution.

5.5.2 Quantification of hydrogen and heat production from the 2 M NaOH experiment

Like in the previous experiments, hydrogen and heat production were analysed for four phases. The results are summarized in Table 11. The detailed calculations and uncertainties are given in Annex F.

Figure 41 and Figure 42 show the comparison between the calculated theoretical maximum (based on the Al feeding rate) and the measured production of hydrogen and heat. The measured values stay more or less constant during the four phases, while the calculated values are exactly constant since the Al feed rate was not changed during the phases. The conversion efficiency for the average of all phases is 82.9% for hydrogen and 85.1% for heat. They are higher than in the 1 M experiments, suggesting that the aluminium is reacting faster under these conditions, but still not fully within the analysed time-span. The usable heat production is with 153 W also higher, as well as the efficiency of heat utilisation with 84.5%.

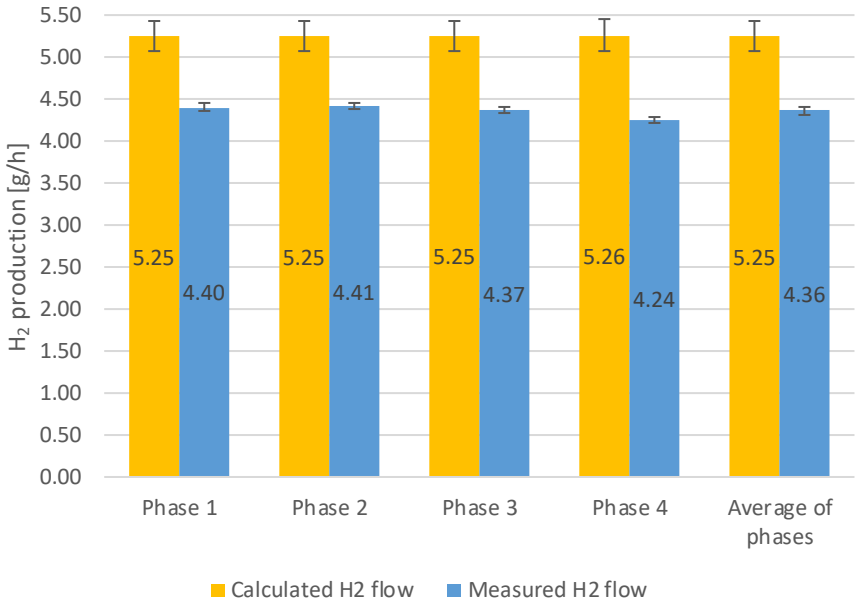

Figure 41: Comparison of the calculated theoretical maximum and of the measured H_2 production of each phase and of average of all phases for the 2 M NaOH experiment; steady state likely not reached at point of evaluation.

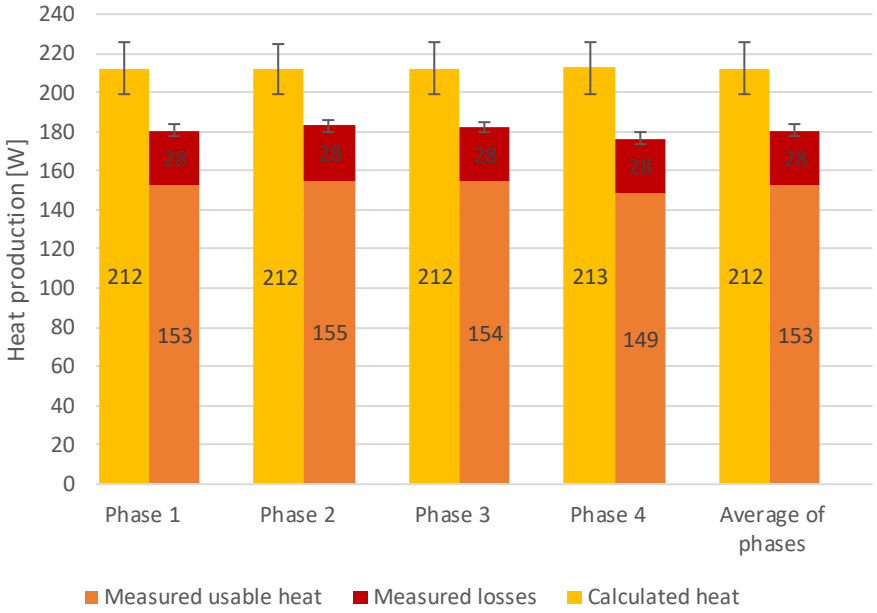

Figure 42: Comparison of the calculated theoretical maximum with the measured heat production of each phase and of average of all phases for the 2 M NaOH experiment.

Table 11: 2 M NaOH experiment: Measured and theoretical maximum values of hydrogen and heat production for each phase and the average of all four phases.

	Phase 1	**Phase 2**	**Phase 3**	**Phase 4**	**Average of 1 to 4**
Start of phase	17:47:23	18:18:34	18:49:43	19:20:51	
End of phase	18:18:33	18:49:42	19:20:50	19:52:01	
Duration of phase [min]	31.15	31.17	31.13	31.12	28.7
Cycles per phase [ ]	4	4	4	4	4
Avg. Al flow [g/h]	46.9 ±1.64	46.8 ±1.64	46.9 ±1.64	46.9 ±1.64	46.9 ±1.64
Temperature of solution [°C]	63.4 ±0.28	63.5 ±0.28	63.5 ±0.28	63.4 ±0.28	63.5 ±0.28
Meas. avg. H_2 flow [g/h]	4.40 ±0.04	4.41 ±0.04	4.37 ±0.04	4.24 ±0.04	4.36 ±0.06
Calculated theoretical maximum of H_2 flow [g/h]	5.25 ±0.18	5.25 ±0.18	5.25 ±0.18	5.26 ±0.18	5.25 ±0.18
H_2 production compared to theoretical maximum [%]	**83.8 ±3.0**	**84.0 ±3.0**	**83.2 ±3.0**	**80.7 ±2.9**	**82.9 ±3.1**
Meas. avg. heat flow [W]	153 ±2.0	155 ±2.0	154 ±2.0	149 ±2.0	153 ±2.49
Meas. heat + losses [W]	181 ±3.0	183 ±3.0	182 ±3.0	177 ±3.0	181 ±3.3
Efficiency heat utilization [%]	84.5 ±1.1	84.7 ±1.0	84.6 ±1.0	84.1 ±1.1	84.5 ±1.1
Calculated theoretical maximum of heat flow [W]	212.3 ±13.0	212.2 ±12.9	212.4 ±13.0	212.5 ±13.0	212.3 ±13.0
Heat production compared to theoretical maximum [%]	**85.1 ±5.4**	**86.3 ±5.5**	**85.8 ±5.4**	**83.1 ±5.3**	**85.1 ±5.4**

Like in the 1 M experiment, the hydrogen and heat conversion were also analysed for the whole experiment from the beginning of Al-feed until the end of Al-feed, respectively until the end of the reaction 8 h after feed stop. The results are given in Table 12. The conversion during the time of feeding is higher than for the 1 M experiment. The conversion efficiencies until the end of the reaction suggest that with enough time, nearly all the aluminium that was added reacts.

Table 12: 2 M NaOH experiment: Conversion efficiency during selected period of the experiment and until the end of the reaction.

	Hydrogen production	**Heat production**
Total conversion efficiency until end of Al-feeding	87.9 ±3.2%	88.1 ±5.6%
Total conversion efficiency until end of reaction	94.5 ±3.4%	97.5 ±6.2%

5.5.3 Measurement of fuel cell performance

Figure 43 shows a section of the fuel cell operation in the experiment with the 2 M NaOH solution. The fuel cell converted the produced hydrogen directly into electricity, which was used to operate variable loads. The hydrogen flow in the graph shows a high fluctuation, this is due to the automatic purging of the fuel cell every 10 seconds, where the flow rises and then drops. After a purging, the pressure after the pressure regulator drops and slowly rebuilds. This pressure drop sometimes caused a short drop in the produced electricity, visible in the yellow line.

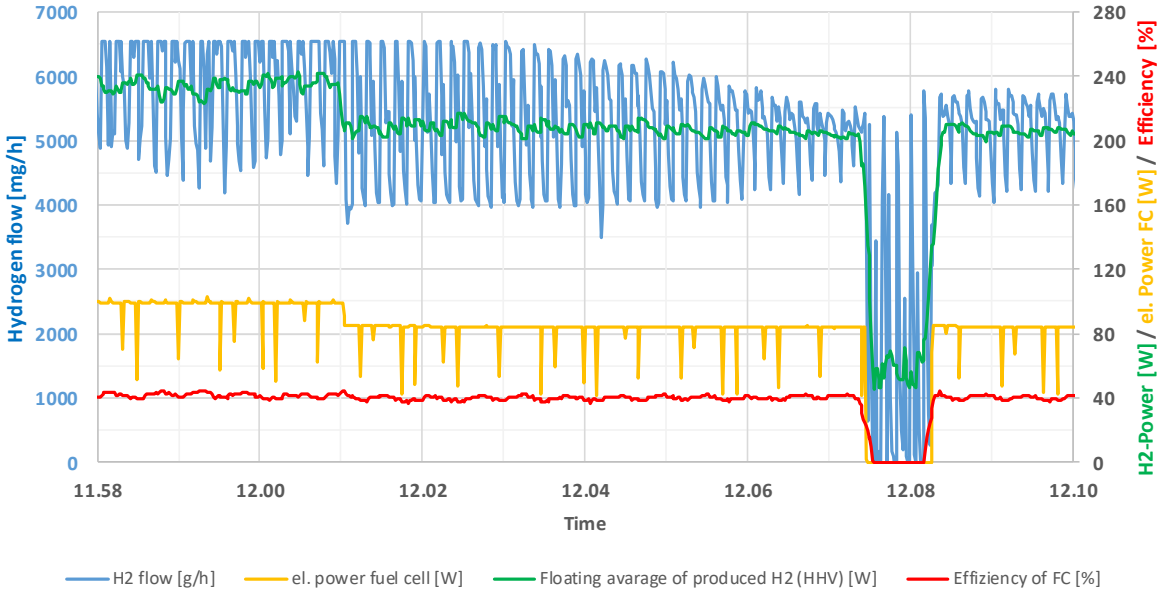

Figure 43: Performance of fuel cell during the experiment with the 2 M NaOH solution.

The fuel cell was operated in three different modes: with a load of 100 W (11:58 – 12:01 in the graph), with a load of 85 W (12:01 – 12:07) and with the loads turned off (around 12:08). When it is operated on 100 W, the hydrogen flow reached with its fluctuations the upper limit of the measuring range of the flow meter at 6553 mg/h. Therefore, the hydrogen flow could not be measured accurately in this operation and subsequently the fuel cell was mainly operated with 85 W. For both operation modes, the electrical efficiency of the fuel cell was around 40% as specified by the manufacturer. The efficiency is calculated from the floating average of the energy content of the hydrogen based on its upper heating value (HHV_{H_2} = 39.4 kWh/kg) and the measured electrical power of the fuel cell. When the load was turned off, the fuel cell still consumed some hydrogen by purging every 10 seconds.

5.5.4 Solid reaction products

The total operation time of the 2 M NaOH experiment was about 10 h and 450 g of aluminium was added. The converter was opened 2 weeks after this experiment ended and visually inspected (Figure 44).

Figure 44: Visual inspection of the converter vessel after the 2 M NaOH experiments, a) upper part with liquid phase, b) lower part with solid phase, c) solid reaction products removed from the converter, d) converter vessel after cleaning.

A liquid phase was observed on top (Figure 44a) as in the case of previous experiments. This was mainly sodium hydroxide solution with dissolved aluminium compounds. After removing the liquid phase, a white-grey colour solid part was observed (Figure 44b). The spherical particles visible in the experiment with 1 M NaOH solution were not observed in this case (Figure 44c). It is assumed that the reaction was faster and thus the shape of the Al grit was not preserved as in the case of the previous experiment. A brown-red layer that is likely due to the presence of iron-based compounds was also observed.

A layer that was not adherent (different from the experiment with 1 M NaOH) was visible in the upper part of the converter walls. This layer was easy to remove and the reactor was perfectly cleaned after removing all the reaction products (Figure 44d).

5.6 Discussion

The experiments showed that the ≈ 400 W prototype with a 6 M NaOH solution produced 194 W of heat, of which 166 W was transferred and extracted with a water cooling system and could be used for DHW and space heating, representing a heat utilisation efficiency of 86%. The system design would allow for an operation of much higher aluminium feeding rates, and respectively higher hydrogen and heat production rates, which would likely increase also the utilisation of heat. Since the solid products are not removed and no water is added, the duration of experiments is currently limited by the converter size.

The aluminium reacts fully when a 6 M NaOH solution is used as a reaction promoter. The expected amount of hydrogen and heat is obtained, according to the reaction stoichiometry. For this experiment, the point where solid aluminium hydroxide is formed was not reached.

For the experiment with 1 M NaOH solution, the reaction is much slower. During the limited operation period, where no steady state was reached, only about 70% of the aluminium converted to hydrogen and heat within the short time-span of evaluation. When Al feeding stops, the reaction still continues for about 20 hours. Including the heat and hydrogen production that occurs during this time, the conversion efficiency reaches about 95%. This indicates that almost all of the added aluminium reacts, albeit slowly.

The reaction was a little faster with the 2 M solution. The conversion efficiency was 88% during the operation period and it took 8 hours for the reaction to stop after the Al feeding has stopped. With a conversion efficiency of about 96% for the whole reaction time, it is expected that nearly all of the added aluminium reacts with time also in this case.

Compared to the 1 M and 2 M NaOH solution, the fast reaction of the 6 M solution makes the system easier to control. For example, if the reaction must be stopped, it takes less than half an hour for the hydrogen production to drop below 10% of its steady state value and about 1.5 h to stop.

The experiment with 1 M and 2 M NaOH showed that the $Al(OH)_3$ precipitates under these conditions after the saturation is reached. When precipitation starts, the reaction is still running, allowing thus for a continuous operation without changes in reaction conditions. At some points even short-term increase in the reaction rate where observed, for which the cause was unclear.

The valve feed system, which was implemented to the converter system, was able to feed the converter with aluminium grit in a quasi-continuous way. The system showed no gas leakage during its operation, except for the inevitable small carry-over leakage of a sluice system. In this time, the feeder clogged one time, which was likely due to humidity raising from the converter, which required a manual intervention. However, measurements of traces of hydrogen above the feeding system indicated that the leakage of the sluice system increased to some extent in the last experiments, suggesting that the feeding system was compromised and required replacement. This increase of gas leakage may also be an explanation for the differences in hydrogen and heat production efficiencies that were measured in later experiments. These are issues that must be solved in order to run the system in a fully automated mode.

The fluctuations in hydrogen and heat production observed in the 6 M NaOH experiments could be minimized by following measures:

- lower the concentration of the reaction promoter to reduce the reaction speed;
- shorten the opening times of the dosing valve, while increasing the amount of dosing per cycle.

The latter is critical however, because the shorter the opening of the dosing valve, the higher the chance of clogging.

6 Analysis of the Precipitate

6.1 Procedures and methodology

Solid products of the Al-water reactions were assumed to be $Al(OH)_3$. To confirm this, the following analytical methods were employed in order to analyse precipitates obtained in the experiments of sections 4.2.4 and 5.4.3:

- scanning electron microscopy (SEM) coupled with energy-dispersive X-ray spectroscopy (EDX);
- X-Ray diffraction (XRD);
- differential scanning calorimetry (DSC) and
- thermogravimetric analysis (TGA).

Samples from small-scale chemical (C) laboratory experiments of section 4.2.4 are identified by the suffix "_C", while samples from the 400 W batch reactor (R) are identified by the suffix "_R". The NaOH concentration at which the reaction of Al was carried out is indicated by "1M" (1 Molar).

Powder samples were prepared by drying the precipitate at room temperature. The solid samples were washed several times with deionized water and filtered using 589/1 filter papers (diameter 125 mm, Lot No. G4997143, Whatman) and a vacuum pump. Precipitate washing was made until neutral pH (7±0.5, measured by pH colour strips). After that, the samples were let to dry at room temperature in the presence of ambient air. The sample 1M_R was homogenised and ball mill grinded (using a Fritsch Pulverisette ball mill) to reduce the particle size. The final aspect of the sample is presented in Figure 45 (1M_C) and Figure 46 (1M_R).

Figure 45: Sample 1M_C from the 1 M NaOH chemical laboratory experiment.

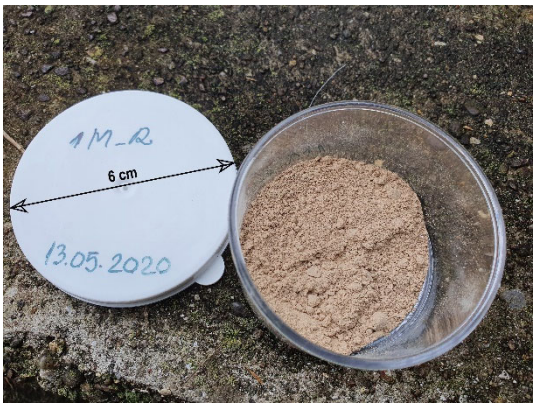

Figure 46: Sample 1M_R obtained after grinding the precipitate from the 1 M NaOH experiment with the 400 W converter.

The morphology of the powder samples was evaluated using a SM-IT200 InTouchScope™ Scanning Electron Microscope from Jeol (accelerating voltage 20.0 kV, magnification x250,

low vacuum mode, pressure 50 Pa) at IWK-HSR[4]. The samples were place on a conductive carbon support. The elemental composition of the samples was determined using energy-dispersive X-ray spectroscopy (EDX).

X-Ray Diffraction was used to identify the crystalline phases and thus obtain information about the chemical composition. A PANalytical X'Pert instrument using a Bragg-Brentano setup was used. Data collection was performed at room temperature using Cu-K_α radiation (λ=1.5406Å). Two types of samples were measured: one dried at room temperature and one thermally treated at 900°C. The XRD measurements were made at the Center for X-ray Analytics at EMPA in Dübendorf and at the ETH X-Ray Platform.

The phase transition behaviour of aluminium hydroxide was investigated using a DSC 3+ from Mettler Toledo at a scanning rate of 10 °C·min^{-1}, in the temperature range from room temperature (25 °C) to 500 °C, in inert atmosphere (50 mL N_2 / min). The change in weight of the precipitate sample as it is heated at constant temperature was evaluated via thermogravimetry. The sample was heated from room temperature to 900°C using an STA 6000 simultaneous thermal analyser from Perkin Elmer. The DSC and TGA measurements were performed at the IWK-HSR. The calcined samples at 900°C were further characterized via XRD to assess the crystalline structure.

6.2 Results

6.2.1 SEM and EDX

SEM images of untreated aluminium hydroxide powder samples 1M_C and 1M_R are shown in Figure 47. The powders are relatively smooth and homogenous, with spherical particles of a few microns. An agglomeration effect is visible in both samples.

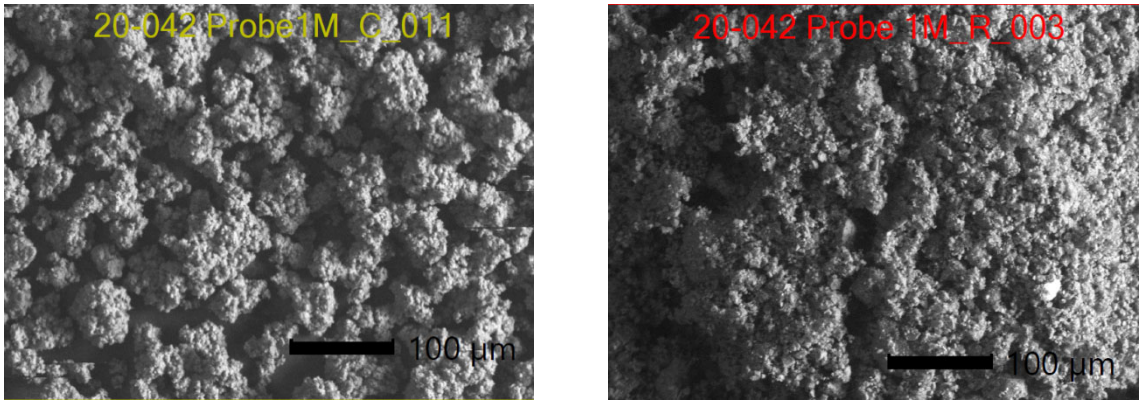

(a) (b)

Figure 47 SEM images of untreated $Al(OH)_3$ powder samples: a) Sample from the 1 M NaOH chemical lab experiment; b) Sample obtained after grinding the precipitate from the 1 M NaOH experiment with the 400 W converter.

[4] IWK Materials Technology and Plastics Processing Institute from HSR University of Applied Sciences Rapperswil.

The EDX results, which are summarized in Table 13, confirmed that the samples consist mainly of oxygen and aluminium. The presence of carbon is likely due to the sample holder made of conductive carbon. Carbon can also be due to environmental gasses (e.g. CO_2) uptake, which occurs during air drying process and sample transfer [22]. The presence of copper is attributed to the measurement setup.

The purity of the used Al samples differed between the chemical laboratory experiments (C): 99% and the experiments with the 400 W reactor (R) 97.5%. The average values of the impurities from the Al grit used in the 400 W reactor was reported by the supplier as follows: Mg 0.80%, Si max. 1%, Fe max. 0.4%, Mn max. 0.3%, C max. 0.10%. This correlated with the EDX results.

Similar concentration for Al was recorded for both categories of samples. This indicates that the same process occurs in both conditions and the effect of impurities is small.

Table 13 Chemical composition (atomic concentration in %) of the solid products from the aluminium water reaction.

		Sample 1M_C		Sample 1M_R	
No.	**Element**	**at. %**	**at. %**	**at.%**	**stdev**
1.	**Al**	27.5	2.39	26.14	0.30
2.	**O**	65.19	1.37	61.32	0.22
3.	**C**	5.64	3.02	7.71	0.56
4.	**Na**	0.45	0.04	0.49	0.01
5.	**Mg**	-	-	0.51	0.01
6.	**Si**	0.05	0.02	0.17	0.05
7.	**P**	0.21	0.04	0.18	0.02
8.	**Mn**	0.01	0.01	0.62	0.02
9.	**Fe**	0.07	0.01	0.56	0.01
10.	**Cu**	0.50	0.38	1.19	0.21
11.	**Zn**	0.40	0.42	1.10	0.21

Based on the atomic concentrations from Table 13, the oxygen/aluminium ratio was calculated (Table 14) and compared with the theoretical one for different possible Al-compounds (Table 15). The calculated values determined experimentally are slightly higher, but are in the range reported by other researchers [22].

Table 14 Atomic concentrations and O/Al ratio – experimental results.

Sample	**Al, at.%**	**O, at.%**	**Ratio O/Al**
1M_C	27.50	65.19	2.37
1M_R	26.14	61.32	2.35

Comparing the experimental (Table 14) and theoretical values (Table 15), it can be concluded that $Al(OH)_3$ (in the form of bayerite/gibbsite) is the likely Al-compound from the Al-water reaction. This is confirmed by the XRD investigations, which are presented below.

Table 15 Atomic concentrations and O/Al ratio – theoretical calculations for different Al-compounds.

Phase name	Chemical formula	Molar mass (g/mol)	Al, at.%	O, at.%	Ratio O/Al
Bayerite	α-$Al(OH)_3$	78.01	34.59	61.53	1.78
Gibbsite	γ-$Al(OH)_3$	78.01	34.59	61.53	1.78
Boehmite	γ-AlOOH	59.99	44.97	53.34	1.19
Diaspore	α-AlOOH	59.99	44.97	53.34	1.19
Gamma alumina	γ-Al_2O_3	101.96	52.92	47.08	0.89

6.2.2 XRD

The crystalline structure of untreated and thermal treated solid reaction products obtained from the Al-water reaction was analysed by X-ray diffraction. Thermal treatment was performed at 900°C for 30 min. The analysis included both samples from the experiments in the chemistry lab described in section 4.2.4 and samples from the 400 W prototype (section 5.4):

- 1M_C0 (untreated);
- 1M_CT (treated at 900°C);
- 1M_R0 (untreated);
- 1M_RT (treated at 900°C).

During the thermal treatment, aluminium hydroxides (bayerite and gibbsite) and aluminium oxide hydroxide (boehmite and diaspore) decompose to aluminium oxide and water according to Eq. 1 and Eq. 2, respectively [22,23]. Aluminium oxide (Al_2O_3) is a polymorphic material that exists in various metastable phases (Figure 48) and one thermodynamically stable phase: α-Al_2O_3. The metastable phases can be obtained after thermal treatment of aluminium hydroxides/ oxide hydroxides (Figure 48), according to [24].

Eq. 1 $$2Al(OH)_3 \rightarrow Al_2O_3 + 3H_2O$$

Eq. 2 $$2\,\gamma AlOOH \xrightarrow{600°C} \gamma Al_2O_3 + H_2O$$

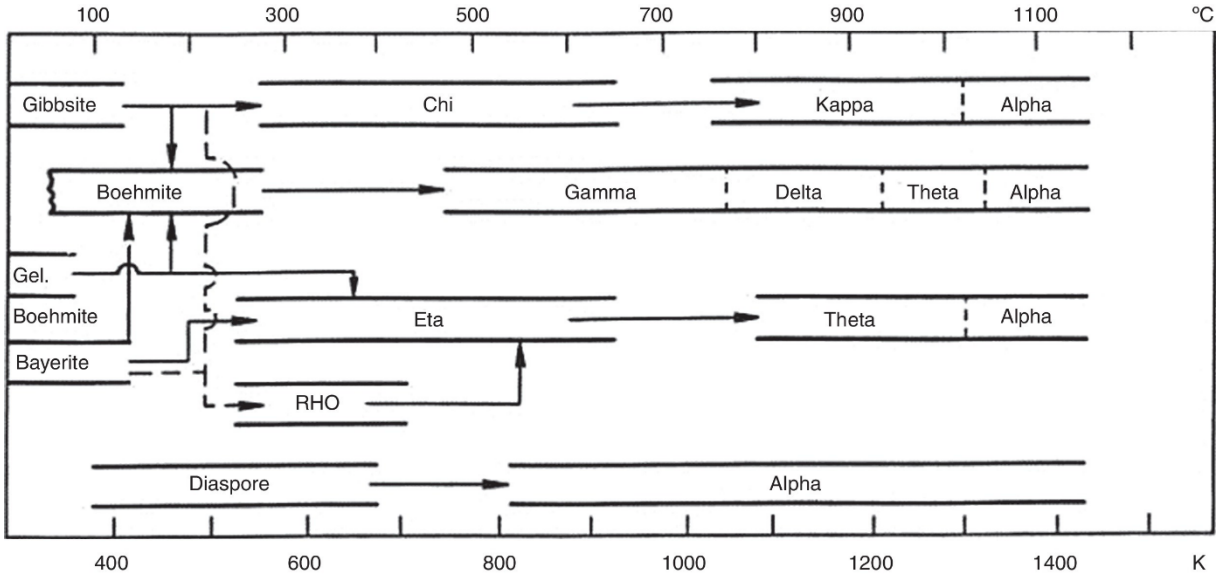

Figure 48: Transformation sequences from $Al(OH)_3$ to α-Al_2O_3 (source: Alcoa Laboratories, Technical Paper No. 19, page 47 [24]).

A summary of the possible Al-compounds that can be formed during the thermal decomposition, including the different aluminium hydroxides/oxide hydroxides and their crystal system is presented in Table 16.

Table 16 Crystal system for different Al-compounds.

Phase name	**Chemical formula**	**Crystal system, other names**
Bayerite	α-$Al(OH)_3$	Hexagonal
Gibbsite / Hydrargilite	γ-$Al(OH)_3$	Monoclinic, triclinic
Boehmite	γ-AlOOH	Orthorhombic
Diaspore	α-AlOOH	Orthorhombic
Rho alumina	ρ-Al_2O_3	Amorphous
Eta alumina	η-Al_2O_3	Face –centered cubic
Chi alumina	χ-Al_2O_3	Hexagonal close-packed
Gamma alumina	γ-Al_2O_3	Face –centered cubic
Delta alumina	δ-Al_2O_3	Tetragonal, orthorhombic
Kappa alumina	κ-Al_2O_3	Hexagonal close-packed (orthorhombic)
Theta alumina	θ-Al_2O_3	Monoclinic
Alpha alumina	α-Al_2O_3	Hexagonal close-packed (trigonal)

The XRD analysis of both precipitate samples consists only of aluminium hydroxide: gibbsite (γ-$Al(OH)_3$, ICDD 96-101-1082) and bayerite (α-$Al(OH)_3$, ICDD 96-900-8136). The sample 1M_C0 seems to have a higher crystallinity than the sample 1M_R0. This might be due to a slightly different growth mechanism influenced by the temperature, which was not exactly the same in both experiments. After annealing at 900°C, only aluminium oxide (γ-Al_2O_3, 96-153-3937) is observed (Figure 50).

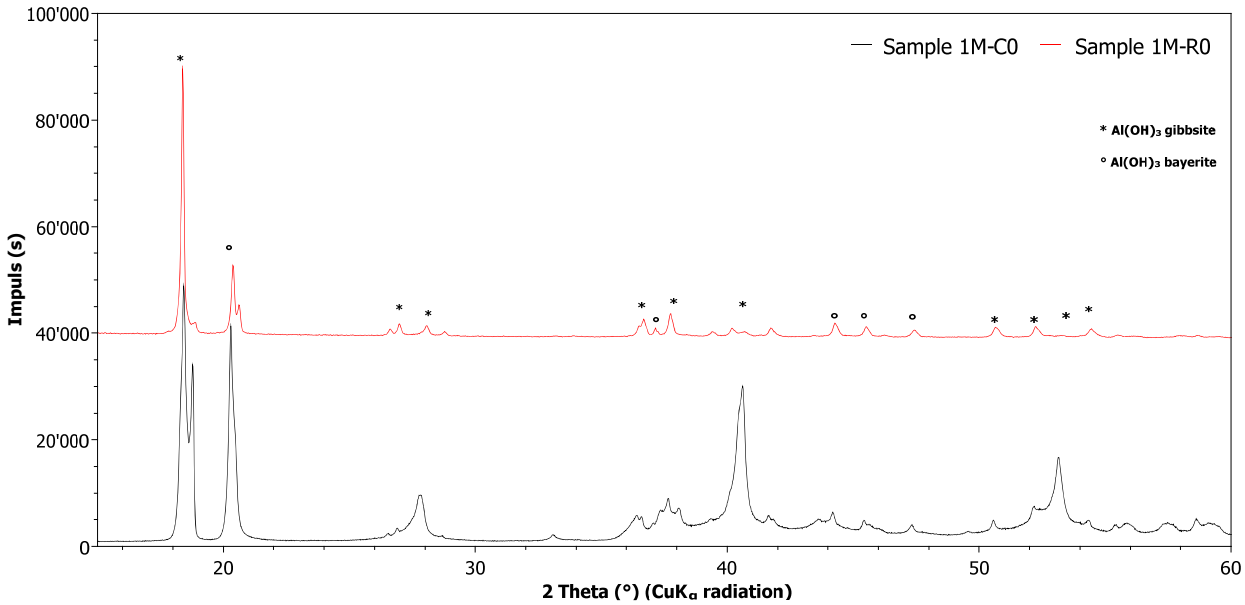

Figure 49: XRD diffraction pattern of the 1M_C sample from the 1 M NaOH chemistry lab experiment and sample 1M_R obtained from the 1 M NaOH experiment with the 400 W converter; the solid by-products consist of gibbsite and bayerite.

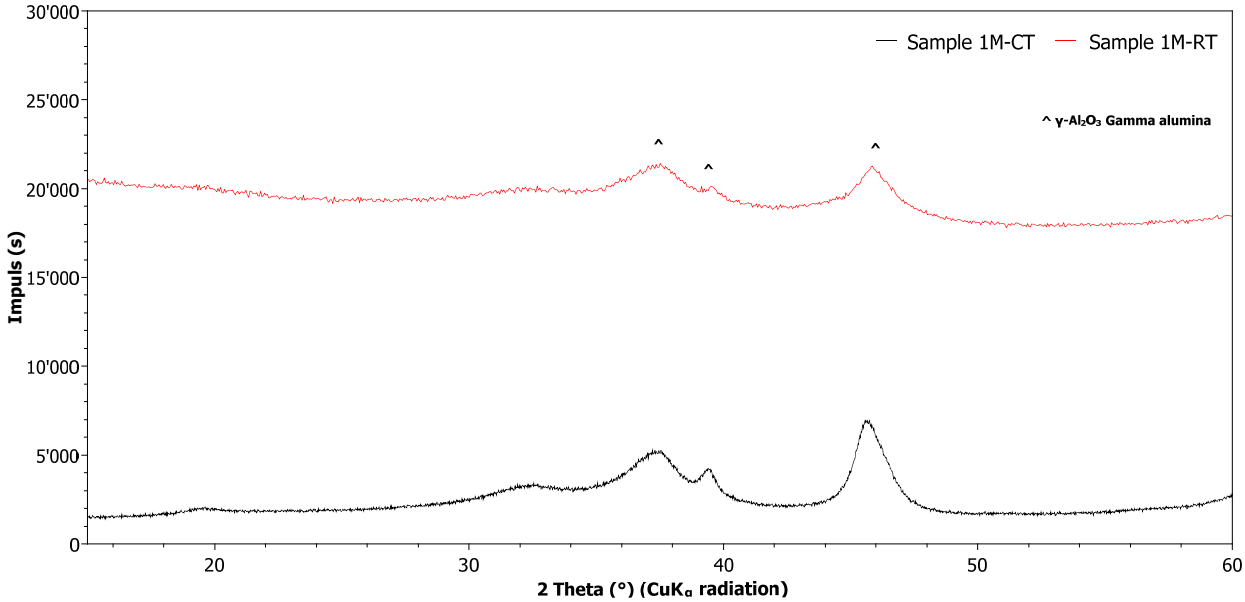

Figure 50: XRD diffraction pattern of the annealed sample (thermal treatment at 900 °C) obtained from the 1 M NaOH chemistry lab experiment (1M-CT) and sample 1M-RT obtained from the 1 M NaOH experiment with the 400 W converter.

6.2.3 DSC

Thermal phase transition of $Al(OH)_3$ (a mixture of gibbsite and bayerite) was studied using DSC from 25°C° to 500°C for the following samples:

- 1M_C sample from the 1 M NaOH chemistry lab experiment;

- 1M_R sample obtained from the 1 M NaOH experiment with the 400 W converter;

The DSC thermograms of these samples are presented in Figure 51 and Figure 52. As can be observed from Figure 51, the DSC thermogram of $Al(OH)_3$ exhibited three endothermic peaks in case of sample 1M_C, respectively two for sample 1M_R. Although both samples consist of $Al(OH)_3$, as indicated by the XRD results, the crystalline structure is not identical, which might explain the differences in the peak's position and heat associated to different phase transition.

All endothermic peaks appear in the range 212-297°C (Table 17). They might be due to elimination of bonded water and possible phase transition from aluminium hydroxide (gibbsite) to aluminium oxide hydroxide (boehmite). The formation of boehmite was reported in the temperature range 177°C - 377°C [25]. Another possible phase transition is from bayerite to boehmite. The formation of boehmite from bayerite was reported in the temperature range of 200°C to 300°C.

Table 17: *Summary of the DSC results.*

	First peak		Second peak		Third peak	
Sample	Heat (J/g)	T (°C)	Heat (J/g)	T (°C)	Heat (J/g)	T (°C)
1M_C	-179.15	222.15	-66.4	244.52	-634.14	281.67
1M_R	-18.21	224.92	-	-	-856.95	297.01

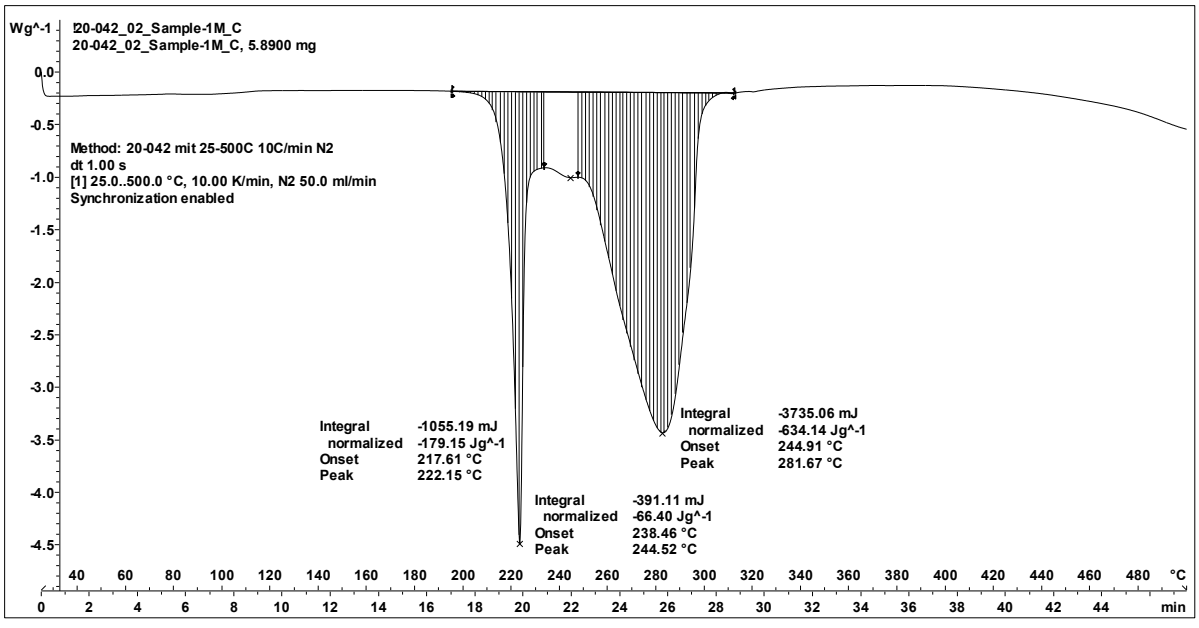

Figure 51: DSC thermogram of the sample 1M_C obtained from 1 M NaOH chemical lab experiments.

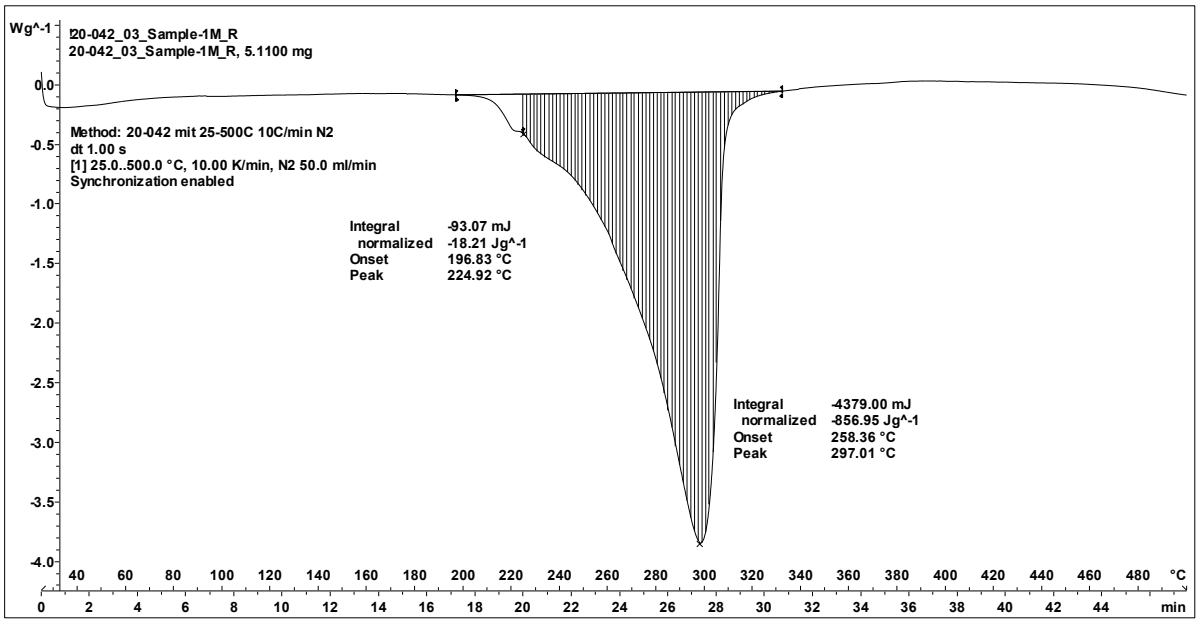

Figure 52: DSC thermogram of the sample obtained from 1 M NaOH experiment with the 400 W converter.

6.2.4 TGA

During the thermal analysis, the weight loss was monitored while the temperature was increased from room temperature (25°C) to 900°C. Based on the mass loss, information about dehydration and phase transitions can be obtained. The mass loss is shown in Figure 53 and Figure 54, together with the heat flow evolution.

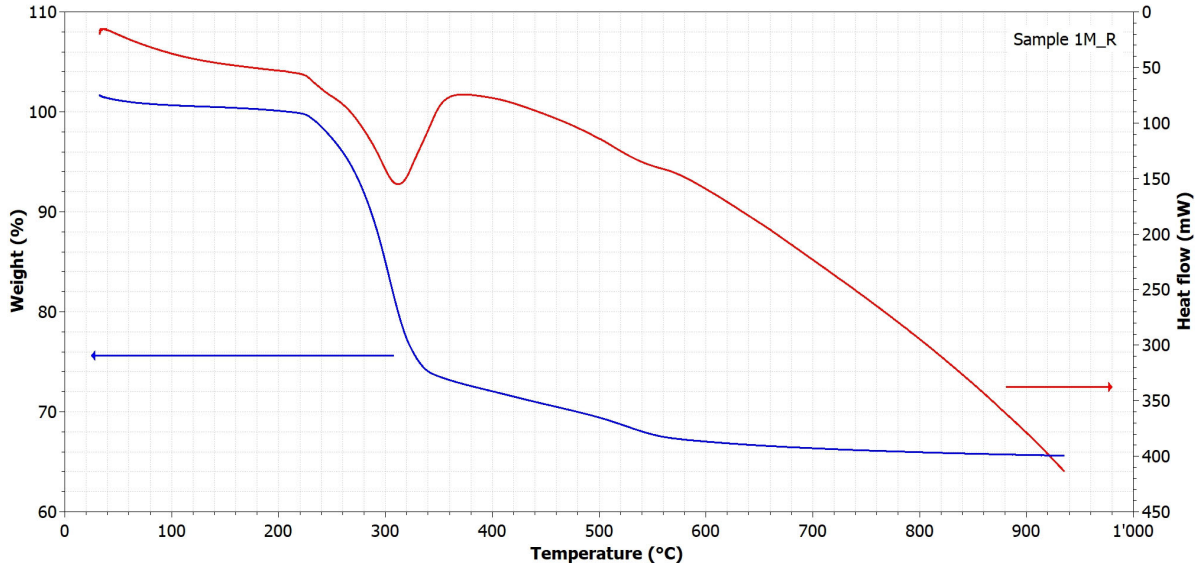

Figure 53: TGA of the sample obtained from 1 M NaOH experiment with the 400 W converter.

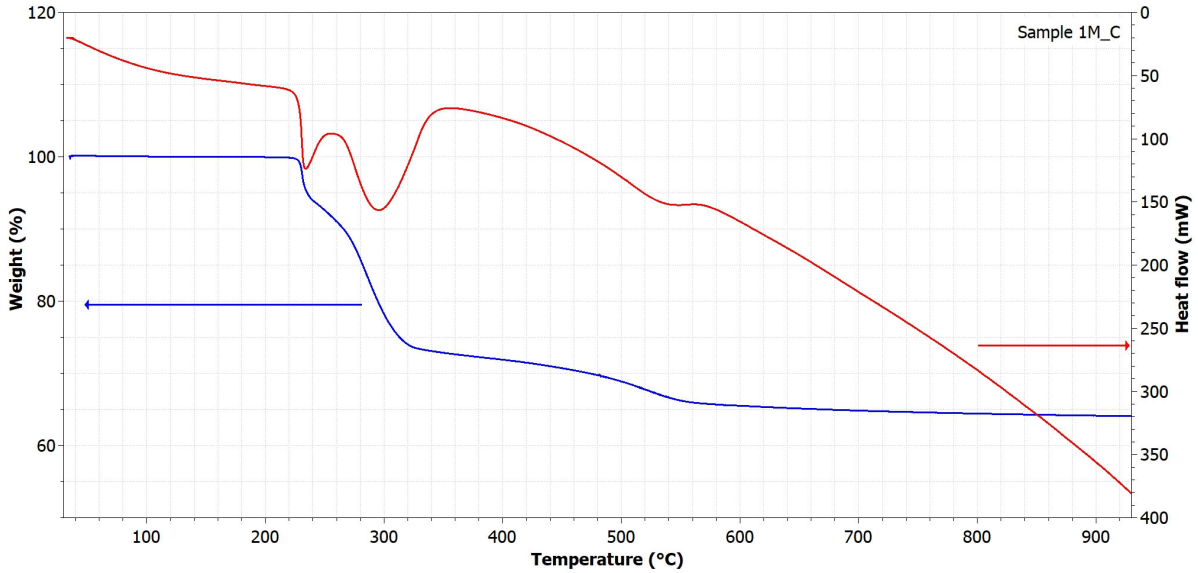

Figure 54: TGA of the sample obtained from 1 M NaOH experiment from the chemistry lab.

The first mass loss (0.2 – 1%, below 210 °C) is associated to (bonded) water loss. The second one of about 27% occurs between 210 °C and 355 °C (including two distinct peaks), indicating a dihydroxylation process and most likely formation of boehmite as reported in [24]. A third mass loss (of about 8-9%) marks the formation of gamma-alumina (confirmed by XRD) from boehmite.

A summary of the water loss on different temperature levels is shown in Figure 55 and Figure 56 for sample 1M_C and 1M_R, respectively.

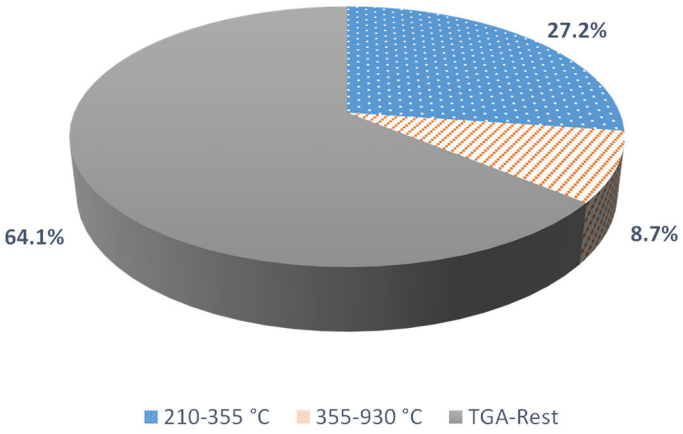

Figure 55: TGA mass fractions for sample 1M_C, temperature ranges are given for the respective weight loss.

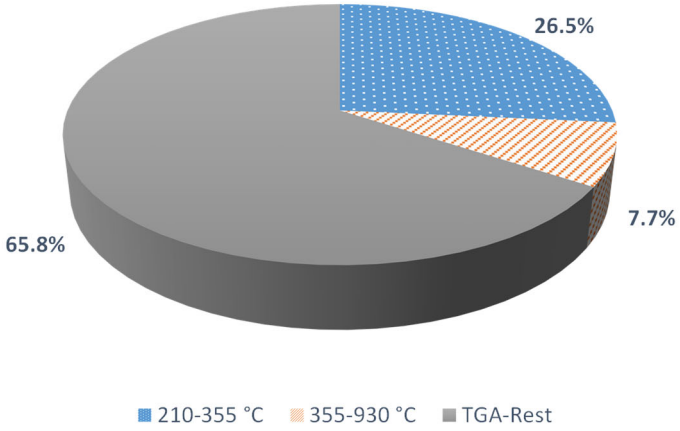

Figure 56: TGA mass fractions for sample 1M_R, temperature ranges are given for the respective weight loss.

Based on the general scheme of thermal decomposition of aluminium hydroxides from [24] (page 46-47), and the results described above, a transformation from gibbsite/bayerite to boehmite and then to gamma alumina is proposed for the HybridStock solid samples in the TGA.

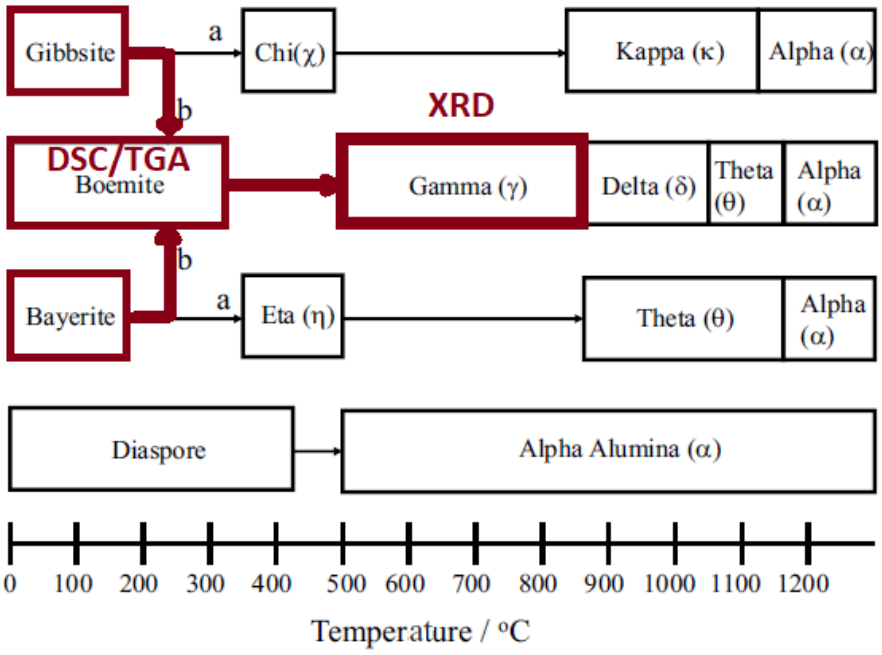

Figure 57: Phase transformation from aluminium hydroxide to gamma-alumina; with dark red indicating the path that the thermal decomposition of aluminium hydroxide is likely to follow, and the measurement techniques used for the corresponding analysis.

6.3 Discussion

The experimental investigations presented in this chapter confirm that the solid product of the Al-water reaction is $Al(OH)_3$. In the temperature range (60-70°C), both gibbsite and bayerite are obtained as the main products. Simple drying procedures at ambient air may be effective for removing most of the additional water. Conversion to gamma-alumina was successful as shown by thermal treatment and subsequent XRD analysis. Thermal energy is required at temperatures of 200 – 250 °C (conversion to oxide-hydroxide / boehmite), and to a smaller extent also above 500 °C (conversion of boehmite to gamma-alumina).

7 Charging Reactions – Power-to-Al

7.1 Methodology

The state of the art on inert anode aluminium production is investigated based on two approaches: Literature review and interviews with experts.

7.2 Results

7.2.1 Literature

The state of the art on inert anodes for aluminium production has been published in a book edited by Galasiu et al. in 2007 [26]. An update on inert anode developments has been written by Pawlek in 2016 [27], and additional information has been published recently (2019) by Gupta and Basu [28]. The principle difference between the more than 100 year old Hall-Héroult process and the newer approaches with inert anodes has been described in the feasibility study that preceded this project and report [9].

Carbon anodes are used and consumed in the Hall-Héroult process at a rate of about 400 kg per tonne aluminium, leading to direct CO_2 emissions as well as emissions of carbon fluorides (CF_X) with strong global warming potential. In contrast, inert anodes or non-consumable anodes release O_2 instead of CO_2 and do not contribute to CF_X emissions. It has to be noted that these inert anodes are never fully inert but only consumed at a very slow rate. Whereas carbon anodes have to be replaced every month or two – thus being a considerable cost factor – inert anodes have the potential to last one or more year before they have to be replaced and the worn anodes are recycled. Furthermore, the cell voltage is likely to be higher for an inert anode process since the reaction at the anode is different (production of O_2 instead of CO_2, decomposition potential 2.2 V instead of 1.2 V). This means that theoretically more electric energy is needed to produce the same amount of aluminium. This is compensated by not converting carbon to CO_2, thereby saving the energy input that can be attributed to the carbon. Thus, the overall energy balance may still be considerably better for the inert anode cell.

As a matter of fact, conventional Hall-Héroult cells consume about 13-15 kWh electric energy per kg Al, with best reported values of 11.5 kWh_{el}/kg Al in a communication by Norsk-Hydro in 2018 [29]. Adding the energy content of 400 kg C (3.6 kWh per kg Al) sums up to a total energy requirement of 15.1 kWh per kg Al. Considering that from the produced aluminium 0.112 kg H_2 and 4.2 kWh heat can be produced, the conversion efficiency of the best case Hall-Héroult cell is 57%:

Eq. 3 $$\eta_{Hall-Héroult} = \frac{m_{H_2} \cdot HHV_{H_2} + \Delta H_r}{W_{el} + m_C \cdot HHV_C} = \frac{0.112kg \cdot 39.4kWh/kg + 4.2kWh}{11.5\ kWh + 0.4kg \cdot 9.11kWh/kg} = 0.57$$

Inert anodes can be arranged vertically, whereas the traditional carbon anodes are always arranged such that the main contact area with the electrolyte is horizontal. Cells with vertical anodes can be constructed more compact, i.e. smaller for the same capacity, and floor area can be saved. Furthermore, also the distance between the cathode and the anode and thus, voltage drop across the electrolyte may be reduced. There is also the potential to reduce the

electrolyte temperatures from 960 °C of the Hall-Héroult cell to around 700 °C and to reduce heat losses. According to expert's opinion, vertical inert anode cells may be operated with as little as 13.2 kWh_{el} per kg Al.

This corresponds to a total efficiency for the aluminium electrolysis of 65%:

$$\eta_{inert-anode\ cell} = \frac{0.112kg \cdot 39.4kWh/kg + 4.2kWh}{13.2kWh} = 0.65$$

Looking at recently filed patents in the field of inert anode aluminium smelter cells[5], the list of companies that are active in this field is long. Some of the well-known players that have been active in this field are Alcoa, Rusal, RioTinto, Aluminium Corporation of China, and Pechiney Aluminium. These companies have little interest to publish their advancements in a scientific way, and thus little to no information can be obtained concerning the type of anode, the composition of the electrolyte, the duration of their experiment or the size of prototype cells used, besides the information given in the patents themselves. Some of the more noteworthy developments were information is available are:

- ***Moltech Technology Center*** successfully tested a horizontal metal anode for aluminium production in a 4 kA pilot cell already in 2006, and then applied this technology also to a 25 kA industrial test cell [30]. There was no continuation of the development because of lack of funding.
- ***Arctus Metals*** and the Innovation Centre Island develop inert anode smelter technology based on patents owned by Arctus [31]. Recent advancement has been published by Gunnarson et al. in 2019 [32]. Production of aluminium was successful with an inert metal (Cu/Fe/Ni) anode in low temperature (800 °C) electrolyte for several hours in a small crucible. Impurities of the aluminium obtained were low with 0.2 wt%, of which 0.1 wt% iron. This development is on-going with goals to test rectangular cells of 1 kA current and then upscale to 100 kA or higher.
- ***RioTinto*** lead the EU funded project AGRAL [33], where anodes made from cermet powders were produced and tested. According to a project report [34], this development will not be exploited but RioTinto will focus on the joint venture ELYSIS instead (see below).
- ***ELYSIS***[6] is a joint venture of RioTinto and Alcoa that started in 2018 and is supported with funding by Apple, the Canadian Government and the Québec Government [29,35]. The development is based on previous work by Alco, and ELYSIS **announced to enter market with inert anode smelter cells for aluminium production by 2024**. According to the online magazine Metalbulletin [12]: “Alcoa had been quietly working on the technology to produce emissions-free metal for some time: it began in 2009 at the US producer’s Pittsburgh Technology Center, with around 700 tonnes produced so far”.

[5] search in Espacenet: CPC: C25C3/12, plus keywords "inert" and "anode" in title or abstract.

[6] https://www.elysis.com, accessed Sep. 6h, 2019.

7.2.2 Interviews with experts

Nine experts on inert anode aluminium production have been contacted and interviewed, most of them we have been able to meet personally.

Out of the nine experts, eight were convinced that inert anode aluminium production is possible also at an industrial scale, and will eventually become the state of the art. Some of them indicated clearly that they believe that governments will increase pressure on aluminium industry in order to push reduction of CO_2 emissions, and that CO_2-taxes may play an important role for the introduction of inert anodes smelter technologies, because economic break-even compared to current technology will be reached faster with higher CO_2-taxes.

Several experts claimed that although upscaling to commercial size smelters is still a challenge, inert anode aluminium production at relevant scale is already possible today. Lifetime of anodes and cell materials, impurities in the produced aluminium that stem from the anode material, and economic reasons have so far hindered the introduction of inert anode technologies in the market.

7.3 Discussion

Inert anode smelters are preferred over the conventional Hall-Héroult smelters because of a much better carbon footprint that stems from the anode process that releases oxygen instead of CO_2.

Although inert anode smelters are not commercially available yet, large industrial players like Elysis (joint venture of Alcoa and Rio Tinto) have announced that they are already today capable of running such a process also at large scale, and that they will introduce this technology into the markets by 2024. This would open the opportunity to use an environmental friendly aluminium production process for "Power-to-Al", the conversion of electric energy into energy that is stored chemically in Al, free of CO_2 emissions and with a conversion efficiency that is estimated by experts to reach 65%.

Most experts agree that eventually inert anode Al smelters will be available and will replace the current Hall-Héroult process. This revolution of the Al industry may come sooner, the sooner the Al industry will have to pay significant CO_2-taxes for the emissions of the currently used Hall-Héroult process.

8 System Simulations

A system that supplies heat and electricity to a multifamily building with six apartments as shown in Figure 58 has been simulated in TRNSYS 18. The only primary energy sources used for this system are a large photovoltaic rooftop installation and on-site harvested ambient heat for the heat pump. Short-term storage of heat in a thermal energy storage (TES) and of electricity in a home battery are used to even out mismatches between solar yield and demand of electricity (and heat). An aluminium energy storage cycle is used to store solar energy seasonally. The approach and results were published in a journal article and in a conference paper [13,36]. The system and simulation results are summarized in the following sections.

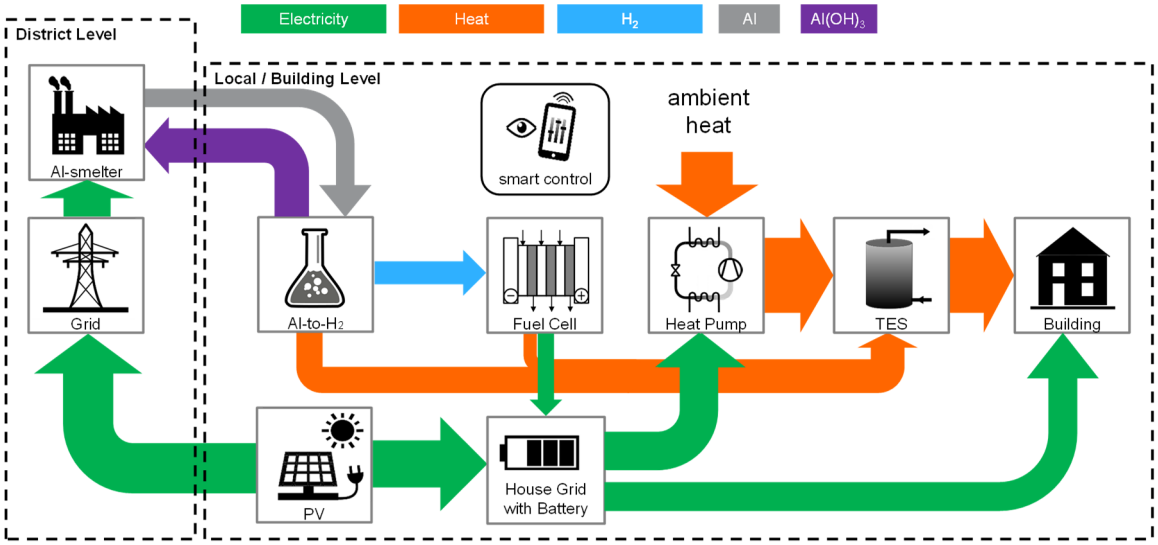

Figure 58: Schematic system concept for heat and electricity provided 100% by a photovoltaic and heat pump system with a seasonal aluminium redox storage cycle [13].

8.1 Procedures and Methodology

8.1.1 Weather data and loads

Weather data was based on Design Reference Years (1984-2003) for Davos (DAV), Geneva (GEN), Zurich (KLO) and Locarno (OTL) from SIA (Swiss society of engineers and architects) [37].

The multi-family house (MFH), described by Mojic et al. [38], with six dwellings has a reference floor area of 1205 m^2 and meets the Swiss Minergie requirements. The Load Profile Generator [39] was used to create Household Electricity (HH_{El}) and Domestic Hot Water (DHW) demand. Different DHW and electricity profiles were chosen for the different apartments, and aggregated into one overall HH_{El} and one DHW profile for the building. An overview of the electricity and heat loads is given in Table 18.

Table 18: Specific and yearly demands for space heating, domestic hot water and electricity for the multi-family building in Zurich.

Energetic use	Specific demand[a)]	Total
	kWh/m^2	MWh
Space heating	27.1	29.1
Domestic hot water (without/with circulation)	15.5/20.2	16.6/21.7
Household electricity	18.4	19.7

a) demand per heated floor surface area.

8.1.2 Sizing, efficiency and cost of components

Sizes of the components in terms of power and capacity are shown in Table 19. The size of the PV field was varied in the range of 25 to 76 kWp, which corresponds to areas of 150 to 450 m^2 for modules with 16.8% efficiency. Assumptions used for the conversion efficiency of the aluminium cycle components and processes are shown in Table 20.

Table 19: Sizes of main components used for the provision of heat and electricity in a multi-family building [13].

Device	***Size***
Al-to-H_2 converter	5 kg/h
Fuel cell	10 kW_{el}
Heat pump	26 kW_{th}
Battery	100 kWh
TES	3 m^3

Table 20: Assumptions for conversion efficiencies and cost of system components.

Device	***Process***	***Efficiency***	***Cost***
Photovoltaics	Solar to AC	Efficiency of module: 16.8%, temperature coefficient: -0.391/K, loss of rectifier 4.7%[a)]	1'000 € + 700 €/kWp
Al-to-Energy	Al to H_2, heat and $Al(OH)_3$	95% of stoichiometric value for H_2 production, 95%[b)] total (H_2 or heat)	1'500 € + 1'300 €/(kg/h)[c)]
Fuel cell	H_2 to electricity and heat	50% of HHV for electricity, 95% of HHV total	1'000 € + 1'000 €/kW_{el}
Power-to-Al	$Al(OH)_3$ to Al	58.7% calcination + smelter[d)]	1.2 €/kg Al[e)]
Home battery	Storage of electricity	88% roundtrip on annual base[f)]	450 € + 230 €/kWh
Heat pump	El. and ambient heat to useful heat	SPF = 4.0[f)]	6'000 € + 450 €/kW_{th}
TES	Storage of heat		700 € + 700 €/m^3

a) rectifier losses have been assumed as depending on the DC power from the PV field, matched to the efficiency curve of Fronius Symo 4.5-3-S

b) based on 8.7 kWh/kg for Al and HHV(Higher Heating Value) of H_2

c) value is extremely uncertain since there are no such devices on the market yet

d) 1.6 kWh/kg Al for calcination and 13.2 kWh/kg Al (65% efficiency) for the inert electrode smelter process

e) including cost of transport between industrial site and end-consumer

f) results from TRNSYS simulations

8.1.3 Key performance indicators

Energetic key performance indicators (KPI) are:

- **PV generation ratio** $\mathbf{R_{PV,gen}} = \boldsymbol{W_{PV}}/(\boldsymbol{W_{used}} + \boldsymbol{W_{smelter}})$,
  where W_{PV} is the electricity generated by the PV field, W_{used} is the electricity consumed in the building including all losses and $W_{smelter}$ is the electricity used to regenerate the aluminium in the Al-smelter;
- **self-sufficiency ratio** $\mathbf{R_{self,suff}} = (\boldsymbol{W_{used}} - \boldsymbol{W_{grid}})/\boldsymbol{W_{used}}$,
  where W_{grid} is the electricity purchased from the grid.

The **economic** KPI used is:

- **levelized cost of energy in €/kWh,**
  using the annuity method described in VDI 2607 [40], interest rate 3%.

And the **environmental** KPI that were used are:

- **CED_{tot}:** Cumulated total primary Energy Demand
- **CED_{nr}:** Cumulated non-renewable primary Energy Demand
- **GWP_{100a}:** Global Warming Potential for 100 years, IPCC 2013

8.1.4 Environmental LCA data sources

LCA data was based on SimaPro 8.3.0.0, with inventory data from the Ecoinvent database version 3.3, using the “cut-off” system model. Linear extrapolation was used to match the size of the component if the data in the database was for a different component size. The impact of the Al-to-H_2 converter is assumed to be negligible. It was assumed that bauxite is only mined once and then the energy cycle can be run for at least 30 years with the alumina obtained, i.e. the impact of bauxite mining was counted with a factor of 0.033. More details are given in [13]. For the environmental evaluation, the new system concept with the aluminium seasonal energy storage was compared with a conventional gas boiler for heating and DHW preparation in combination with electricity from the ENTSO-E grid (low voltage level).

8.1.5 OPEX

Maintenance cost are assumed to be 1% of the investment cost (CAPEX) per year. Transport of electricity through the grid, mainly from local PV production to the smelter plant, is reimbursed with 0.05 €/kWh. Additionally, the energy service company that is running the aluminium smelter plant (including calcination and transport of Al_2O_3 and $Al(OH)_3$) is reimbursed with 1.2 € per kg Al. Based on literature [30] it can be assumed that aluminium can be produced at a cost of 150 – 300 US$/ton with non-carbon electrode technology. Assuming an operation only during summer season increases this value to at least 400 €/ton. Thus, from the 1.2 € per kg, 0.4 €/kg are used for smelter operation and 0.8 €/kg are left for transport cost and margins.

8.2 Results

8.2.1 Energetic balance for Zurich

Monthly energy balances for the system are shown in Figure 59, and are composed of:

Inputs

- **Heat from air:** renewable heat from air used by the air source heat pump.
- **Heat from Al-to-H_2 and fuel cell:** heat released by the Al-converter and the fuel cell.
- **PV to system**: total net AC electricity provided by the PV system (field and inverters) to local equipment (battery, household, heat pump system), i.e. without PV to grid.
- **El from grid:** total electricity purchased from the grid.
- **El from fuel cell:** electricity provide by the fuel cell.

Outputs

- **DHW:** demand of Domestic Hot Water.
- **SH:** space heating demand
- **HH El:** household electricity demand
- **Loss heat and El:** heat losses of the storage tank, pipes and the electrical losses of the battery.

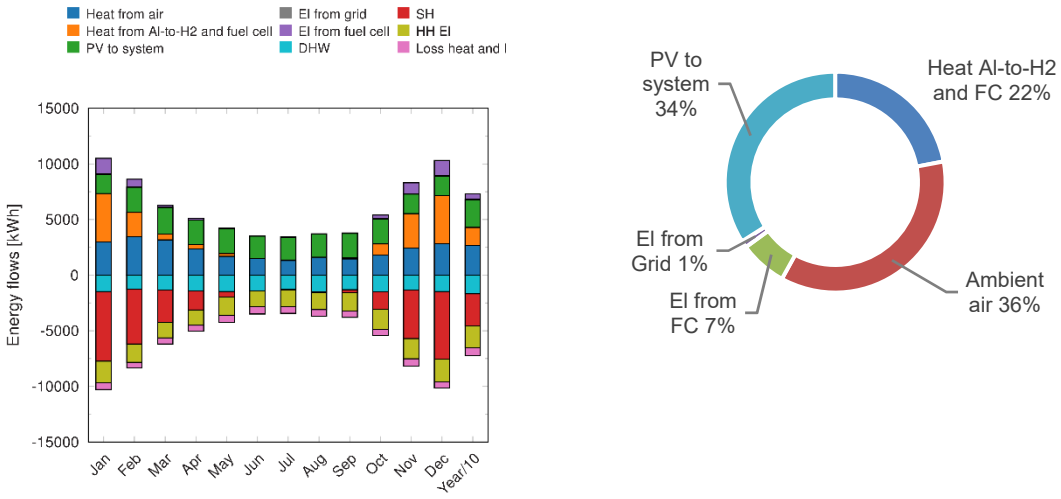

Figure 59: Monthly distribution of overall energy flows (left) and yearly share of energy flows into the system (right). Results for Zurich with 60 kW_p PV field and a battery of 100 kWh with a $R_{PV,gen}$ of 100% and $R_{self,suff}$ of 99%,[13].

8.2.2 Energy cost for Zurich

Table 21: Investment cost and energy generation cost using a 100 kWh battery for Zurich. Interest rate for annuity calculation: 3% *[13]*.

Major Component	Costs [€]	Size	Life time [years]	Total Costs [€]
PV	1'000+700/kW_p	60 kW_p	25	43'350
Battery	450+230/kWh	100 kWh	15	23'450
Thermal Storage	700+700/m^3	3.5 m^3	40	3'150
Heat pump	6'000+450/kW	26 kW	25	17'700
Fuel Cell	1'000+1'000/kW_{el}	10 kW_{el}	20	11'000
Al converter	1'500+1300/kg/h	5 kg/h	25	8'000
	Total Investment Cost			**106'650**
Annuity cost	yearly costs over lifetime			13'131/a
	Investment			6'805/a
	Electricity from grid (0.3 €/kWh)		289 kWh	87/a
	Maintenance (1% of investment cost)			1'066/a
	Aluminium fuel service (1.2 €/kg)		2'662 kg	3'195/a
	Transmission grid (0.05 €/kWh)		39'934 kWh	1'997/a
Energy generation costs	Based on annuity cost		**0.20**	**€/kWh**

8.2.3 PV size, energy cost and amount of Al needed for different locations

Differences in heat demand for the different locations and climates that were simulated are shown in Table 22.

Table 22: Specific and yearly demands for space heating depending on the location, [13].

Location	***Specific SH demand***[a)]	***Total SH demand***
	kWh/m²	***MWh***
Davos	42.0	42.9
Zurich	27.1	29.1
Geneva	24.2	22.6
Locarno	16.6	17.8

a) Demand per heated floor surface area.

Size of the PV generation system, levelized cost of energy and the amount of Al needed for the Al seasonal energy storage cycle vary between different locations and climates, as shown in Table 23 for results where $R_{PVgen} \approx 100\%$.

Table 23: Cost and installed PV capacity that reach an R_{PVgen} > 99% and $R_{self,suff}$ >98% with a battery of 100 kWh, [13].

Location	Capacity of PV system	Cost	Amount of Al
	kW_p (m^2)[a)]	€/kWh	kg
Davos	42.3 (252 m^2)	0.14	2198
Zurich	60.5 (360 m^2)	0.20	2662
Geneva	48.7 (290 m^2)	0.20	2740
Locarno	39 (232 m^2)	0.19	1858

a) Area is calculated with a nominal power of 186 W/m^2. Lower areas are needed for modules with higher efficiency.

8.2.4 Global warming potential – GWP100

The GWP (100a) of the new system, compared to conventional natural gas heating and electricity from ENTSO-E grid, are displayed in Figure 60. Two variants for the electricity for the system and the location of the smelter are shown. The first variant is a smelter plant in Island that uses local hydropower, and local hydropower is also assumed as a source for the electricity whenever PV was able to provide the electricity in the simulations shown before. In this case, the Al fuel is transported from Island to Switzerland and $Al(OH)_3$ back to Island by waterways between Island and Basel, and an additional 100 km by road (conventional lorry) to the site of the building. Thus, CO_2 emissions of transport (dark blue bar below the brown bar) are quite more significant than in the second case where local Swiss PV is used for the smelter and on-site, and only 100 km road transport is included between the smelter plant and the building. However, in neither of the two cases CO_2 emissions of the transport play a significant role. The production, installation and later disposal of the PV-system of the Swiss PV variant is the largest contributor to the overall GWP. Another important contributor to the GWP are the carbon anodes that are used if the aluminium smelter process is run with the conventional Hall-Héroult process (shown in light grey). With inert anode smelter cells, these emissions can be avoided. Using hydroelectricity in combination with an inert electrode Al-smelter process, GWP_{100} can be reduced by a factor of five, even though a smelter in Island and a building in Switzerland have been assumed with corresponding transport distances for the Al fuel and for the $Al(OH)_3$. Using local produced PV electricity, the reduction factor is more than two.

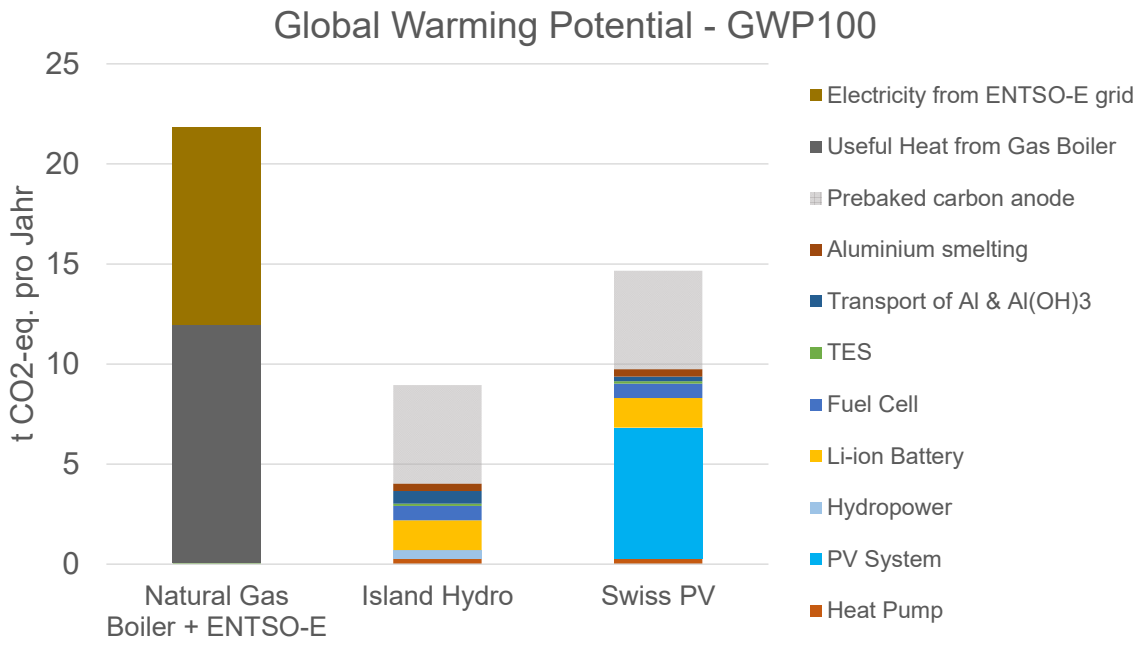

Figure 60: Global warming potential (GWP 100a) for a conventional gas boiler and grid electricity system and for the 100% solar driven heat and electricity system with seasonal Al energy storage (Swiss PV), as well as for a variant where PV electricity has been replaced by local hydropower for an aluminium smelter in island as well as for the local supply of electricity at times when PV is usually available in Switzerland. The impact of the carbon electrode consumption of the conventional Hall-Héroult process is shown light texturized since it is not envisaged to be part of the final system concept, [13].

It is worth noting that the contribution by the PV system is also due to the fact that data that was used was based on small rooftop installations and the data-set may not have been updated to the newest research findings. Thus, the GWP of the PV production was 107 $gCO_{2,aq}$/kWh (lifetime 25 years), whereas publications since 2014 show values between 20 and 80 $gCO_{2,aq}$/kWh for irradiations of 1200 – 2000 kWh/m^2 [41]. Using electricity from wind with 10.6 $gCO_{2,aq}$/kWh, [42] similar results as for hydropower (12.4 $gCO_{2,aq}$/kWh, [42]) can be achieved.

8.3 Discussion

The simulation of a multifamily building in the climate of Zurich shows, that 300 – 500 kg Al per living unit would be enough for seasonal storage of energy needed in order to supply the building with heat and with electricity all year around in combination with PV, a heat pump, a PEM fuel cell and thermal as well as electrical short term (diurnal) storage options.

The economic analysis shows that by the year of 2030, with the expected cost decrease for PV systems, batteries and fuel cells, a mixed end-user all-inclusive (CAPEX + OPEX) energy price of 0.2 €/kWh seems possible.

The LCA of the overall energy cycle shows that even with the conventional Hall-Héroult process run by rooftop PV electricity the system that uses the Power-to-Al and Al-to-Energy seasonal storage cycle reduces GWP of the heat and electricity supply compared to a

conventional gas boiler and electricity from the ENTSO-E grid considerable. Even larger reductions are possible when the conventional Hall-Héroult process is replaced with an inert anode Al smelter process, and when hydro or wind power can be used instead of rooftop photovoltaics. Transport of Al from a smelter plant to the end-user and of $Al(OH)_3$ back to the plant has no significant effect on the GWP when road transport of 100 km between the two sites is included. Even additional transport from Basel to Island and back by waterways does not increase the GWP of the transport to significant levels compared to the overall system emissions.

9 Conclusions

The oxidation of aluminium in aqueous solution under alkaline conditions (aqueous NaOH solutions) is straightforward and highly efficient. No significant obstacles have been encountered so far. Aluminium samples of different shapes and different origins have been tested and it showed – as expected – that the main influencing parameters that determine the hydrogen production rate are temperature, alkalinity, and the specific surface area of the aluminium samples. Based on an analysis of feasibility and risk, small aluminium grains (larger than 0.5 mm) have been identified as a promising solution for the shape of the aluminium renewable fuel.

Laboratory experiments have shown that with higher alkalinity of the solution, also the maximum concentration of dissolved Al species increases. However, for all concentrations of NaOH that were tested, eventually a point is reached where precipitation of Al species occurs. Just before this point is reached, reaction has been shown to slow down temporarily, but recover to a steady value after precipitation starts. Just as expected, the solid products that precipitated were $Al(OH)_3$ (bayerite and gibbsite), which was confirmed by XRD analysis. With thermal treatment, these solid products were successfully converted to gamma-alumina, which may serve as a starting point for obtaining smelter grade alumina that can be re-introduced into the aluminium production process and thus the material cycle may eventually be closed.

A small unit for the conversion of 0.5 g Al per batch has been able to provide hydrogen gas of extremely high purity that was used directly (after dehumidification) in a 12 W PEM fuel cell. Based on this first small scale prototype batch converter, a larger unit for operation with 5.1 g Al per hour and a total power of 400 W (200 W thermal and 200 W in from of the energy contained in the produced hydrogen) was successfully designed and tested for several hours. Conversion efficiencies were higher than 95% of the theoretical maximum for some of the reaction conditions that were tested. Thus, the Al-to-H_2 unit produced roughly the amount of heat and hydrogen expected from the stoichiometry of the reaction and of the enthalpy of reaction. A combination with a 100 W commercial PEM fuel cell has been demonstrated successfully.

Although within this project only units for Al-to-Energy, i.e. units for the production of heat and electricity from Al, have been developed, also the likelihood for an environmental friendly Power-to-Al process has been investigated. There are good chances that inert anode smelters for the conversion of alumina to elementary Al will start replacing the conventional Hall-Héroult process within this decade, as industry has announced the market introduction of the new process by 2024. These new processes are expected to reach a Power-to-Al efficiency of roughly 65% when fully implemented and optimized. This will open up the opportunity to further reduce the carbon footprint and GWP of the seasonal energy storage cycle based on Al as a chemical energy carrier.

Last but not least, also the economic viability of small CHP units based on Al renewable fuel for covering the buildings' heat and electricity needs look promising: final end-user prices of 0.2 €/kWh (mixed heat and electricity, CAPEX and OPEX included). This values is calculated for the entire heat and electricity providing system that includes roughly 300 – 500 kg Al as a seasonal energy storage material and covers both heat and electricity all year around based on solar energy from the roof.

10 Outlook and Next Steps

The next steps will be the development of a larger conversion unit for 1 kW electric power and 3 kW thermal output, in combination with attempts to close the material cycle by using the solid products from the Al-to-Energy conversion unit – after pre-treatment – for an inert electrode smelter process. For these next steps, further funding is needed.

11 National and International Collaboration

The topic of energy storage in aluminium is currently only investigated in a few places in Europe and internationally.

Contacts have been established with the relevant working groups and industry in Europe that can provide inert anode aluminium smelters at lab-scale. Several groups with known activity in this field have been visited on site. The impression of field visits and expert interviews confirms that significant progress has been made in this field.

Contacts to research groups and experts on topics related to this project included former employees of Alu-Suisse and related companies in Switzerland as well as experts from Spain, Israel, Norway, Island, Romania, and Canada.

Applications for funding further cooperative work under the EU H2020 programme have been filed with some of the national or international contacts.

12 Communication

12.1 Conferences and Symposia

The project and its results have been presented in the following conferences and symposia:

- Keynote presentation at ***EuroSun 2018***, Rapperswil [43];
- ***IRES 2019***, Düsseldorf, presentation;
- ***Clima 2019***, Bucharest, presentation and conference paper [44];
- ***Solar World Congress 2019***, Chile, presentation and conference paper [45];
- ***SPF Industrietag SPF 2019***, poster and presentation / demonstration;
- ***Annual Symposium of the SCCER HaE,*** 5. Nov. 2019, invited oral presentation;
- ***Conexio Symposium Thermische Solarenergie 2020***, Bad Staffelstein, Mai 2020, presentation and conference paper [36];
- ***Brenet Status Seminar 2020***, 3.+4. September 2020, Aarau, oral presentation.

12.2 Media

A ***press release*** on the new seasonal storage concept has been launched on 25.09.2018 [46] and has received much attention especially in Germany. Additionally, a coverage by Benedikt Vogel on behalf of the SFOE has led to some reports in magazines and online-news. Some of the media that have reported on the project are:

- Ostschweiz am Sonntag [47];
- Solarthemen+ (www.solarthemen.de) [48,49];
- PV Magazine (www.pv-magazine.de) [50];
- Windjournal (www.windjournal.de) [51];
- ee-news (www.eenews.ch) [52];
- Sonnenseite (www.sonnenseite.com) [53];
- Sonnenenergie (www.sonnenenergie.de) [54];
- NZZ am Sonntag [55];
- energate messenger (www.energate-messenger.ch) [56];
- ee-news (www.ee-news.ch) [57];
- Aluminium Praxis [58];
- etc.

13 Publications

13.1 Journal Articles

- Haller MY, Carbonell D, Dudita M, Zenhäusern D, Häberle A. Seasonal energy storage in aluminium for 100 percent solar heat and electricity supply. ***Energy Conversion and Management: X*** 2020:100017. https://doi.org/10.1016/j.ecmx.2019.100017, [13].
- Haller MY, Amstad D, Dudita M, Englert A, Häberle A. Combined Heat and Power Production based on Renewable Aluminium-Water Reaction. ***Renewable Energy*** 2021. https://doi.org/10.1016/j.renene.2021.04.104, [14].

13.2 Conference Papers

- Dudita M, Farchado M, Englert A, Carbonell Sanchez D, Haller M. Heat and power storage using aluminium for low and zero energy buildings. E3S Web Conf 2019;111:04008. https://doi.org/10.1051/e3sconf/201911104008 [44];
- Haller M, Dudita M, Amstad D, Carbonell Sanchez D, Häberle A. Seasonal Energy Storage in Aluminium for 100 Percent Solar Space Heat, DHW and Electricity. ISES Solar World Congress 2019, Santiago, Chile: 2019, p. 1312–20. https://doi.org/10.18086/swc.2019.24.04 [45];
- Haller M, Dudita M., Amstad D, Carbonell Sanchez D, Zenhäusern D, Häberle A. Aluminium als saisonaler Energiespeicher für Solarenergie, Online Conference Due to

Corona Virus - Usual Place: Kloster Banz, Bad Staffelstein, Germany: 2020, p. 80–87 [36];

- Haller M, Amstad D, Dudita M, Carbonell D, Zenhäusern D. Aluminium als Heizölersatz – Auf dem Weg zu einem erneuerbaren Energieträger der auch Winterstrom liefert, Brenet Status Seminar 2020, Aarau.

14 References

[1] Jenni J. Das Sonnenhaus - mit hohem solarem Deckungsgrad für Warmwasser und Heizung. 3. Auflage. Oberburg Bei Burgdorf: Jenni Energietechnik AG; 2010.
[2] Jenni J. Speicher in Theorie und Praxis. Oberburg Bei Burgdorf: Jenni Energietechnik AG; 2000.
[3] Energieautarkes MFH Brütten. Umwelt Arena 2018. http://www.umweltarena.ch/uber-uns/energieautarkes-mfh-brutten/ (accessed November 23, 2018).
[4] Vetterli N, Ammann A, Fischer L. Praxisnahe Modellierung für die Planung eines energieautarken Gebäudes. HK-Gebäudetechnik 2015;3/15:36–7.
[5] Wellstein J. Symphonie der Speicher. HK-Gebäudetechnik 2015;3/15:38–9.
[6] Wochele J, Ludwig Chr. Aluminium als Brennstoff und Speicher. Paul Scherrer Institut, im Auftrag des Bundesamtes für Energie; 2004.
[7] Elitzur S, Rosenband V, Gany A. Study of hydrogen production and storage based on aluminum–water reaction. International Journal of Hydrogen Energy 2014;39:6328–34. https://doi.org/10.1016/j.ijhydene.2014.02.037.
[8] Soler L, Macanás J, Munoz M, Casado J. Aluminum and Aluminum Alloys as Sources of Hydrogen for Fuel Cell Applications. Journal of Power Sources 2007;169:144–9. https://doi.org/doi:10.1016/j.jpowsour.2007.01.080.
[9] Haller M, Carbonell D, Dudita M, Zenhäusern D. HePoStAl – Heat and Power Storage in Aluminum. Rapperswil: SPF Institute for Solar Technology; 2018.
[10] Huang X, Gao T, Pan X, Wei D, Lv C, Qin L, et al. A review: Feasibility of hydrogen generation from the reaction between aluminum and water for fuel cell applications. Journal of Power Sources 2013;229:133–40. https://doi.org/10.1016/j.jpowsour.2012.12.016.
[11] Shkolnikov EI, Zhuk AZ, Vlaskin MS. Aluminum as energy carrier: Feasibility analysis and current technologies overview. Renewable and Sustainable Energy Reviews 2011;15:4611–23. https://doi.org/10.1016/j.rser.2011.07.091.
[12] Wang HZ, Leung DYC, Leung MKH, Ni M. A Review on Hydrogen Production Using Aluminum and Aluminum Alloys. Renewable and Sustainable Energy Reviews 2009;13:845–53. https://doi.org/10.1016/j.rser.2008.02.009.
[13] Haller MY, Carbonell D, Dudita M, Zenhäusern D, Häberle A. Seasonal energy storage in aluminium for 100 percent solar heat and electricity supply. Energy Conversion and Management: X 2020;5:100017. https://doi.org/10.1016/j.ecmx.2019.100017.
[14] Haller MY, Amstad D, Dudita M, Englert A, Häberle A. Combined Heat and Power Production based on Renewable Aluminium-Water Reaction. Renewable Energy 2021. https://doi.org/10.1016/j.renene.2021.04.104.
[15] Scholz F, Kahlert H. The calculation of the solubility of metal hydroxides, oxide-hydroxides, and oxides, and their visualisation in logarithmic diagrams. ChemTexts 2015;1:7. https://doi.org/10.1007/s40828-015-0006-0.
[16] Hem JD, Roberson CE. Form and stability of aluminum hydroxide complexes in dilute solution. U.S. G.P.O.,; 1967.
[17] Lydersen E. The Solubility and Hydrolysis of Aqueous Aluminium Hydroxides in Dilute Fresh Waters at Different Temperatures. Hydrology Research 1990;21:195–204. https://doi.org/10.2166/nh.1990.0015.
[18] Gayer KH, Thompson LC, Zajicek OT. The Solubility of Aluminum Hydroxide in Acidic and Basic Media at 25 °c. Can J Chem 1958;36:1268–71. https://doi.org/10.1139/v58-184.
[19] Saukkoriipi J. Theoretical study of the hydrolysis of aluminum complexes. PhD Thesis. University of Oulu, 2010.
[20] Sarpola A. The hydrolysis of aluminium, a mass spectrometric study. 2007.
[21] Teng H-T, Lee T-Y, Chen Y-K, Wang H-W, Cao G. Effect of Al(OH)3 on the hydrogen generation of aluminum–water system. Journal of Power Sources 2012;219:16–21. https://doi.org/10.1016/j.jpowsour.2012.06.077.

[22] Urbonavicius M, Varnagiris S, Pranevicius L, Milcius D. Production of Gamma Alumina Using Plasma-Treated Aluminum and Water Reaction Byproducts. Materials (Basel) 2020;13. https://doi.org/10.3390/ma13061300.
[23] Lamouri S, Hamidouche M, Bouaouadja N, Belhouchet H, Garnier V, Fantozzi G, et al. Control of the γ-alumina to α-alumina phase transformation for an optimized alumina densification. Boletín de La Sociedad Española de Cerámica y Vidrio 2017;56:47–54. https://doi.org/10.1016/j.bsecv.2016.10.001.
[24] Wefers K, Misra C. Oxides and Hydroxides of Aluminum. Alcoa Laboratories; 1987.
[25] Levin I, Brandon D. Metastable Alumina Polymorphs: Crystal Structures and Transition Sequences. Journal of the American Ceramic Society 1998;81:1995–2012. https://doi.org/10.1111/j.1151-2916.1998.tb02581.x.
[26] Galasiu I, Galasiu R, Thonstad J. Inert anodes for aluminium electrolysis. Düsseldorf, Germany: Aluminium-Verlag; 2007.
[27] Pawlek RP. Update on Inert Anodes. Light Metal Age 2016:38–41.
[28] Gupta A, Basu B. Sustainable Primary Aluminium Production: Technology Status and Future Opportunities. Trans Indian Inst Met 2019. https://doi.org/10.1007/s12666-019-01699-9.
[29] Otzen-Odrich K. Bald noch grüneres Aluminium. Aluminium-Praxis 2018;2018:3.
[30] von Kaenel R. Technical and economical evaluation of the de NORA inert metallic anode in aluminum reduction cells. In: Galloway TJ, editor. Light Metals, TMS (The Minerals, Metals & Materials Society); 2006, p. 397–402.
[31] Patent US8480876B2. Aluminum Production Cell. US8480876B2, 2013.
[32] Gunnarsson G, Óskarsdóttir G, Frostason S, Jón Hjaltalín M. Aluminum electrolysis with multiple vertical non-consumable electrodes in a low temperature electrolyte. Light Metals 2019, San Antonio, Texas: Springer, Cham; 2019, p. 803–10.
[33] AGRAL project. Primary aluminium production : AgrAl Project (Advanced Green Aluminum Anodes) 2017. https://www.agral-project.com/the-agral-project/primary-aluminium-production/ (accessed July 10, 2017).
[34] European Commission. Periodic Reporting for period 2 - AGRAL (Development of the optimum AGRAL cermet manufacturing process for aluminium inert anode application and fuel cell interconnect plates.). European Union; 2017.
[35] Alcoa. Alcoa -- Elysis 2018. https://www.alcoa.com/global/en/what-we-do/elysis/default.asp (accessed November 23, 2018).
[36] Haller MY, Dudita M, Amstad D, Carbonell D, Zenhäusern D, Häberle A. Aluminium als saisonaler Energiespeicher für Solarenergie. Proceedings of the 29. Symposium Solarthermie und Innovative Wärmesysteme, Online Conference Due to Corona Virus - Usual Place: Kloster Banz, Bad Staffelstein, Germany: 2020.
[37] Schweizerischer Ingenieur- und Architektenverein, 2015. SIA Merkblatt 2024: Standard-Nutzungsbedingungen für die Energie- und Gebäudetechnik n.d.
[38] Mojic I, Luzzatto M, Haller M, Lehmann M, Benz M, Van Velsen S. ImmoGap - Einfluss der Kombination aus Nutzerverhalten und Gebäudetechnik auf den Performance Gap bei Mehrfamilienhäuser. Rapperswil: SPF Institut für Solartechnik, HSR Hochschule für Technik Rapperswil; 2018.
[39] Pflugradt N. Load Profile Generator Version 1.3.5. Chemnitz: Prof. Technische Thermodynamik, Germany; 2010.
[40] VDI 2607. Economic efficiency of building installations, Fundamentals and economic calculation, Part 1 2012.
[41] Ludin NA, Mustafa NI, Hanafiah MM, Ibrahim MA, Asri Mat Teridi M, Sepeai S, et al. Prospects of life cycle assessment of renewable energy from solar photovoltaic technologies: A review. Renewable and Sustainable Energy Reviews 2018;96:11–28. https://doi.org/10.1016/j.rser.2018.07.048.
[42] Memmler M, Lauf T, Wolf K, Schneider S. Emissionsbilanz erneuerbarer Energieträger - Bestimmung der vermiedenen Emissionen im Jahr 2016. Dessau-Roßlau: Umweltbundesamt; 2017.
[43] Haller M. Solar Energy and Heat Pumps - Short Term (and Long Term) Storage Options 2018.

[44] Dudita M, Farchado M, Englert A, Sanchez DC, Haller M. Heat and power storage using aluminium for low and zero energy buildings. E3S Web Conf 2019;111:04008. https://doi.org/10.1051/e3sconf/201911104008.
[45] Haller M, Dudita M, Amstad D, Carbonell Sanchez D, Häberle A. Seasonal Energy Storage in Aluminium for 100 Percent Solar Space Heat, DHW and Electricity. ISES Solar World Congress 2019, Santiago, Chile: 2019, p. 1312–20. https://doi.org/10.18086/swc.2019.24.04.
[46] HSR. Aluminium als Heizöl-Ersatz? HSR forscht an innovativer Energiespeicher-Lösung für die Energiewende. www.hsr.ch 2018. https://www.hsr.ch/de/die-hsr/aktuell/medien/detail/article/aluminium-als-heizoel-ersatz-hsr-forscht-an-innovativer-energiespeicher-loesung-fuer-die-energiewende/ (accessed November 23, 2018).
[47] Genova M. Wenn Aluminium den Ofen heizt. Ostschweiz Am Sonntag 2018:11.
[48] Witt A. Schweizer entwickeln neues Speicherkonzept. Solarthemen+Plus 2018;507/2.
[49] Witt A. Schweizer HSR entwickelt neues Speicherkonzept. Solarthemen 2018. https://www.solarthemen.de/index.php/2018/09/27/schweizer-hsr-entwickelt-neues-speicherkonzept/ (accessed September 27, 2018).
[50] pv magazine. Aluminium als Heizöl-Ersatz? pv magazine 2018.
[51] Aluminium als Heizöl-Ersatz? - Link zu diesem Artikel auf: www.windjournal.de 2018. https://www.windjournal.de/alle-artikel/aluminium_als_heizoel_ersatz-101304#.W65J82cyWpp (accessed September 28, 2018).
[52] Niederhäuser A. SPF: Taugt Aluminium – mit einer doppelt so hohen Speicherdichte wie Erdöl – als Saisonspeicher für Wärme und Strom? (ee-news.ch) 2018. https://www.ee-news.ch/de/erneuerbare/article/39460/spf-taugt-aluminium-mit-einer-doppelt-so-hohen-speicherdichte-wie-erdol-als-saisonspeicher-fur-warme-und-strom (accessed September 28, 2018).
[53] Aluminium als Heizöl-Ersatz? Sonnenseite 2018. http://www.sonnenseite.com/de/wissenschaft/aluminium-als-heizoel-ersatz.html (accessed September 28, 2018).
[54] Haller M. Aluminium als Heizöl-Ersatz - Schweizer Forschungsinstitut forscht an einer Energiespeicher-Lösung. Sonnenenergie 2018:54–5.
[55] Diermann R. Kraftpaket im Heizungskeller. NZZ 2019.
[56] Ballinari Y. Energiespeicherung durch Aluminium wird genauer erforscht - energate messenger Schweiz 2019. p:\SPF-in-Medien-und-Fachmagazinen\2019\2019-03-06_Energiespeicherung in Aluminium-Energate-messenger_Schweiz.pdf (accessed April 5, 2019).
[57] Vogel B. HSR-Forschungsprojekt: Aluminium bringt die Sonne in den Winter. WwwEe-NewsCh 2019.
[58] HSR. HSR forscht an innovativer Energiespeicher-Lösung für die Energiewende - Aluminium als Heizöl-Ersatz. Aluminium-Praxis Report Schweiz 2019;2019:6.
[59] ISO. Guide to the expression of uncertainty in measurement. Switzerland: 1995.
[60] Suva, editor. Explosionsschutz – Grundsätze, Mindestvorschriften, Zonen 2015.
[61] Rolf K. Eckhoff. Dust explosions in the process industries. Second ed. Oxford: Butterworth-Heinemann; 1997.
[62] IFA. Datenbank Brenn- und Explosionskenngrössen von Stäuben 2001. http://staubex.ifa.dguv.de/ (accessed April 10, 2019).
[63] Dufaud O, Traoré M, Perrin L, Chazelet S, Thomas D. Experimental investigation and modelling of aluminum dusts explosions in the 20 L sphere. Journal of Loss Prevention in the Process Industries 2010;23:226–36. https://doi.org/10.1016/j.jlp.2009.07.019.
[64] Hong-Chun Wu, Hsin-Jung Ou, Hsiao-Chi Hsiao. Explosion Characteristics of Aluminum Nanopowders. Taiwan Association for Aerosol Research 2009;38–42. https://doi.org/10.4209/aaqr.2009.06.0043.
[65] Castellanos D, Carreto-Vazquez VH, Mashuga CV, Trottier R, Mejia AF, Mannan MS. The effect of particle size polydispersity on the explosibility characteristics of aluminum dust. Powder Technology 2014;254:331–7. https://doi.org/10.1016/j.powtec.2013.11.028.
[66] Ian Fraser. Leitfaden für die Anwendung der Maschinenrichtlinie. 2009.
[67] Bundesrat. Verordnung über die Unfallverhütung VUV. 1984.

[68] Man AIP. Geochemistry of Epigenesis. Springer Science & Business Media; 2012.
[69] Gaffney JS, Marley NA. Chemistry of Environmental Systems: Fundamental Principles and Analytical Methods. John Wiley & Sons; 2019.
[70] Wesolowski DJ, Palmer DA. Aluminum speciation and equilibria in aqueous solution: V. Gibbsite solubility at 50°C and pH 3–9 in 0.1 molal NaCl solutions (a general model for aluminum speciation; analytical methods). Geochimica et Cosmochimica Acta 1994;58:2947–69. https://doi.org/10.1016/0016-7037(94)90171-6.
[71] Cusano G, Rodrigo Gonzalo M, Farrell F, Remus R, Roudier S, Delgado Sancho L. Best Available Techniques (BAT) Reference Document for the Non-Ferrous Metals Industries. 2017.
[72] Fara I. Aluminiul de la materia prima la produsele finite. Editura Tehnica; 2000.
[73] Bagshaw AN. Bauxite to alumina: the Bayer process. 2017.
[74] Lubin MI, Bylaska JH, Weare JH. Ab initio molecular dynamics simulations of Aluminum solvation. Chemical Physics Letters 2000;322:447–53. https://doi.org/10.1016/S0009-2614(00)00434-6.
[75] Kumar PV, Tembe BL. Solvation structure and dynamics of the Fe2+–Fe3+ ion pair in water. J Chem Phys 1992;97:4356–67. https://doi.org/10.1063/1.463905.

Annex A Measurement Uncertainty of Hydrogen Production

For the estimation of measurement uncertainties, Type A measurement uncertainty (random errors based on measurement results) and Type B measurement uncertainty (based on prior knowledge of accuracy of measurement devices and data) were calculated separately [59] and then combined with Gaussian error propagation. Type A measurement uncertainty was taken as the uncertainty of the average of at least three measurement results that were obtained under same conditions. The estimation of the uncertainty of type B has been carried out as follows:

The efficiency η_{H_2} of the hydrogen production experiment is calculated as:

Eq. 4 $$\eta_{H_2} = \frac{V_{n,H_2}}{V_{n,H_2,max}}$$

Where V_{n,H_2} is the normal volume of hydrogen produced an $V_{n,H_2,max}$ is the maximum volume of hydrogen that could be produced theoretically based on a stoichiometric reaction of the aluminium that is introduced into the reactor:

Eq. 5 $$V_{n,H_2,max} = \frac{m_{Al}}{M_{Al}} \cdot \frac{n_{H_2}}{n_{Al}} \cdot V_M$$

With M_{Al} = 26.982 g/mol and n_{H_2}/n_{Al}= 3/2 according the stoichiometry of reaction:

Eq. 6 $$2Al + 6H_2O \rightarrow 2Al(OH)_3 + 3H_2$$

In a typical experiment, 0.1 g of Al is used for the measurement by volume displacement, and 0.05 g is used for the measurement by pressure increase. Thus, in the worst case of 0.05 g of material, the relative uncertainty of this value is 0.2%. Additional uncertainties have to be assumed depending on the purity of the material.

For 100% pure material, 0.1 g of Al-sample produces $V_{n,H_2,max}$= 124.6 mL ±0.4% (±2σ)

Table 24: More or less constant values and their absolute and relative uncertainties (1 σ).

Parameter	Physical unit	Typical value	Typical uncertainty	Rel. uncertainty
m_{Al}	g	0.05 (0.1)	0.0001	0.2% (0.1%)
M_{Al}	g/mol	26.982	negligible	negligible
V_M	l/mol	22.42	±0.01	negligible
n_{H_2}/n_{Al}	-	3/2	0, by definition	negligible

A.1 Measurement by volume displacement

When measuring the amount of hydrogen produced by the volume displacement method, the produced normal volume of hydrogen V_{n,H_2} is calculated as:

Eq. 7 $$V_{n,H_2} = V_{H_2} \cdot \frac{T_n}{T_{H_2}} \cdot \frac{p_{H_2}}{p_n}$$

Table 25: Typical values and their absolute and relative uncertainties for the volume displacement method (1 σ).

Parameter	Physical unit	Typical value	Typical uncertainty	Rel. uncertainty (u)
V_{H_2}	mL	130	3	2.3%
T_{H_2}	K	293	4	1.4%
p_{H_2}	Pa	99.8	5	5.0%

T_n, p_n have by definition no uncertainty.

Since all values can be considered independent, and the calculation of the efficiency is based on multiplications of divisions only, the Gaussian error propagation of relative errors u can be written as follows for the volume displacement method:

$$u(\eta_{H_2}) = \sqrt{u(V_{H_2})^2 + u(T_{H_2})^2 + u(p_{H_2})^2 + u(m_{Al})^2}$$

and thus, for perfectly pure aluminium:

$u(\eta_{H_2}) = \sqrt{(2.3\%)^2 + (1.4\%)^2 + (5.0\%)^2 + (0.1\%)^2}$ = ***±5.7%***

As long as the setup of the experiment is not changed considerably and the amount of hydrogen produced remains about the relative type B uncertainty can be assumed as ±10.6% (±2σ) if the impurity of the Al sample can be neglected.

For experiments with ordinary kitchen aluminium foil, the impurity is largely unknown[7]. therefore, an increased uncertainty u of 2% (u=1 σ) has been assumed in this case for the uncertainty $u(m_{Al})$. Thus, the typical uncertainty of these experiments is ±12% (±2σ).

[7] later, ICP-OES measurements of the precipitate revealed a content of less than 2% of non-aluminium metals.

A.2 Measurement by pressure increase

The gas pressure measured during the experiment was converted to moles of gas produced using the ideal gas law, and then converted to millilitres (mL) of gas produced using Avogadro's law.

Ideal gas law

Eq. 8 $n_{H_2} = \frac{p \cdot V}{R \cdot T}$

where:

n = hydrogen gas produced in moles (mol)
p = pressure in kilopascal (kPa)
V = head-space volume in the glass bottle in liters (L)
T = temperature in Kelvin (K)
R = gas constant (8.314472 L·kPa·K^{-1}·mol^{-1})

Avogadro's law

Using Avogadro's Law, at atmospheric pressure measured in psi (1 psi = 6.8947 kilopascal), 1 mole will occupy 22.4 L at 273.15 K and 101.325 kPa (standard conditions). In this way, the hydrogen measured in moles was converted to gas measured in mL as follows:

Eq. 9 $V_{H2}\ produced\ in\ mL = n_{H2} \cdot 22.4 \frac{L}{mol} \cdot 1000\ \frac{mL}{L}$

Table 26: Typical values and their absolute and relative uncertainties for the pressure increase method (1 σ).

Parameter	Physical unit	Typical value	Typical uncertainty	Rel. uncertainty (u)
V_{H_2}	mL	60	1	1.7%
T_{H_2}	K	296.35	2	0.7%
p_{H_2}	kPa	43.44	0.01	0.02%

Since all values can be considered independent, and the calculation of the efficiency is based on multiplications of divisions only, the Gaussian error propagation of relative errors u can be written as follows for the volume displacement method:

$$u(\eta_{H_2}) = \sqrt{u(V_{H_2})^2 + u(T_{H_2})^2 + u(p_{H_2})^2 + u(m_{Al})^2}$$

and thus, for perfectly pure aluminium:

$u(\eta_{H_2}) = \sqrt{(1.7\%)^2 + (0.7\%)^2 + (0.02\%)^2 + (0.1\%)^2}$ = ***±1.8%***

Annex B Material Used for Laboratory Experiments

In order to characterize the composition of the aluminium samples used, Scanning Electron Microscopy coupled with Energy Dispersive X-ray Spectroscopy (SEM/EDX) was performed for the different form of aluminium investigated in section 3.1.3.

B.1 Aluminium samples

Commercial Aluminium foil

The study of the composition of the commercial aluminium foil via EDX establishes that the purity of this aluminium shape is around 98%, containing traces of iron and manganese.

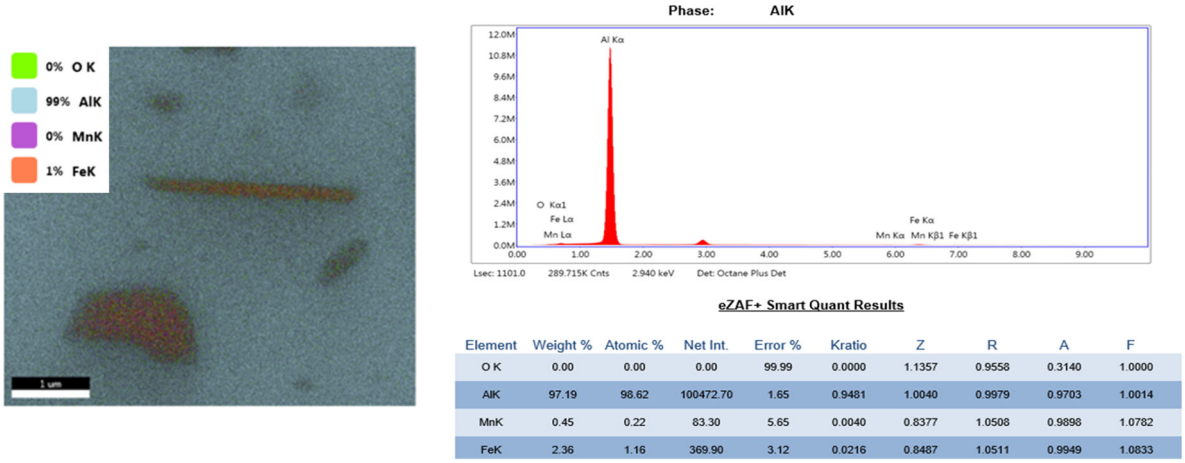

eZAF+ Smart Quant Results

Element	Weight %	Atomic %	Net Int.	Error %	Kratio	Z	R	A	F
O K	0.00	0.00	0.00	99.99	0.0000	1.1357	0.9558	0.3140	1.0000
AlK	97.19	98.62	100472.70	1.65	0.9481	1.0040	0.9979	0.9703	1.0014
MnK	0.45	0.22	83.30	5.65	0.0040	0.8377	1.0508	0.9898	1.0782
FeK	2.36	1.16	369.90	3.12	0.0216	0.8487	1.0511	0.9949	1.0833

Figure 61: EDX map and pattern of the commercial aluminium foil.

Aluminium granular

The results determine that the granular aluminium contains apart from aluminium (98.42%), traces of titanium (0.26) and iron (0.12%). The iron is present in small inclusions and along grain boundaries.

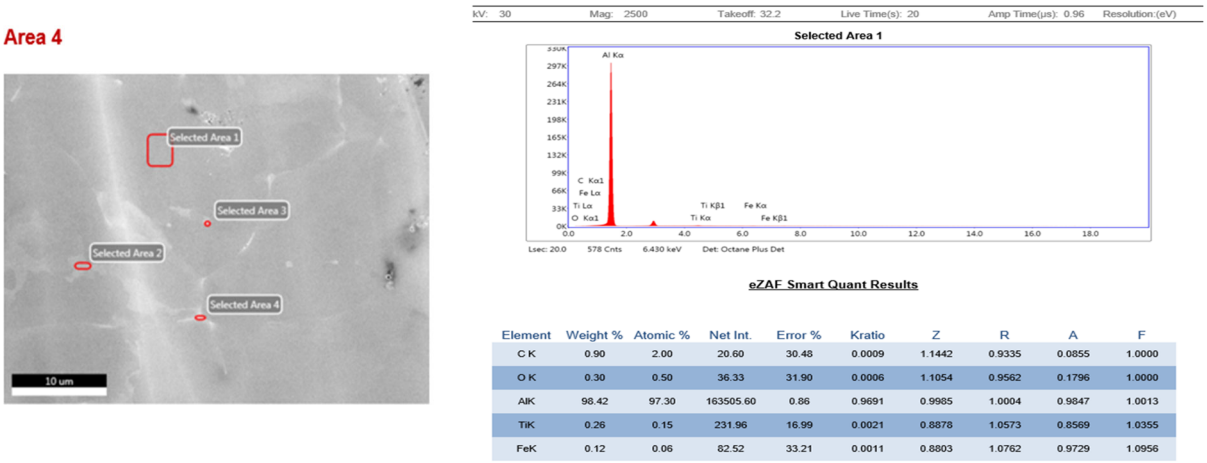

Element	Weight %	Atomic %	Net Int.	Error %	Kratio	Z	R	A	F
C K	0.90	2.00	20.60	30.48	0.0009	1.1442	0.9335	0.0855	1.0000
O K	0.30	0.50	36.33	31.90	0.0006	1.1054	0.9562	0.1796	1.0000
AlK	98.42	97.30	163505.60	0.86	0.9691	0.9985	1.0004	0.9847	1.0013
TiK	0.26	0.15	231.96	16.99	0.0021	0.8878	1.0573	0.8569	1.0355
FeK	0.12	0.06	82.52	33.21	0.0011	0.8803	1.0762	0.9729	1.0956

Figure 62: EDX map and pattern of the aluminium granular.

Aluminium pellet

The results establish that the aluminium pellet contains apart from aluminium (96.36%), traces of iron (0.08%) and nickel (0.04%).

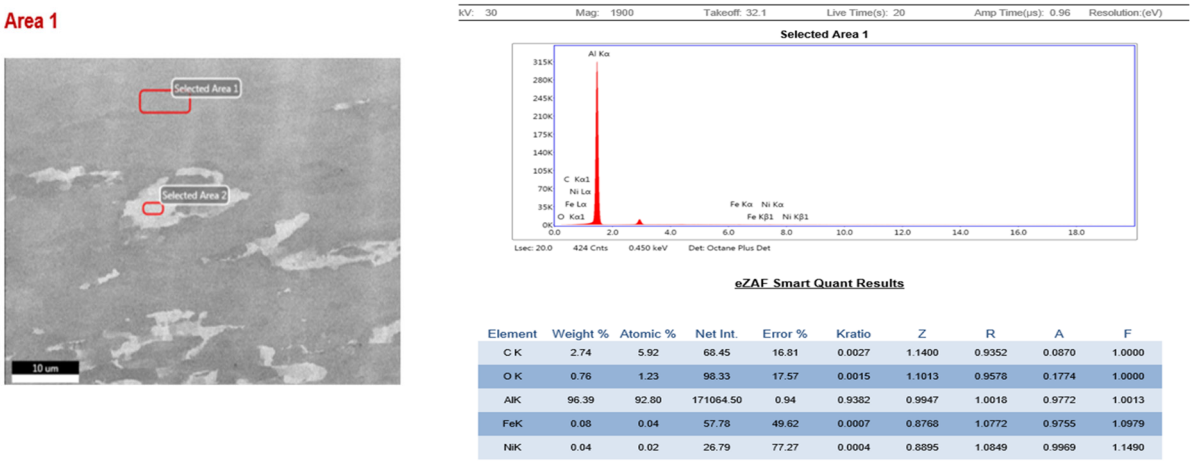

Element	Weight %	Atomic %	Net Int.	Error %	Kratio	Z	R	A	F
C K	2.74	5.92	68.45	16.81	0.0027	1.1400	0.9352	0.0870	1.0000
O K	0.76	1.23	98.33	17.57	0.0015	1.1013	0.9578	0.1774	1.0000
AlK	96.39	92.80	171064.50	0.94	0.9382	0.9947	1.0018	0.9772	1.0013
FeK	0.08	0.04	57.78	49.62	0.0007	0.8768	1.0772	0.9755	1.0979
NiK	0.04	0.02	26.79	77.27	0.0004	0.8895	1.0849	0.9969	1.1490

Figure 63: EDX map and pattern of the aluminium pellet.

Aluminium wire

The results determine that the aluminium wire contains apart from aluminium (97.08%), traces of iron (2.92%). There is a structure (different intermetallic phases) in the regions where the iron is present.

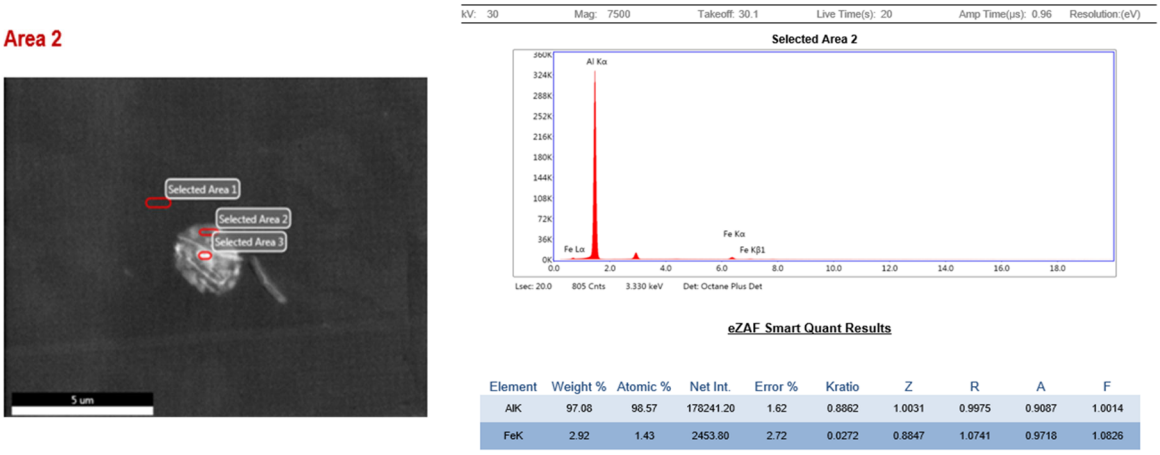

Figure 64: EDX map and pattern of the aluminium wire.

B.2 Measurement by volume displacement

Material used:

- Mettler Toledo AT 261 Delta Range balance
- Water bath 5.0 L (Büchi 461)
- Reactor 250 mL 2 DIN NB 14/23 and 1 DIN NS 29/32 (Schott Duran)
- Cylinder 250 mL:2 ISO/4788 (VWR)
- Water bucket 10 L (VWR)
- Temperature sensor x3
- Pressure sensor (testo)
- Silicone connection tubes 1.30 m long, 8 mm diameter.
- Joint grease K_aW_eS. for vacuum and high vacuum (-40° to +200 °C)

B.3 Measurement by pressure increase

Material used:

- Mettler Toledo AT 261 Delta Range balance
- Glass bottles 500 mL
- Bottle gaskets
- Modules (ANKOM^{RF} Gas Production System)
- Reference module zero (ambient pressure)
- Multipoint stirring system with magnets
- Synthetic grease K_aW_eS. for vacuum and high vacuum (-40° to +200 °C)
- Antenna extension assembly
- Base coordinator with USB cable and antenna
- 10 station battery charger
- Luer check valves

Figure 65: Material used for the ANKOM pressure increase experiments.

Annex C Explosion Risk of Aluminium Powders

This section presents the results of a literature study on the explosion risks of fine aluminium powders.

C.1 Explosion sensitivity and indices

The main influencing factors of the ignition sensitivity and explosion violence of dust clouds are:

- particle size, respectively the specific surface area
- degree of dispersion/ agglomeration of the particles
- turbulence in the dust cloud

The following indices are used to describe the behaviour of different dust shapes.

- **The minimum explosion concentration (MEC):** Starting with a dust concentration that can explode, the dust concentration is stepwise reduced until no more explosion occurs. There must be at least three tries with the same dust concentration resulting in no ignition until the dust concentration in g/m^3 is defined as the MEC.
- **Maximal explosion overpressure and the K_{st} value:** The maximum rate of pressure rise is volume dependent and described by the maximal explosion overpressure. By applying the "cubic law", it can be converted to the K_{st}-value, a characteristic that is independent of the vessel volume.

K_{st} [bar m/s]	Explosion characteristics	Dust explosion class
0	No explosion	-
0 – 200	Weak or medium scale explosion	St 1
200 – 300	Large scale explosion	St 2
>300	Extremely large scale explosion	St 3

The K_{st}-value can be calculate according the following equation.

Eq. 10 $$\frac{dp}{dt} \cdot V^{\frac{1}{3}} = K_{st}$$

For a given dust material, the maximum explosive pressure and the maximum rate of pressure rise increases systematically with decreasing particle size.

- **Minimum Ignition Energy (MIE)** The MIE describes the energy used to ignite a dust cloud at room temperature and generally decreases with decreasing particle size and moisture content. This is not of major importance for this report, since we are only interested at which particle size and concentration an explosion occurs.

Therefore, the indices of most interest are the maximum explosion overpressure, the K_{st}-value respectively and the minimal explosive concentration (MEC).

C.2 Explosion risk of aluminium powder derived from literature

In general, combustible dusts with a particle size of less than 0.5 mm can form explosive atmospheres according to [60]. This fact was also mentioned by Mischa Schwanninger (058 517 80 37, Process safety Tüv Süd 8.02.2019) in a phone call with Ivo Caduff, SPF.

According to another source [61] does the hazard increase with decreasing particle size down into the range below 1 µm. The MIE does not decrease further due to agglomeration of the aluminium particles when the range of nm is reached. Coarser Aluminium powder with particle diameter larger than 100 µm has only a moderate explosion potential. The particle diameter of a coarser powder can decrease e.g. during transportation when friction occurs. Even a small fine fraction in the aluminium powder can increase the hazardous potential dramatically. Keeping a watch on the particle size allows however, in the case of aluminium, to control the explosion hazard. The book does not clarify the particle size or the weight percentage of the fine fraction at which a risk arises.

The Institute for Accident Insurance of the Industrial Sector (IFA, Germany) has collected a list with more than 4'300 dust samples taken from nearly all branches of industry. The database is available under [62]. The available data regarding aluminium includes different shapes as powders, pellets, grits and chips made by drilling or milling. Normally the particle size distribution and the median particle size are listed in the database. Depending on the conducted experiments, the resulting MEC, K_{st}-value or the MIE were determined. Not every experiment investigated all three parameters with the same particle size distribution and a comparison is therefore not always possible.

The data of the experiment is valid under the following conditions:

- Pressure from 0.9 bar to 1.1 bar
- Oxygen approx. 21 Vol.-%
- Temperature from 0 °C to 30 °C
- No flammable liquids or gases mixed with the sample

Figure 66 shows the maximum explosion overpressure depending on the median particle size on a logarithmic scale for all different aluminium shapes found in the database. A distinction between aluminium powder and all the other shapes was made. In some of the experiments when no explosion occurred, then the sample was sieved and the behaviour of the smaller particle size of the same sample was tested again. The new median of the sample was often not determined again, which is indicated by the range of the error bar in the figure. An overpressure of zero means that no explosion occurred.

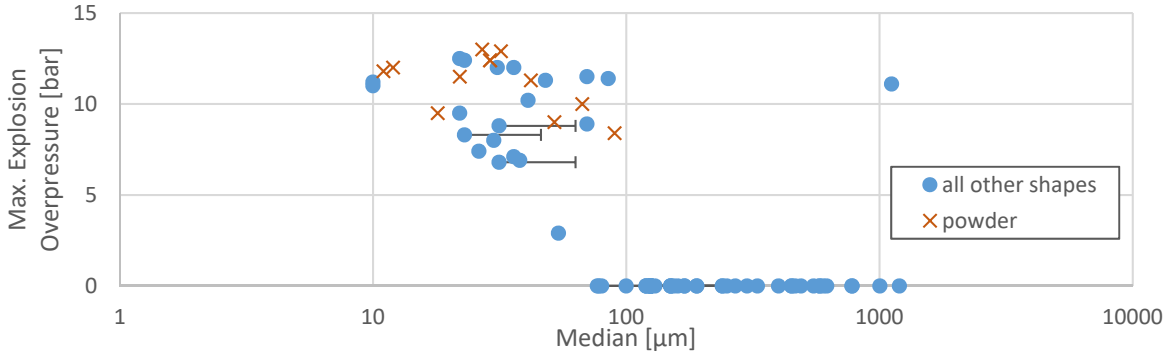

Figure 66: Explosion overpressure for different particle sizes according to the IFA.

High pressures are reached when an explosion occurs, independent of the particle size. However, the highest overpressures are reached when powder is used due to the high surface ratio. The maximum explosion pressure decreases when the particle sizes increases except for one outlier. If the aluminium shapes have a median smaller than 100 µm, then the chance of an explosion is reduced. The outlier with particle size of 1117 µm is an aluminium pellet (with 20% binding agent and 23 weight-% smaller than 125 µm). An assumption could be that the pellet decayed and formed a fine dust cloud when it was tested.

Figure 67 shows the K_{st}-value and the minimal explosion concentration respectively in function of the median particle size. Again, all different aluminium shapes found in the IFA database have been used. The error bar indicates the range of the median particle size when it was unknown.

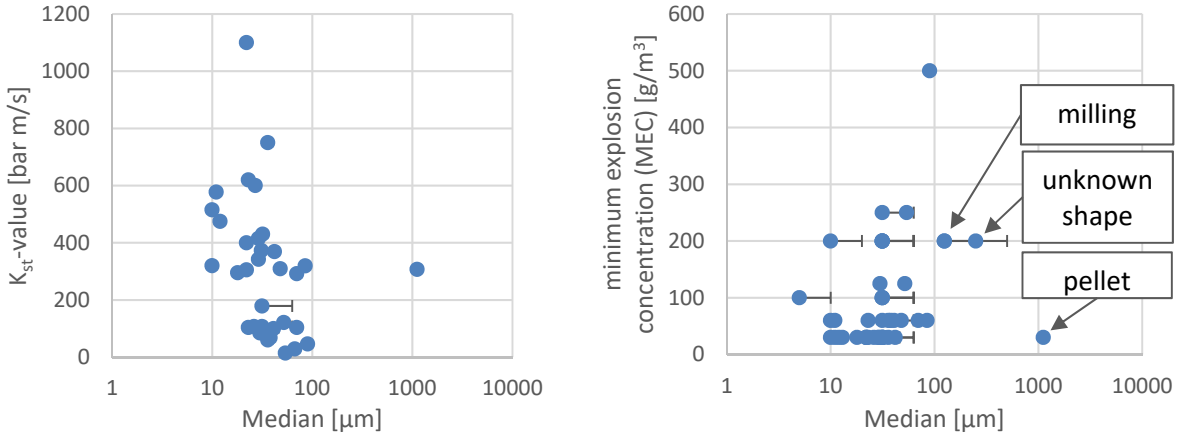

Figure 67: MEC and K_{st}-value depending on the particle size according to data from IFA.

The K_{st}-value does decrease by increasing particle size. No explosions occurred when the particle size was larger than 100 µm and therefore no K_{st}-value was recorded. The only explosion observed was for the pellet shaped aluminium sample. The minimum explosion concentration (MEC) however, does not follow the same behaviour as the K_{st}-value and the maximum explosion overpressure figures suggested. No trend towards increasing explosion

concentration with increasing particle size is visible as expected. On the other hand, there were many experiments conducted in the particle range larger than 100 µm and no explosions occurred.

The K_{st}-value and the MEC of dust and powder samples are compared in Figure 68. Therefore data from the IFA database has been used and was complemented by the data of [63–65]. The particle median size was plotted on a logarithmic scale.

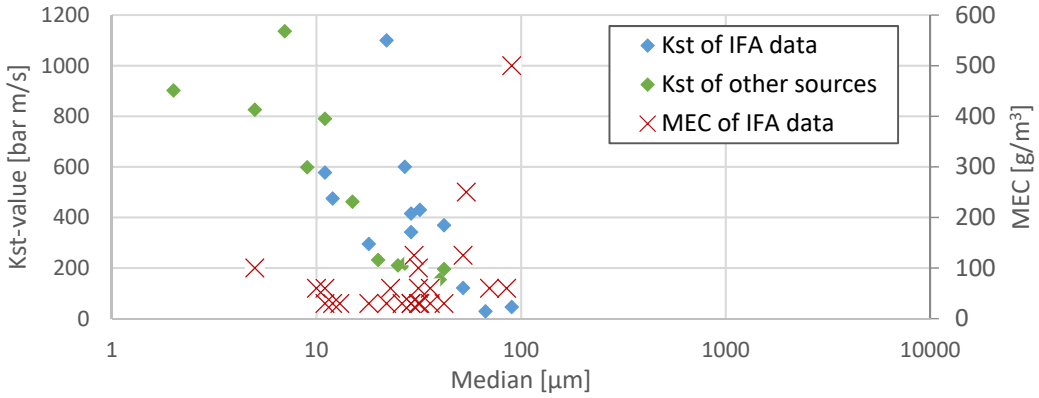

Figure 68: Comparison of K_{st}-value and MEC of different aluminium powder and dust samples.

The MEC increases whereas the K_{st}-value decreases with increasing particle size when only powder is considered. The maximal explosion concentration exceeds 500 g/m³ and does not increase further when the median particle size is larger than 100 µm. The smaller the particle size, the higher is the explosion potential. Similar results for the K_{st} were obtained by using data from different sources.

The explosion potential increases dramatically when the particle size is smaller than 100 µm, as already seen in Figure 68. Therefore the question arises which amount of fine dust is needed to cause an explosion risk.

Figure 69 shows selected samples out of the IFA database, which did not explode with the shown particle size distribution. Shown are aluminium shapes as powders and chips made by drilling or milling. All the samples were sieved and the fraction smaller than 125 µm tested again but no explosion occurred. An explosion occurred only when 100% of the particles mass weight was smaller than 63 µm. A dust explosion class of 1 was reached which is equivalent to a K_{st}-value of 0-200 bar m/s.

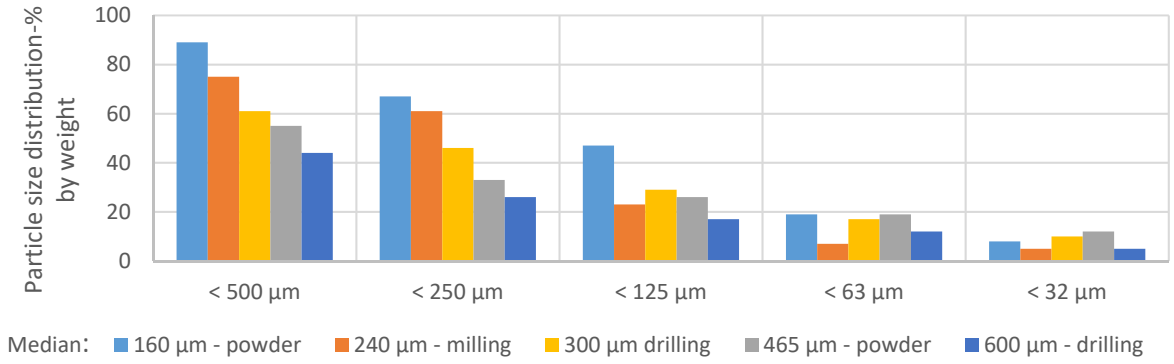

Figure 69: Particle size distribution where no explosion occurred until sample was sieved and the fine fraction smaller than 63 µm was tested.

A high amount of fine dust is needed until an explosion occurs. For most of the samples as shown above is the percentage of the dust fraction, which is smaller than 63 µm, almost 20%. The exact percentage of the fine dust fraction, which should not be undershoot is unknown but the critical particle size is in the range between 63 and 125 µm.

As long as the size of the greatest particle is still larger than 125 µm, no harm should occur. If all the particles are reduced during transportation and fall below the limit of 63 µm, then the explosion risks will be high. Unfortunately, it is not possible to determine the limit value of the fine dust fraction as a percentage of the samples weight distribution with the available data.

C.3 Standards and regulations

Chapter 1.5.7 of the Maschinenrichtline [66] states that every machine must be built and constructed in such a way that any risk of explosions can be avoided. No risk must arise for all gasses, liquids, vapours, dusts or other harmful substances used or released by the machine. The requirement in the first paragraph of point 1.5.7 refers to the explosion risks caused by the actual operation of the machinery or by materials or substances used or produced by the machine.

To prevent the risk, a combination of the following measures has to be followed [60,66,67]:

- Avoid the accumulation of explosive mixtures in areas in or around the machine by avoiding flammable materials or substances or maintain the concentration permanently at a level outside the lower or upper explosion limits;
- Avoid the presence of ignition sources in hazardous areas;
- Reduce the oxygen concentration in hazardous areas (unless this leads to additional risks for persons).

If the explosion risk cannot be reduced completely, then additional protection measures have to be undertaken. This can be constructive measures such as explosion proof construction, pressure relief devices etc. This is further specified in the standard EN 1127-1:2007 Explosionsfähige Atmosphären – Explosionsschutz –Teil 1: Grundlagen und Methodik.

Another important standard is the ATEX (ATmosphères EXplosibles).The ATEX directive does not apply to explosion risks arising within the machine itself. However, it states that in areas where explosions can occur only equipment, which meets the ATEX directive, can be installed. This is important for the aluminium storage of the HybridStock device and especially for the aluminium feed mechanism when dust is used.

As long as the mean diameter of the particles is greater 0.5 mm, no standards and regulations regarding explosion safety have to be considered because then, the material is not considered as explosive. Further comments to the risk assessment procedure and which regulations can be considered in detail is further described in [60]. In this booklet, all necessary information's are summarized.

C.4 Conclusion

The finer the powder, the higher are the risks of dust explosions. According to SUVA, dust explosions can be avoided by using particle sizes above 500 µm. Different sources showed that aluminium shapes as powder or chips made by drilling or milling with particle sizes smaller than 63 µm have a high explosion risk and can ignite even at small concentrations (MEC). The risk does decrease when the particle size is larger than 100 µm and is almost zero when the particle size is greater than 125 µm. As long as the particles do not decay as suggested by the aluminium pellet.

Therefore, it is recommended to use particles, which have a median particle size of 500 µm in order to be on the safe side. This has the further advantage that also during transportation no explosion risk occurs. In addition, no special regulations regarding explosion safety have to be considered. However, a further request is to test the explosion potential of the aluminium once the final shape is determined. Criteria's as the minimum ignition energy or the combustibility were not determined in this report. They are only becoming of increasing importance when the median particle size is smaller than 250 µm.

Annex D Literature Study on Precipitation of $Al(OH)_3$ from Aqueous Solutions

The discharging of the aluminium storage can be described as a corrosion or an oxidation process ($Al \rightarrow Al^{3+}$). The reaction product aluminium hydroxide $Al(OH)_3$ needs to be removed from the converter continuously or after a certain period. It is known that above pH 8, the major Al^{3+} specie is aluminate ion $[Al(OH)_4^+]^-$ in solution, that may also form polynuclear complexes. Aluminium hydroxide precipitates easily at pH 5-8 in the form of a white or semitransparent gel. In this case, the solid precipitate is amorphous $Al(OH)_3$ [20]. However, decreasing the pH by adding water or acids (e.g. HCl) is not desired because it would decrease reaction speed, and add additional elements, and complicate the conversion process. Furthermore, NaCl may precipitate together with $Al(OH)_3$ and have to be separated from it in an additional step.

D.1 Solubility of aluminium ions

Aluminium is a reactive metal that forms a thin oxide layer on its surface in the presence of oxygen, which protects it from further oxidation. The oxidation behaviour of aluminium in alkaline solutions is directly related to the stability of the oxide film. Typically, the oxidation rate of aluminium increases exponentially for pH values lower than 3 or higher than 9. At room temperature and pH 7.5, the oxidation rate is about 10^{-8} g/(cm^2 h), while at pH 12 it is 10^{-4} g/(cm^2 h), indicating a four orders of magnitude increase from the neutral to the alkaline pH range [1].

Aluminium hydroxide can act as a Brønsted–Lowry base by accepting protons from an acidic solution, or as a Lewis acid by accepting an electron pair from hydroxide ions in a basic solution. The central aluminium atom (Figure 70) is electron deficient because it forms only three bonds, and the octet rule is not fulfilled; thus, Al^{3+} is ready to accept a pair of electrons and form another bond. In strongly alkaline solution, it forms a bond with an OH^- ion, pulling it out of solution and thus lowering the solution's pH.

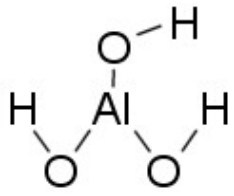

Figure 70: Structural formula of $Al(OH)_3$.

In solution, one mole of aluminium hydroxide gives one mole of aluminium ions and three moles of hydroxide ions.

Eq. 11 $Al(OH)_{3(s)} \leftrightarrow Al^{3+}_{(aq)} + 3OH^-_{(aq)}$

The solubility constant (K_{sp}) expression for $Al(OH)_3$ is given by the equation below. More solubility parameters are given in Table 27. Solubility of aluminium hydroxide strongly depends on temperature.

Eq. 12 $K_{sp} = [Al^{3+}][OH^-]^3 = 1.9 \times 10^{-33}$

Table 27 Solubility parameters for $Al(OH)_3$.

Parameter	Details	Reference
Solubility in water	0.001 g/L	[68]
Solubility product ($K_{sp,\ 25\ °C}$)	1.9×10^{-33}	[69]
Solubility constant ($pK_{s,\ 25°C}$)	31.5	[70]
Solubility	soluble in acids and alkalis	[15]

In neutral water, a very small amount of aluminium hydroxide will already lead to a saturated solution, thus the solubility is limited. For example, 2.2 x 10^{-7} g $Al(OH)_3$ will saturate 1 L of water at 25°C. In alkaline solutions, the solubility will be much higher because of the formation of the charged species $[Al(OH)_4]^-$ [15].

Eq. 13 $Al(OH)_3 + OH^- \leftrightarrow Al(OH)_4^-$

D.2 Precipitation of $Al(OH)_3$ in the Bayer process

Precipitation of $Al(OH)_3$ (also written as $Al_2O_3{\cdot}3H_2O$ – a hydrate - or gibbsite) from an aqueous solution is part of the Bayer process that is used for the extraction of aluminium from bauxite in large quantities worldwide. In this process, bauxite or other ores that are rich in aluminium are first ground and digested in order to obtain dissolved Al^{3+} in caustic soda (highly alkaline solutions). The digestion takes place at high temperature (100 – 320 °C), pressure (25 – 40 bar) and 100 g/L to 250 g/L of Na_2O [71,72], corresponding to 7-16% NaOH or 1 to 4 M NaOH aqueous solution. Temperature, pressure and caustic soda concentration are dependent on the ore or bauxite that is digested.

The result of the digestion in the Bayer process is a highly alkaline liquor, consisting mainly of water and aluminate ions. From this digested solution, unwanted elements such as iron and silicon are precipitated first, before precipitation of $Al(OH)_3$ is initiated. Precipitation of $Al(OH)_3$ is started by cooling and addition of water (dilution) and hydrargillite (gibbsite, $Al(OH)_3$) crystals as crystallization seeds. The precipitation temperature varies from 55-70°C [71] to 75-80°C [73].

The slurry that results from the initiation of the precipitation flows through a tank cascade and in each tank, $Al(OH)_3$ is precipitated. The solid phase is removed by filtration or thickeners and after that is washed with condensate and send to calcination. The solid-free liquor is sometimes passed through an evaporation plant in order to remove excessive water and re-used in the digestion area. Typically, the pregnant liquor entering the precipitation phase will have an Al content of 140 g/L (expressed as Al_2O_3), while at exit will have circa 50 g/L, thus giving a yield of 90 g/L. Precipitation of aluminate based solution occurs until the following molar ration is reached: Na_2O:Al_2O_3= 6:1.

As the aluminium concentration in the liquor is well above its equilibrium values, precipitation occurs in uncontrolled ways. Scale is forming in pipes and vessels, and precipitators. This represents a loss of the hydrate yield as well as decreased efficiency due to the reduced flows in pipework and volume loss in tanks. Therefore, maintenance programs are ensuring that the hydrate scale is regularly removed.

The precipitation mechanism involves a combination of agglomeration and controlled growth. Depending on the temperature and impurities from the liquor, the final particles after precipitation phase may have a radial or mosaic structure [73]. The radial particles are preferred because they are tougher compared to mosaic shapes and they are less prone to break up into smaller particles during transport and calcination. The optimum particle diameter ranges from 45 to 150 μm. At the end of the precipitation phase, the particles are separated from the spent liquor and washed carefully with good quality water.

The precipitation step is the most critical step in the Bayer process and it aims to maximize the product recovery in the minimum time and with maximum efficiency. It aims for growing large enough particles in a controlled and slow way so that the resulting particles meet the size and toughness specification for the next step: calcination [73].

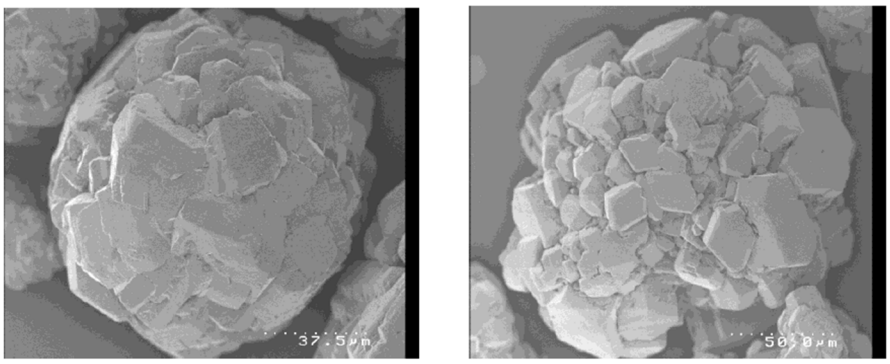

Figure 71: Scanning electron microscopy images illustrating the two types of particles after precipitation occurs [73]: left radial, strong gibbsite and right mosaic, weak gibbsite.

Regarding the nature of aluminate solutions from the Bayer process, there are more theories in literature: colloidal, chemical (ionic) and mix (colloidal-ionic). These theories and the experimental investigations were triggered by the need of understanding the complex behaviour of aluminate solutions from the Bayer process.

According to the colloidal theory, the aluminate solutions contain colloidal aluminium hydroxide and aluminium oxide hydrosols. The aluminium hydroxide precipitation occurs as a coagulation process.

The ionic theory claims that the reactions from Eq. 14 to Eq. 16 will occur when dissolving $Al(OH)_3$, neglecting the presence of colloidal species.

Eq. 14 $Al(OH)_3 + OH^- \rightarrow Al(OH)_4^-$

Eq. 15 $Al(OH)_3 + OH^- \rightarrow AlO_2^- + 2\,H_2O$

Eq. 16 $AlOOH + OH^- \rightarrow AlO_2^- + H_2O$

The precipitation of $Al(OH)_3$ includes complex processes that are combined (nucleation, crystal growth or crystal breakdown), and the mechanism is still poorly understood on a microscopic scale.

Annex E Analysis of Non-Al Precipitate

All the small-scale laboratory experiments performed with aluminium foil have led to the formation of a black precipitate, before $Al(OH)_3$ started to precipitate. The chemical composition of this black precipitate was evaluated using the following method:

- Precipitate was obtained from a 50 mL assay of 6 M NaOH solution after reaction of 1.04 g of commercial aluminium foil.
- The precipitate is magnetic, thus part of the precipitate was taken out of the solution with the magnetic stirring bar retriever
- The initial weight of a filter was determined with a Mettler Toledo balance, model MS6002S/01, d= 0.01 g
- The solution resulting from the chemical reaction between NaOH solution and Al foil was filtered
- The filter was washed with deionised water
- The filter with the precipitate was dried at 105°C for 2 h
- The weight of the precipitate was determined after weighting the dried filter
- The precipitate was chemically digested (dissolved) in a microwave process
- The resulting solution was analysed using ICP-OES, a technique in which elements in water-dissolved samples can be determined (qualitative and quantitative)
- For ICP-OES quantitative evaluation, the elements identified in the Al foil via the SEM/EDX analysis made at ETH-SCOPEM[8] lab were used as input.

Table 28 shows the concentrations and absolute weights of the most important elements identified in the precipitate. Other elements were also measured, but they could not be quantified (Ag, Al, B, Ba, Bi, Ca, Cd, Co, Cr, Cu, Fe, Ga, In, K, Li, Mg, Mn, Na, Ni, Pb, Sr, Tl, Zn).

Figure 72: Aspect of the precipitate resulted from the reaction between Al foil – NaOH 6M.

The main component from the precipitate is iron (Fe, see Table 28), which explains the magnetic behaviour. It is a trace element in the aluminium foil, already identified in the SEM-EDX measurements from ETH SCOPE-M lab, like manganese (Mn). Very small amounts of Al and Na were also measured. They are likely to stem from the solution, which was incompletely washed out of the precipitate. The other elements were measured only in very low quantities

[8] https://scopem.ethz.ch/

and with high uncertainties. The difference between the initial filter weight (23.6 mg) and the amount evaluated via ICP-OES (15.2) might be attributed to water, which may have been physical bound to the metal ions (hydration) and evaporated during sample preparation or measurement[9].

The analysis of the precipitate shows that only a small fraction (less than 0.1%) of the reacted Al is found in the precipitate[10]. Instead, iron is the main component of the precipitate. Considering the aspect (e.g. colour) and the magnetic behaviour of the black precipitate, iron should be in the form of iron(II,III) oxide (Fe_3O_4), which is the stable iron form in alkaline solutions.

Thus, assuming that the identified aluminium stems from the solution, which was imperfectly washed out of the precipitate, we can conclude that after the HybridStock discharging reaction, aluminium is to be found predominantly dissolved in solution and not as $Al(OH)_3$ precipitate. This is also in agreement with literature on hydration and solubility of Al-cations in alkaline solution that is discussed in chapter 4.

Table 28: Results of the ICP-OES measurement of the precipitate from the oxidation of Al foil in aqueous NaOH (6 M) solution, digested in aqua regia to form 50 mL of solution.

Element	Concentration	Amount absolute	Amount per kg Al	Remark
	mg/L	mg	g/kg	
Fe	240	12	11.5	Main compound of precipitate
Cu	2.8	0.14	0.1	Value with high uncertainty
Al	18	0.9	0.9	Possibly from solution in the filtrate
Mn	13.2	0.66	0.6	Side compound of precipitate
Na	28	1.4	1.3	Possibly from solution in the filtrate
Zn	2	0.1	0.1	Value with high uncertainty
	Sum	15.2	14.5	

[9] It is known that in aqueous solutions, hydration occurs. This interaction of a solute (like metal ions, e.g. Al^{3+}, Fe^{3+}) with the solvent (water) leads to stabilization of the solute species in the solution. In the hydrated state, an ion in a solution is surrounded or complexed by water molecules. Metal ions form then hydrated ions also called aqua ions with the formula $[M(H2O)_n]^{z+}$. The solvation number, n, is 6 for aluminium and iron, e.g. hexa-hydrates ions are formed: $Fe(H_2O)_6^{2+}$, $Fe(H_2O)_6^{3+}$, $Al(H_2O)_6^{3+}$ [74,75].

[10] 0.9 mg compared to 1040 mg Al that has been added in the experiment.

Annex F Measurement Uncertainty of 400 W Prototype Results

For the estimation of measurement uncertainties, Type A measurement uncertainty (random errors based on measurement results) and Type B measurement uncertainty (based on prior knowledge of accuracy of measurement devices and data) were calculated separately [59] and then combined with Gaussian error propagation. Type A measurement uncertainty was taken as the uncertainty of the average of at least three measurement results that were obtained under same conditions. The estimation of the uncertainty of type B is described in this section.

F.1 Aluminium feeding rate

The mass flow of aluminium into the converter $\dot{m}_{Al}$ could not be measured directly due to the construction of the feeding system. In an additional experiment with the same conditions, the aluminium that was added to the reservoir of the feed system was weighted. After the experiment, the left over aluminium in the reservoir was weighted to calculate the total mass that was inserted to the converter. Dividing this mass by the number of cycles N_{cycles} in this experiment results in the mass of Al alloy that is fed in one cycle ($m_{Al-alloy\ per\ cycle}$). The amount of aluminium in one phase (of four cycles) is calculated taking into account the purity of the aluminium grit f_{purity}, and the mass flow rate is calculated by dividing the amount of Al per phase by the duration of four cycles t_{phase}:

Eq. 17 $$m_{Al\ per\ phase} = f_{purity} \cdot 4 \cdot \frac{(m_{Al,initial} - m_{Al,leftover})}{N_{cycles}}$$

Eq. 18 $$\dot{m}_{Al} = \frac{m_{Al\ per\ phase}}{t_{phase}}$$

To estimate the uncertainty of $m_{Al\ per\ phase}$, the feeder was dismounted from the converter in order to measure the amount of aluminium that is fed in one cycle. The average value out of 20 measurements is 5.32 g with a standard deviation of σ = 0.216 g for a single value. This value is smaller than the 5.81 g calculated according to Eq. 28 because when the feeder is dismounted, there is no backpressure from the converter, which is increasing the opening time of the pinch valve slightly. The standard deviation of one opening of the valve is estimated to be in the same range with or without backpressure. The standard deviation of $m_{Al\ per\ cycle}$ as the average of 4 cycles is $\sigma_{avg} = \sigma/\sqrt{n} = 0.216\ g/\sqrt{4} = 0.108\ g$ and its uncertainty u = 2*σ_{avg} = 0.216 g (3.72%). The Al flow per phase has the same relative uncertainty as the average of four cycles.

Table 29: Type B uncertainties for the measurement of Al mass flow rate.

Parameter	Physical unit	Typical value	Typical uncertainty (u)	Rel. Uncertainty (urel) (of typical value)
$m_{Al,initial}$	g	362.4	0.02	negligible
$m_{Al,leftover}$	g	14.3	0.02	negligible
$m_{Al\ per\ cycle}$	g	5.81	0.216	3.72%
$m_{Al\ per\ phase}$	g	23.24		3.72%
f_{purity}	%	97.5	0.5	0.51%
t_{phase}	h	0.49…0.57	<1/3600	negligible
N_{cycles}	-	60	0	0

For the calculation of the uncertainty of $\dot{m}_{Al}$ only the uncertainty of f_{purity} and $\mathrm{m}_{\mathrm{Al\ per\ phase}}$ are used, since the other uncertainties are negligible. Since f_{purity} and $\mathrm{m}_{\mathrm{Al\ per\ cycle}}$ are independent, and the calculation is based on multiplication only, the Gaussian error propagation of relative uncertainties u_{rel} can be written as follows:

Eq. 19 $$u_{rel}(\dot{m}_{Al}) = u_{rel}(\dot{m}_{H_2,calc}) = \sqrt{u_{rel}(f_{purity})^2 + u_{rel}(m_{Al\ per\ phase})^2}$$

F.2 Hydrogen production rate and hydrogen production efficiency

The hydrogen production rate $\dot{\mathrm{m}}_{H_2,avg}$ is the average of the measured hydrogen flow within a time-span (a phase) of four feed cycles, (four dosings per cycle, i.e. 16 dosings in a phase). The uncertainty of the measured hydrogen flow rate is given by the accuracy of the H_2 mass flow sensor *mini CORI-FLOW™ M12* by Bronkhorst used in this experiment and is 0.02 g/h + 0.5% of reading.

The maximum mass flow rate $\dot{\mathrm{m}}_{H_2,\mathrm{calc}}$ that could be produced theoretically, based on a stoichiometric reaction of the aluminium that is introduced into the converter, is:

Eq. 20 $$\dot{m}_{H_2,calc} = \frac{3}{2} \cdot \frac{\dot{m}_{Al} * M_{H2}}{M_{Al}}$$

With M_{Al} = 26.982 g/mol, M_{H2} = 2.016 g/mol and n_{H_2}/n_{Al}= 3/2 according to the stoichiometry of reaction. The uncertainty of $\dot{m}_{H_2,calc}$ equals the uncertainty of the mass flow rate of Al into the reactor, since the uncertainties of the other terms of Eq. 20 are negligible.

Eq. 21 $$u_{rel}(\dot{m}_{H_2,calc}) = u_{rel}(\dot{m}_{Al})$$

The efficiency η_{H_2} of the conversion of aluminium and water to hydrogen in the experiment is calculated for different phases of the measurement as:

Eq. 22 $$\eta_{H_2} = \frac{\dot{m}_{H_2,avg}}{\dot{m}_{H_2,calc}}$$

The uncertainty of the conversion efficiency of H_2 is calculated with the same method as in Eq. 19, using the uncertainties of $\dot{\mathrm{m}}_{\mathrm{H_2,avg}}$ and $\dot{\mathrm{m}}_{\mathrm{Al,exp}}$.

Eq. 23 $$u_{rel}(\eta_{H_2}) = \sqrt{u_{rel}(\dot{m}_{H_2,avg})^2 + u_{rel}(\dot{m}_{Al,exp})^2}$$

Where an average of the four phases is calculated (see Table 8, Table 10 and Table 11), the uncertainty of type A (standard deviation of four phases) and type B (prior known uncertainty of each phase according to measurement devices and data used) are combined with Gaussian error propagation of absolute uncertainties with:

Eq. 24 $$u_{TypeA} = stdev(\overline{x}) = \frac{\sigma}{\sqrt{N}} = \frac{\sqrt{\frac{\Sigma_{i=1}^{4}(x_i - \overline{x})^2}{(4-1)}}}{\sqrt{4}}$$

Table 30: Type B uncertainties for the hydrogen production rate and efficiency.

Parameter	Physical unit	Typical value	Typical uncertainty (u)	Rel. Uncertainty (urel) (of typical value)
$\dot{m}_{H_2,avg}$	g/h	4 - 5.5	0.02 + 0.5% o.r.	0.86 - 1%
M_{Al}	g/mol	26.982	negligible	negligible
M_{H_2}	g/mol	2.016	negligible	negligible
n_{H_2}/n_{Al}	-	3/2	0, by definition	0, by definition
t_{phase}	h	0.49…0.57	<1/3600	negligible

F.3 Heat production rate and efficiencies

The measured utilized heat production rate $\dot{Q}_{avg}$ is the average heat flow measured over one phase (four cycles), that is calculated based on the input and output temperatures of the heat exchanger and the mass flow rate of the cooling water as follows:

Eq. 25 $\dot{Q} = \dot{m}_{water} \cdot c_{p,water} \cdot \Delta T$ *with* $\Delta T = (T_{out} - T_{in})$

The uncertainty of ΔT is 0.1 K, it was measured in the calibration of the two temperature sensors *in* and *out*.

The heat loss rate $\dot{Q}_{loss}$ was measured while heating and keeping the converter at 60°C before starting the aluminium reaction. It is calculated analogue to Eq. 25. In this case, ΔT for the measurement of the losses is smaller (1.26 K), thus the relative uncertainty is higher (8%).

The total heat production rate $\dot{Q}_{total}$ is taken as the sum of the measured heat production $\dot{Q}_{avg}$ plus the loss rate $\dot{Q}_{loss}$:

Eq. 26 $\dot{Q}_{total} = \dot{Q}_{avg} + \dot{Q}_{loss}$

The expected heat production is calculated from the added aluminium and the reaction enthalpy ΔH_r as follows:

Eq. 27 $\dot{Q}_{calc} = \frac{\Delta H_{r,333K^*} \dot{m}_{Al}}{M_{Al}}$

Where $\Delta H_{r,333K}$ is the enthalpy of reaction at the temperature of 60 °C (333K)[11].

Eq. 28 $2Al + 6H_2O \rightarrow 2Al(OH)_3 + 3\,H_2$ $\Delta H_{r,333K}$ = -880 kJ/mol

Eq. 29 $2Al + 2NaOH + 6H_2O \rightarrow 2Na[Al(OH)_4] + 3\,H_2$ $\Delta H_{r,333K}$ = -830 kJ/mol

In order to determine the degree of conversion of Al to heat and hydrogen according to Eq. 28 and 29, the conversion efficiency of heat is defined as:

[11] These reaction enthalpies derive from the formation enthalpies of H_2O, $Al(OH)_3$, NaOH and $Na[Al(OH)_4]$. The formation enthalpy of water at 333 K (where our reaction takes place) is -284.73 kJ/mol *[NIST]*. The value at 333 K for solid $Al(OH)_3$ is -1293.69 kJ/mol, for NaOH -474.66 kJ/mol and for $Na[Al(OH)_4]$ -1743.62 kJ/mol. *[CHEN]*. We expect that, before saturation is reached, about 20% of the aluminium reacts according to Eq. 28 and 80% according to Eq. 29, and after saturation only reaction according to Eq.28 takes place. Therefore, for the 6 M experiment a weighted $\Delta H_{r,333}$ of 420 kJ/mol Al is used and for the 1 M experiment $\Delta H_{r,333}$ is 440 kJ/mol Al. An uncertainty of ±5% is assumed.

[NIST]: NIST Chemistry WebBook, NIST Standard Reference Database Number 69, National Institute of Standards and Technology, Gaithersburg (MD), https://janaf.nist.gov/tables/H-063.html (retrieved 2020-03-26).

[CHEN]: Chen Q., Xu Y., Hepler L.G. Calorimetric study of the digestion of gibbsite, A1(OH)3(cr), and thermodynamics of aqueous aluminate ion, A1(OH)4-(aq). Department of Chemistry and Department of Chemical Engineering, University of Alberta, Edmonton, Alta, Canada. 1991.

Eq. 30 $\eta_{conv.heat} = \frac{\dot{Q}_{total}}{\dot{Q}_{calc}}$

The efficiency of the heat utilization is defined as the ration of the measured usable heat $\dot{Q}_{avg}$ and $\dot{Q}_{\mathrm{total}}$, where $\dot{Q}_{\mathrm{total}}$ is the sum of the usable heat and the previously measured losses. Since $\dot{Q}_{\mathrm{total}}$ and $\dot{Q}_{avg}$ are not independent variables, the formula is first converted in order to reach a form with only independent variables in order to be able to apply Gaussian propagation of uncertainties for independent variables:

Eq. 31 $\eta_{heat} = \frac{\dot{Q}_{avg}}{\dot{Q}_{total}} = \frac{\dot{Q}_{avg}}{\dot{Q}_{avg}+\dot{Q}_{loss}} = \frac{1}{\frac{\dot{Q}_{avg}+\dot{Q}_{loss}}{\dot{Q}_{avg}}} = \frac{1}{1+\frac{\dot{Q}_{loss}}{\dot{Q}_{avg}}}$

According to uncertainty propagation, $\mathrm{u}(\eta_{\mathrm{heat}})$ is calculates as:

Eq. 32
$$u(\eta_{heat}) = \sqrt{\left(\frac{\partial\left(\frac{1}{1+\frac{\dot{Q}_{loss}}{\dot{Q}_{avg}}}\right)}{\partial\dot{Q}_{loss}}\right)^2 * u(\dot{Q}_{loss})^2 + \left(\frac{\partial\left(\frac{1}{1+\frac{\dot{Q}_{loss}}{\dot{Q}_{avg}}}\right)}{\partial\dot{Q}_{avg}}\right)^2 * u(\dot{Q}_{avg})^2}$$

$$= \sqrt{\left(-\frac{\dot{Q}_{avg}}{(\dot{Q}_{loss}+\dot{Q}_{avg})^2}\right)^2 * u(\dot{Q}_{loss})^2 + \left(\frac{\dot{Q}_{loss}}{(\dot{Q}_{loss}+\dot{Q}_{avg})^2}\right)^2 * u(\dot{Q}_{avg})^2}$$

$$= \sqrt{\frac{\dot{Q}_{avg}{}^2 * u(\dot{Q}_{loss})^2 + \dot{Q}_{loss}{}^2 * u(\dot{Q}_{avg})^2}{(\dot{Q}_{loss}+\dot{Q}_{avg})^4}}$$

For the other equations, the propagation of uncertainties is much simpler:

Eq. 33 $u_{rel}(\dot{Q}) = \sqrt{u_{rel}(\dot{m}_{water})^2 + u_{rel}(c_{p,water})^2 + u_{rel}(\Delta T)^2},$

Eq. 34 $u_{rel}(\dot{Q}_{calc}) = \sqrt{u_{rel}(\Delta H_{r,333})^2 + u_{rel}(\dot{m}_{Al})^2}$

Eq. 35 $u(\dot{Q}_{total}) = \sqrt{u(\dot{Q}_{avg})^2 + u(\dot{Q}_{loss})^2}$

Eq. 36 $u_{rel}(\eta_{conv.heat}) = \sqrt{u_{rel}(\dot{Q}_{total})^2 + u_{rel}(\dot{Q}_{calc})^2}$

Table 31: Type B uncertainties for the heat production rate and efficiencies.

Parameter	Physical unit	Typical value	Typical uncertainty (u)	Rel. Uncertainty (urel) (of typical value)
$\Delta H_{r,333,6M,unsaturated}$	kJ/mol	420	21	5%
$\Delta H_{r,333,1M,saturated}$	kJ/mol	440	22	5%
$\dot{m}_{water}$	kg/h	18.7		0.1%
$c_{p,water}$	kJ / (kg*K)	4.183	0.003	0.07%, negligible
ΔT	K	1.26 / 7.7	0.1	8% / 1.3%
$\dot{Q}_{loss}$	W	28	2.2	8%

F.4 Fuel cell power

The power of the fuel cell was calculated using the measured voltage U and the current, which was calculated from the voltage drop U_R over a measuring shunt R of 0.05 Ω.

Eq. 37 $$P_{el} = U * I = U * \frac{U_R}{R}$$

The uncertainty of the power measurement of the fuel cell was calculated with the Gaussian error propagation.

Eq. 38 $$u_{rel}(P_{el}) = \sqrt{u_{rel}(U)^2 + u_{rel}(U_R)^2 + u_{rel}(R)^2}$$

The electrical efficiency of the fuel cell was calculated using the measured hydrogen flow $\dot{m}_{H_2,avg}$ and its upper heating value HHV_{H2}.

Eq. 39 $$\eta_{FC} = \frac{P_{el}}{\dot{m}_{H_2,avg} \cdot HHV_{H2}}$$

The uncertainty of η_{FC} is calculated as follows, the uncertainty of HHV_{H2} is neglected.

Eq. 40 $$u_{rel}(\eta_{FC}) = \sqrt{u_{rel}(P_{el})^2 + u_{rel}\left(\dot{m}_{H_2,avg}\right)^2}$$

Table 32: Type B uncertainties for the fuel cell power calculation

Parameter	Physical unit	Typical value	Typical absolute uncertainty (u)	Rel. Uncertainty (urel) (of typical value)
U	V	12	0.051	0.4%
R	Ω	0.05		1%
U_R	V	0.417	0.0008	0.2%
I	A	8.3		
P_{el}	W	100		1.1%
HHV_{H2}	kWh/kg	39.4	negligible	negligible
η_{FC}	%	42	0.6	1.5%

F.5 Measuring Devices and Materials

Table 33: Measuring devices used for the experiments in chapter 5

Device	Manufacturer	Type	Unit	Uncertainty		
Analytical balance	Mettler Toledo	MS6002S	g	± 0.02		
Temperature sensors	Transmetra	PT-100	°C	± (0.15 + 0.002 * T[°C])		
Hydrogen flow meter	Bronkhorst	mini CORI-FLOW™ M12	g/h	± 0.02 + 0.5% of reading		
Water flow sensor	Endress + Hauser	Cubemass DCI	kg/h	± 0.1% of reading (for >1 kg/h)		
Thermostat bath	Lauda	RE 420 G	-	-		
Electrical data reader	National Instruments	NI CompactDAQ (9172) Module 9219	V	Range	± 15 V	± 1 V
				Gain error	± 0.4%	± 0.18%
				Offset error	± 180 ppm	± 45 ppm

Table 34: Materials used for the experiments in chapter 5

Material	Manufacturer	Note
Aluminium grit	Metallpulver24	size: 0.8 – 1.2 mm; bulk density: ca. 1.2 g/cm3 purity: 97.5 ±0.5%; impurities: Mg 0,80%, Si max. 1%, Fe max. 0,4%, Mn max. 0,3%, C max. 0,10%
NaOH	Sigma Aldrich	NaOH 50 wt.% (±2%) in H2O; density: 1.515 g/mL at 25 °C, MW: 400 g/mol, CAS Number: 1310-73-2; Sigma-Aldrich Code 415413, Lot #STBH6577